SANDIA REPORT
SAND2021-0996
Printed January 2021

Modeling Study of Reduced Tubing Size Effects on Flow in Depleted Reservoir Natural Gas Storage Wells

David L. Lord; Raymond G. Allen

Prepared by
Sandia National Laboratories
Albuquerque, New Mexico
87185 and Livermore,
California 94550

Issued by Sandia National Laboratories, operated for the United States Department of Energy by National Technology & Engineering Solutions of Sandia, LLC.

NOTICE: This report was prepared as an account of work sponsored by an agency of the United States Government. Neither the United States Government, nor any agency thereof, nor any of their employees, nor any of their contractors, subcontractors, or their employees, make any warranty, express or implied, or assume any legal liability or responsibility for the accuracy, completeness, or usefulness of any information, apparatus, product, or process disclosed, or represent that its use would not infringe privately owned rights. Reference herein to any specific commercial product, process, or service by trade name, trademark, manufacturer, or otherwise, does not necessarily constitute or imply its endorsement, recommendation, or favoring by the United States Government, any agency thereof, or any of their contractors or subcontractors. The views and opinions expressed herein do not necessarily state or reflect those of the United States Government, any agency thereof, or any of their contractors.

Printed in the United States of America. This report has been reproduced directly from the best available copy.

Available to DOE and DOE contractors from
U.S. Department of Energy
Office of Scientific and Technical Information
P.O. Box 62
Oak Ridge, TN 37831

Telephone: (865) 576-8401
Facsimile: (865) 576-5728
E-Mail: reports@osti.gov
Online ordering: http://www.osti.gov/scitech

Available to the public from
U.S. Department of Commerce
National Technical Information Service
5301 Shawnee Rd
Alexandria, VA 22312

Telephone: (800) 553-6847
Facsimile: (703) 605-6900
E-Mail: orders@ntis.gov
Online order: https://classic.ntis.gov/help/order-methods/

ABSTRACT

This report explores the effects of tubing size reductions on natural gas flow from representative depleted reservoir underground storage wells and fields using basic models for coupled reservoir and pipe flow. This work was motivated by interest at the U.S. Department of Transportation, Pipeline and Hazardous Materials Safety Administration, in evaluating the effects of tubing and packer as a potential safety upgrade to implement double-barrier systems to existing underground natural gas storage wells. Reservoir and well flow models were developed from widely accepted industry equations, verified against a commercial process simulator model, and validated against field data. The study utilized U.S. operator survey data to provide context and assure that modeling parameters including average deliverability rates for wells and fields, operating pressures, well depths, and storage capacities were all carefully considered to keep the modeling relevant to the known range of U.S. operations. The models generally found that wells and fields with inherently low deliverability were relatively insensitive to reductions in tubing diameter, primarily because the hydraulics in those cases were controlled by reservoir properties. For the high-producing wells and fields, the models found that reducing tubing diameter could produce significant reductions in deliverability, both at the field- and well- level. When put into context with occurrence data regarding average deliverability of fields and wells, it appears that most wells and most fields across the U.S. would experience deliverability reductions on the low end of what was simulated here, generally below 20%. For fields with moderate to high deliverability, reductions were generally larger, and could reach as high as 60% for the highest-producing wells and fields.

ACKNOWLEDGEMENTS

This work was funded by the U.S. Department of Transportation, Pipeline and Hazardous Materials Safety Administration through a contract with the Battelle Corporation.

The authors would like to thank Mr. Stephen Nowaczewski (Nova Northstar, LLC) and Dr Jiann Su (Sandia National Laboratories) for technical reviews and assistance with access to natural gas storage operations data.

CONTENTS

1. Introduction 13
   1.1. Background 14
2. Approach 15
   2.1. Modeling Domain 15
   2.2. Flow Equations 16
      2.2.1. Vertical Gas Well 16
         2.2.1.1. Darcy Equation 16
         2.2.1.2. Weymouth Equation 17
         2.2.1.3. Cullender and Smith 17
         2.2.1.4. Gas Equation of State 19
         2.2.1.5. Gas Mixture Properties 20
      2.2.2. Well and Reservoir Deliverability 21
   2.3. Numerical Models 22
      2.3.1. Sandia in-House Models 22
         2.3.1.1. Darcy Model for Vertical Pipe Flow 22
         2.3.1.2. Weymouth Model for Vertical Pipe Flow 23
         2.3.1.3. Cullender-Smith Model for Vertical Pipe Flow 23
      2.3.2. Commercial Process Simulator (PSM) for Vertical Pipe Flow 23
      2.3.3. Combined Pipe and Well Flow Model 24
3. Model Verification and Validation 27
   3.1. Vertical Pipe Flow Model Verification 27
      3.1.1. Verification Cases 27
      3.1.2. Verification Results 27
      3.1.3. Summary Comments on Verification Results 31
   3.2. Combined Pipe and Well Flow Model Validation 32
      3.2.1. Summary Comments on Combined Model Validation 33
4. Simulation Cases 35
   4.1. Deliverability within a Field 35
   4.2. Fields, Wells, and Working Gas Capacities Across the U.S. 38
   4.3. Simulation Cases 38
      4.3.1. Run Matrices 41
5. Modeling Results 45
   5.1. Field C (Hockey Stick Distribution) Results Across Selected $Q_{avg/well}$ Bins 45
   5.2. Field G (Linear Distribution) Results Across Selected $Q_{avg/well}$ Bins 50
   5.3. Field C vs. G Comparison 53
   5.4. Effects of Depth and Liners on Deliverability for Field C 55
   5.5. Effects of Reservoir Shut-In Pressure on Deliverability for Field C 58
   5.6. Comparison Across Multiple Bins, Fields 58
   5.7. Interpretation for U.S. Depleted Reservoir Storage 59
6. Summary 63
7. References 65

Appendix A. Reservoir Performance Simulations for Field C (Hockey Stick Distribution) 67

Appendix B. Reservoir Performance Simulations for Field G (Linear Distrbution) 75

Appendix C. Reservoir Perfomance Simulations Showing Depth Dependence.....81
Appendix D. Reservoir Perfomance Simulations Showing Reservoir Shut-In Pressure Dependence 87

LIST OF FIGURES

Figure 1-1. Schematic of tubing and packer configuration in a gas storage well. Gas flow direction indicates drawdown mode.....13
Figure 2-1. Conceptual sketch of modeling domain.....15
Figure 2-2. Abstracted version of modeling domain showing pressure nodes connected by flow resistances in drawdown configuration.....16
Figure 2-3. Screenshot of combined pipe and well flow model showing 20 model runs for a given well field.....25
Figure 3-1. Case 1 model verification results, volumetric flowrate with pipe inner diameter.....28
Figure 3-2. Case 1 model verification results, mass flowrate with pipe inner diameter.....28
Figure 3-3. Case 1 model verification results, gas velocity at wellhead with pipe inner diameter. 29
Figure 3-4. Case 2 model verification results, volumetric flowrate with pipe inner diameter.....29
Figure 3-5. Case 2 model verification results, mass flowrate with pipe inner diameter 30
Figure 3-6. Case 2 model verification results, gas velocity at wellhead with pipe inner diameter.....30
Figure 3-7. Case 1 relative changes in volumetric flow with reductions in pipe inner diameter.....31
Figure 3-8. Model overlay with field data for four wells to validate model performance.....32
Figure 4-1. Deliverability distribution for field "A" comprising 4 wells with $Q_{avg/well}$ = 9.1 MMSCFD @ dP^2 = 500,000 psi^2.....35
Figure 4-2. Deliverability distribution for field "C" comprising 92 wells based on field data scaled by the authors to yield a Qavg/well = 0.5 MMSCFD.....36
Figure 4-3. Deliverability distribution for field "G" comprising 29 wells based on field data scaled by the authors to yield a $Q_{avg/well}$ = 2.4 MMSCFD. 37
Figure 4-4. Deliverability distribution for field "D" comprising 71 wells based on field data scaled by the authors to yield a $Q_{avg/well}$ = 1.7 MMSCFD. 37
Figure 4-5. Overview of U.S. Depleted Reservoir Storage showing relative occurrence of number of fields, number of wells, and working gas capacity versus average deliverability per well for all reported fields in 2016-2017. Data from AGA (2017).....38
Figure 4-6. Overview of simulation cases (red and green bars) run in association with the AGA data (blue bars) on average deliverability per well in U.S. gas storage fields.....39
Figure 4-7. Plot of P_{max} versus D as interpreted from AGA (2017). Linear fit equation is shown on plot.....40
Figure 5-1. Q25 flowrates for Field C wells with baseline $Q_{avg/well}$ = 0.5 MMSCFD in 4.95" ID wells showing reductions at two liner sizes, 2.992 and 2.441".....46
Figure 5-2. Q250 flowrates for Field C wells with baseline $Q_{avg/well}$ = 2.5 MMSCFD in 4.95" ID wells showing reductions at two liner sizes, 2.992 and 2.441".....46
Figure 5-3. Q500 flowrates for Field C wells with baseline $Q_{avg/well}$ = 5.5 MMSCFD in 4.95" ID wells showing reductions at two liner sizes, 2.992 and 2.441".....47
Figure 5-4. Q1000 flowrates for Field C wells with baseline $Q_{avg/well}$ = 19.5 MMSCFD in 4.95" ID wells showing reductions at two liner sizes, 2.992 and 2.441".....47
Figure 5-5. Q250 flowrates for Field C wells with baseline $Q_{avg/well}$ = 3.5 MMSCFD in 6.276" ID wells showing reductions at two liner sizes, 3.958 and 3.476".....48

Figure 5-6. Q500 flowrates for Field C wells with baseline $Q_{avg/well}$ = 11.5 MMSCFD in 6.276" ID wells showing reductions at two liner sizes, 3.958 and 3.476". 48
Figure 5-7. Q1200 flowrates for Field C wells with baseline $Q_{avg/well}$ = 46.5 MMSCFD in 6.276" ID wells showing reductions at two liner sizes, 3.958 and 3.476". 49
Figure 5-8. Summary results for Field C (hockey-stick distribution) for all $Q_{avg/well}$ and liners run against base case production casing ID = 4.95" and 6.276". 50
Figure 5-9. Q25 flowrates for Field G wells with baseline $Q_{avg/well}$ = 0.5 MMSCFD in 4.95" ID wells showing reductions at two liner sizes, 2.992 and 2.441". 51
Figure 5-10. Q500 flowrates for Field G wells with baseline $Q_{avg/well}$ = 11.5 MMSCFD in 4.95" ID wells showing reductions at two liner sizes, 2.992 and 2.441". 51
Figure 5-11. Q500 flowrates for Field G wells with baseline $Q_{avg/well}$ = 11.5 MMSCFD in 6.276" ID wells showing reductions at two liner sizes, 3.958 and 3.476". 52
Figure 5-12. Q1200 flowrates for Field G wells with baseline $Q_{avg/well}$ = 46.5 MMSCFD in 6.276" ID wells showing reductions at two liner sizes, 3.958 and 3.476". 52
Figure 5-13. Summary results for Field G (linear distribution) for all $Q_{avg/well}$ and liners run against base case production casing ID = 4.95" and 6.276". 53
Figure 5-14. Q250 flowrates for Field C wells with baseline $Q_{avg/well}$ = 3.5 MMSCFD in 6.276" ID wells showing reductions at two liner sizes, 3.958 and 3.476". 54
Figure 5-15. Q250 flowrates for Field G wells with baseline $Q_{avg/well}$ = 3.5 MMSCFD in 6.276" ID wells showing reductions at two liner sizes, 3.958 and 3.476". 54
Figure 5-16. Summary results for Field C (hockey stick distribution) and Field G (linear distribution) for all $Q_{avg/well}$ bins and with Liner 1 run against base case production casing ID = 4.95" and 6.276". 55
Figure 5-17. Field-level reductions in deliverability with well depth for baseline $Q_{avg/well}$ = 0.5 MMSCFD in 4.95" ID wells in Field C (hockey stick distribution) showing reductions at two liner sizes, 2.992 and 2.441". 56
Figure 5-18. Field-level reductions in deliverability with well depth for baseline $Q_{avg/well}$ = 3.5 MMSCFD in 4.95" ID wells in Field C (hockey stick distribution) showing reductions at two liner sizes, 2.992 and 2.441". 56
Figure 5-19. Field-level reductions in deliverability with well depth for baseline $Q_{avg/well}$ = 25.5 MMSCFD in 6.276" ID wells in Field C (hockey stick distribution) showing reductions at two liner sizes, 3.958 and 3.476". 57
Figure 5-20. Field-level reductions in deliverability with well depth for baseline $Q_{avg/well}$ = 46.5 MMSCFD in 6.276" ID wells in Field C (hockey stick distribution) showing reductions at two liner sizes, 3.958 and 3.476". 57
Figure 5-21. Summary plot of field deliverability across a broad range of $Q_{avg/well}$ bins for 4.95" and 6.276" ID base case wells with the addition of liners. 59
Figure 5-22. Hybrid graph showing overlay of field, well, and working gas capacity occurrence data from AGA (2017) with field-level deliverability modeling results for selected tubing size reductions. 61

Figure A- 1. Q25 flowrates for Field C wells with baseline $Q_{avg/well}$ = 0.5 MMSCFD in 4.95" ID wells showing reductions at two liner sizes, 2.992 and 2.441" 67
Figure A- 2. Q100 flowrates for Field C wells with baseline $Q_{avg/well}$ = 1.5 MMSCFD in 4.95" ID wells showing reductions at two liner sizes, 2.992 and 2.441" 67
Figure A- 3. Q250 flowrates for Field C wells with baseline $Q_{avg/well}$ = 2.5 MMSCFD in 4.95" ID wells showing reductions at two liner sizes, 2.992 and 2.441" 68

Figure A- 4. Q250 flowrates for Field C wells with baseline $Q_{avg/well}$ = 3.5 MMSCFD in 4.95" ID wells showing reductions at two liner sizes, 2.992 and 2.441" 68
Figure A- 5. Q500 flowrates for Field C wells with baseline $Q_{avg/well}$ = 5.5 MMSCFD in 4.95" ID wells showing reductions at two liner sizes, 2.992 and 2.441". 69
Figure A- 6. Q500 flowrates for Field C wells with baseline $Q_{avg/well}$ = 11.5 MMSCFD in 4.95" ID wells showing reductions at two liner sizes, 2.992 and 2.441". 69
Figure A- 7. Q1,000 flowrates for Field C wells with baseline $Q_{avg/well}$ = 19.5 MMSCFD in 4.95" ID wells showing reductions at two liner sizes, 2.992 and 2.441". 70
Figure A- 8. Q250 flowrates for Field C wells with baseline $Q_{avg/well}$ = 3.5 MMSCFD in 6.276" ID wells showing reductions at two liner sizes, 3.958 and 3.476". 70
Figure A- 9. Q500 flowrates for Field C wells with baseline $Q_{avg/well}$ = 11.5 MMSCFD in 6.276" ID wells showing reductions at two liner sizes, 3.958 and 3.476". 71
Figure A- 10. Q1,000 flowrates for Field C wells with baseline $Q_{avg/well}$ = 25.5 MMSCFD in 6.276" ID wells showing reductions at two liner sizes, 3.958 and 3.476". 71
Figure A- 11. Q1,200 flowrates for Field C wells with baseline $Q_{avg/well}$ = 46.5 MMSCFD in 6.276" ID wells showing reductions at two liner sizes, 3.958 and 3.476". 72

Figure B- 1. Q25 flowrates for Field G wells with baseline $Q_{avg/well}$ = 0.5 MMSCFD in 4.95" ID wells showing reductions at two liner sizes, 2.992 and 2.441". 75
Figure B- 2. Q100 flowrates for Field G wells with baseline $Q_{avg/well}$ = 1.5 MMSCFD in 4.95" ID wells showing reductions at two liner sizes, 2.992 and 2.441". 75
Figure B- 3. Q500 flowrates for Field G wells with baseline $Q_{avg/well}$ = 11.5 MMSCFD in 4.95" ID wells showing reductions at two liner sizes, 2.992 and 2.441". 76
Figure B- 4. Q1000 flowrates for Field G wells with baseline $Q_{avg/well}$ = 19.5 MMSCFD in 4.95" ID wells showing reductions at two liner sizes, 2.992 and 2.441". 76
Figure B- 5. Q250 flowrates for Field G wells with baseline $Q_{avg/well}$ = 3.5 MMSCFD in 6.276" wells showing reductions at two liner sizes, 3.958 and 3.756". 77
Figure B- 6. Q500 flowrates for Field G wells with baseline $Q_{avg/well}$ = 11.5 MMSCFD in 6.276" wells showing reductions at two liner sizes, 3.958 and 3.756". 77
Figure B- 7. Q1,000 flowrates for Field G wells with baseline $Q_{avg/well}$ = 25.5 MMSCFD in 6.276" wells showing reductions at two liner sizes, 3.958 and 3.756". 78
Figure B- 8. Q1,200 flowrates for Field G wells with baseline $Q_{avg/well}$ = 46.6 MMSCFD in 6.276" wells showing reductions at two liner sizes, 3.958 and 3.756". 78

Figure C- 1. Q25 flowrates for Field C wells with baseline $Q_{avg/well}$ = 0.5 MMSCFD in 4.95" ID wells showing reductions at two liner sizes, 2.992 and 2.441" and reservoir/well depth = 4,000 ft. 81
Figure C- 2. Q25 flowrates for Field C wells with baseline $Q_{avg/well}$ = 0.5 MMSCFD in 4.95" ID wells showing reductions at two liner sizes, 2.992 and 2.441" and reservoir/well depth = 6,000 ft. 81
Figure C- 3. Q250 flowrates for Field C wells with baseline $Q_{avg/well}$ = 3.5 MMSCFD in 4.95" ID wells showing reductions at two liner sizes, 2.992 and 2.441" and reservoir/well depth = 2,000 ft. 82
Figure C- 4. Q250 flowrates for Field C wells with baseline $Q_{avg/well}$ = 3.5 MMSCFD in 4.95" ID wells showing reductions at two liner sizes, 2.992 and 2.441" and reservoir/well depth = 6,000 ft. 82

Figure C- 5. Q500 flowrates for Field C wells with baseline $Q_{avg/well}$ = 25.5 MMSCFD in 6.276" wells showing reductions at two liner sizes, 3.958 and 3.756" and reservoir depth = 4,000 ft.....83
Figure C- 6. Q500 flowrates for Field C wells with baseline $Q_{avg/well}$ = 25.5 MMSCFD in 6.276" wells showing reductions at two liner sizes, 3.958 and 3.756" and reservoir depth = 7,000 ft.....83
Figure C- 7. Q1,200 flowrates for Field C wells with baseline $Q_{avg/well}$ = 46.5 MMSCFD in 6.276" wells showing reductions at two liner sizes, 3.958 and 3.756" and reservoir depth = 4,000 ft.....84

Figure D- 1. Q250 flowrates for Field C wells with baseline $Q_{avg/well}$ = 3.5 MMSCFD and P_{RSI} = 1200 psia in 4.95" ID wells showing reductions at two liner sizes, 2.992 and 2.441".....87
Figure D- 2. Q250 flowrates for Field C wells with baseline $Q_{avg/well}$ = 3.5 MMSCFD and P_{RSI} = 1500 psia in 4.95" ID wells showing reductions at two liner sizes, 2.992 and 2.441".....87
Figure D- 3. Q250 flowrates for Field C wells with baseline $Q_{avg/well}$ = 3.5 MMSCFD and P_{RSI} = 1600 (=P_{max}) psia in 4.95" ID wells showing reductions at two liner sizes, 2.992 and 2.441". 88
Figure D- 4. Q500 flowrates for Field C wells with baseline $Q_{avg/well}$ = 11.5 MMSCFD and P_{RSI} = 1200 psia in 4.95" ID wells showing reductions at two liner sizes, 2.992 and 2.441".....88
Figure D- 5. Q500 flowrates for Field C wells with baseline $Q_{avg/well}$ = 11.5 MMSCFD and P_{RSI} = 1500 psia in 4.95" ID wells showing reductions at two liner sizes, 2.992 and 2.441".....89
Figure D- 6. Q500 flowrates for Field C wells with baseline $Q_{avg/well}$ = 11.5 MMSCFD and P_{RSI} = 1720 (=P_{max}) psia in 4.95" ID wells showing reductions at two liner sizes, 2.992 and 2.441". 89

LIST OF TABLES

Table 2-1. Representative natural gas component mixture used in this study.....20
Table 2-2. Component critical properties and MW for natural gas components from Frick and Taylor (1962). Bottom row represents mixture value computed from simple mole-weighted mixing rule.....21
Table 3-1. Summary of test cases for vertical pipe flow verification 27
Table 4-1. Run matrix for Field C (hockey stick distribution) across $Q_{avg/well}$ bins for 5.5 and 7-in OD base casing size.....42
Table 4-2. Run matrix for field G (linear distribution) across $Q_{avg/well}$ bins for 5.5 and 7-in OD base casing size.....42
Table 4-3. Run matrix for Field C (hockey stick distribution) across selected depths and $Q_{avg/well}$ bins for 5.5 and 7-in OD base casing size.....43
Table 4-4. Run matrix for Field C (hockey stick distribution) across selected P_{RSI} and $Q_{avg/well}$ bins for 5.5-in OD base casing.....43
Table 5-1. Summary of field-level reductions in deliverability for Field C with liner size and reservoir shut-in pressure for base well ID = 4.95". 58

Table A- 1. Results matrix for Field C showing % reductions in field deliverability for all simulated $Q_{avg/well}$ bins in 4.95" ID wells with reductions at two liner sizes, 2.992 and 2.441". 73
Table A- 2. Results matrix for Field C showing % reductions in field deliverability for all simulated $Q_{avg/well}$ bins in 6.276" ID wells with reductions at two liner sizes, 3.958 and 3.476"...73

Table B- 1. Results matrix for Field G showing % reductions in field deliverability for all simulated $Q_{avg/well}$ bins in 4.95" ID wells with reductions at two liner sizes, 2.992 and 2.441". 79

Table B- 2. Results matrix for Field G showing % reductions in field deliverability for all simulated $Q_{avg/well}$ bins in 6.276" ID wells with reductions at two liner sizes, 3.958 and 3.476"...79

Table C- 1. Results matrix for Field C showing % reductions in deliverability with depth for selected $Q_{avg/well}$ bins in 4.95" ID wells showing reductions at two liner sizes, 2.992 and 2.441"....84
Table C- 2. Results matrix for Field C showing % reductions in deliverability with depth for selected $Q_{avg/well}$ bins in 6.276" ID wells showing reductions at two liner sizes, 3.958 and 3.476"....85

EXECUTIVE SUMMARY

This report explores the effects of tubing size reductions on natural gas flow from representative underground storage wells using basic models for coupled reservoir and pipe flow. This work was motivated by national-level interest in improving safety in underground storage operations following the Aliso Canyon natural gas leak that occurred in 2015 near Los Angeles, California, which was the largest-known methane release from a natural gas storage facility in U.S. history. Both government and industry reports have proposed adding tubing and packer as possible solutions to upgrading from a single point of failure design to a double-barrier system, particularly in existing wells many decades old where materials and design pre-date modern standards.

This report is intended to provide a quantitative overview of the range of effects of tubing size reductions on deliverability in typical U.S. gas storage fields. Reservoir and well flow models were developed from widely accepted industry equations, and the flow models were verified against a commercial process simulator model and validated against field data. The study also utilized a recent survey from the American Gas Association summarizing the properties of gas storage fields across the U.S. to provide context for the simulations and assure that operating parameters including average deliverability rates for wells and fields, operating pressures, well depths, and storage capacities were all considered to keep the modeling relevant to the known range of U.S. operations.

The models generally found that wells and fields with inherently low deliverability were relatively insensitive to reductions in tubing diameter, primarily because the hydraulics in those cases were controlled by reservoir properties. For the high-producing wells and fields, reductions in tubing diameter could produce significant reductions in deliverability, both at the field- and well- level. When put into context with occurrence data regarding average deliverability of fields and wells, it appears that most wells and most fields across the U.S. would experience deliverability reductions on the low end of what was simulated here, generally below 20%. For fields with moderate to high deliverability, reductions were generally larger, and could reach as high as 60% for the highest-producing wells and fields. Operator concerns noted from the public record stating that reductions in deliverability could reach 40% for their current wells or even exceed 60% in some wells on the peak day appear to be validated by the current work for the highest-deliverability wells and fields. These 40-60% reductions do not represent the majority of wells or fields in the U.S., but are possible under the right conditions for the highest-flowing wells and fields.

ACRONYMS AND DEFINITIONS

Abbreviation	Definition
AGA	American Gas Association
C_i	Deliverability constant for well *i*
ϵ	Absolute roughness
DOT	U.S. Department of Transportation
d	Well or tubing inner diameter
dP^2	Difference in squares of pressures
ϵ	Absolute roughness
f	Friction factor
G	Specific gravity of gas
ID	Well or tubing inner diameter
L	Length of pipe
MW_{air}	Molecular weight of air
MW_g	Molecular weight of the natural gas mixture
n_i	Deliverability exponent for well *i*
PHMSA	Pipeline and Hazardous Materials Safety Administration
P_{BHF}	Bottomhole flowing pressure
P_{max}	Maximum reservoir pressure
P_{RSI}	Shut-in reservoir pressure
P_{sc}	Pressure at standard conditions (14.7 psia)
PSM	Process Simulation Model
P_{WHF}	Wellhead flowing pressure
Q_{field}	Gas flowrate for a given field
Q_i	Gas flowrate for well *i*
q_{msc}	Gas volumetric flowrate at standard conditions
R	Gas constant
Re	Reynolds number
ρ_{sc}	Mass density at standard conditions
T_{BHF}	Bottomhole flowing temperature
T_{sc}	Temperature at standard conditions (60°F; 520°R)
μ	Gas mixture absolute viscosity
$\bar{V}$	Specific volume of fluid
W	Mass rate of flow
Z	Compressibility factor

1. INTRODUCTION

This report summarizes a modeling study exploring the effects of hypothetical tubing and packer installations on available flowrates from representative natural gas storage configurations. Tubing and packer installations have the potential to provide an extra layer of protection against product loss in natural gas wells that connect a storage reservoir with surface piping, though their addition will reduce the effective internal diameter and, in turn, could reduce fluid flow rate for given pressure boundary conditions. A simple schematic of tubing and packer installed in a gas storage well is given in Figure 1-1 for illustration. The original cemented production casing is shown connecting the gas storage reservoir to the surface, with an inner diameter and resulting cross-sectional flow area that is determined principally by the production casing size at the time of installation. The tubing and packer may be added at a later time and involves setting a packer deep in the original casing just above the completion zone that stabilizes the end of the tubing creates a static annulus that is hydraulically isolated from reservoir pressure. This double-barrier configuration is more robust against casing leaks than a single barrier, and with pressure monitoring of the static annulus, can provide immediate notice of loss of primary containment from the tubing. A caveat of this configuration, however, is that the cross-sectional area available in the well to transport gas into or out of the reservoir is reduced relative to the original production casing, which was likely sized according to design calculations intended to optimize for reservoir performance and economic return on investment. The magnitude of flow reduction is also affected by the deliverability of the reservoir into the given well. This study quantifies the magnitude of flowrate reductions associated with selected tubing configurations relative to base cases by applying basic numerical models for gas flow in pipes and reservoir deliverability. Three types of underground gas storage are used in the U.S., including depleted oil & gas reservoir, aquifer, and salt cavern. This study focuses on depleted reservoir storage.

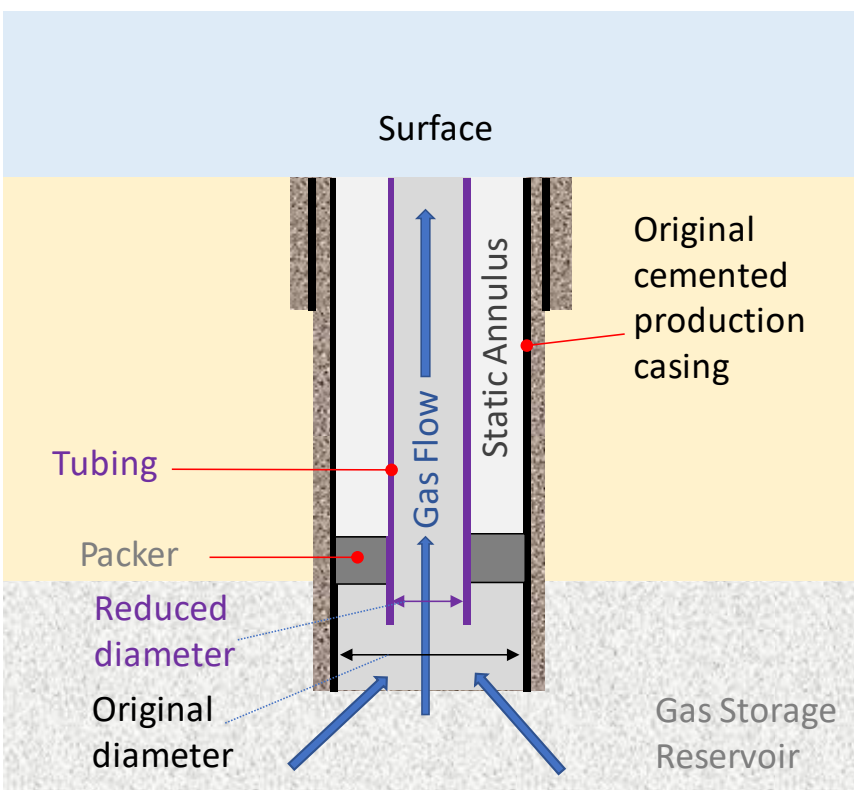

Figure 1-1. Schematic of tubing and packer configuration in a gas storage well. Gas flow direction indicates drawdown mode.

1.1. Background

Underground storage of natural gas is critical component of the U.S. energy supply infrastructure. The natural gas leak from the Aliso Canyon underground natural gas storage facility near Los Angeles, California in 2015 that lasted nearly four months and led to numerous extended residential evacuations, was judged the largest single methane release from a natural gas storage facility in U.S. history, and brought significant national attention to the issue of safety around natural gas storage facilities. Soon after this event, the U.S. Federal Government formed an Interagency Task on Natural Gas Storage Safety, which issued a report in October 2016 entitled Ensuring Safe and Reliable Underground Natural Gas Storage (USDOE 2016). One of the primary recommendations from this report was that operators should phase out wells with single point of failure designs. Among several options, the addition of tubing and packers to underground storage wells was identified as a strategy to mitigate the single point of failure, though concerns were raised about the additional equipment restricting cross-sectional flow area and therefore reducing deliverability, especially in high-capacity wells (API, AGA et al. 2016).

The impact of reducing cross-sectional area on flowrate in a pipe is relatively straightforward, estimated by the basic pipe flow equations, which will be introduced in detail in the next chapter. Generally speaking, the flowrate is proportional to the pipe inner diameter raised to the ~5/2 power. As such, a decrease in pipe inner diameter will decrease flow for given pressure boundary conditions. Implications for operators are less straightforward than this simple pipe flow equation, however. The properties of the storage reservoir and the well completion will affect this overall flow regime, and coupled analysis taking into account both reservoir and well features must be included.

Industry concerns with the implications of tubing and packer have been documented in several publicly available reports (API, AGA et al. 2016; Freifield, Oldenburg et al. 2016; Johnson 2016). One operator indicated that installing liners would results in a 40% reduction in deliverability with their current wells (Freifield, Oldenburg et al. 2016). Another operator indicated that well flow on a peak day may be reduced by > 60% in some wells (Johnson 2016). Part of the purpose of the current work is to conduct an independent analysis to see if these types of numbers can be reasonably expected in U.S. storage fields with the addition of tubing and packers.

2. APPROACH

2.1. Modeling Domain

The modeling domain includes a vertical (non-deviated) pipe that originates at reservoir depth z_1 and ends at the ground surface z_2 as shown in Figure 2-1. The well has a specified inner diameter *d,* absolute roughness *e,* and a length *L* equal to the elevation difference between z_2 and z_1. The wellhead flowing pressure, P_{WHF} and bottomhole flowing pressure, P_{BHF}, are related through vertical gas well flow equations. The bottom of the well is coupled through perforations with a reservoir that exhibits a shut-in pressure P_{RSI}. P_{BHF} and P_{RSI} are related through a simple well deliverability equation with empirical constant *C* and exponent *n*. Only dry gas flow is simulated, with no condensation or particulates or free liquids of any phase.

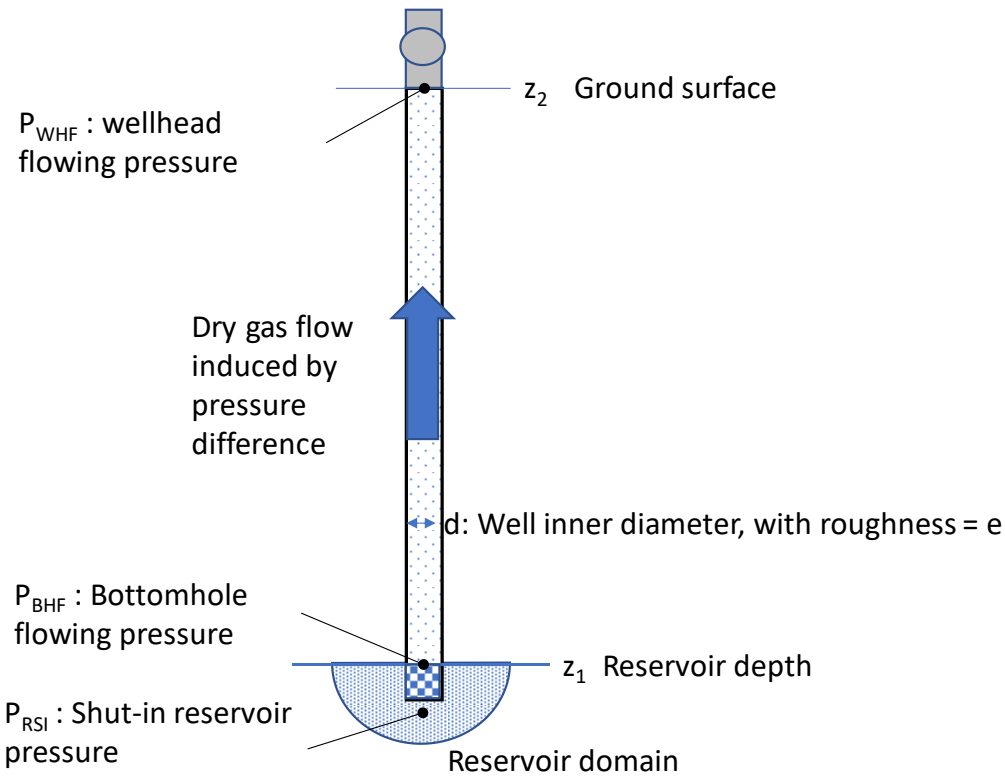

Figure 2-1. Conceptual sketch of modeling domain.

The system may be represented in a more abstracted form as three nodes of pressure potential connected by flow resistances, illustrated in Figure 2-2. For reservoir drawdown operations, the highest-pressure node is the reservoir at shut-in pressure, connected to the well bottomhole through a flow resistance associated with reservoir and well completion properties. The bottomhole is further connected to the wellhead through a second flow resistance associated with well/tubing properties. For a given reservoir shut-in pressure, flowing wellhead pressure, and flow resistance equations, there will be a unique flowrate that satisfies both flow equations and results in a common bottomhole flowing pressure.

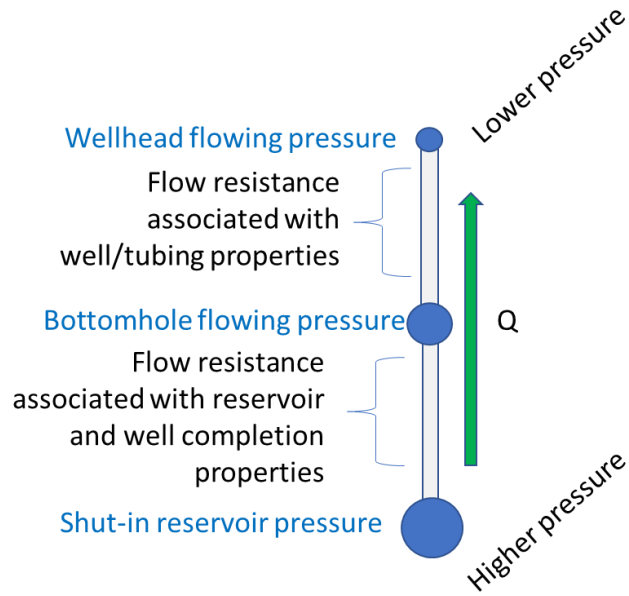

Figure 2-2. Abstracted version of modeling domain showing pressure nodes connected by flow resistances in drawdown configuration.

2.2. Flow Equations

2.2.1. Vertical Gas Well

Through literature research and confirmation with industry experts, several basic equations were selected for use and comparison here. All derive from the fundamental principle of conservation of energy as expressed in the Bernoulli equation. These include the Darcy equation for pressure loss in a vertical pipe (Crane 1982), the Weymouth equation for vertical gas well flow (King 2018), and the Cullender Smith solution of a general equation for gas flow in wells and pipelines with large temperature gradients (Cullender and Smith 1956).

2.2.1.1. Darcy Equation

One specific adaptation of the Bernoulli equation that has widespread use for simulating gas flow in pipes is the Darcy equation (Eq. 111) arranged to solve for pressure drop ΔP (psi) along a tubing section (Crane 1982):

$$\Delta P = 0.000\,003\,36 \times \left\{ \frac{fLW^2\bar{V}}{d^5} \right\} \tag{1}$$

where:

- f = friction factor, dimensionless
- L = length of pipe, ft
- W = rate of flow, lb/hr
- $\bar{V}$ = specific volume of fluid, ft^3/lb
- d = internal diameter of pipe, in

2.2.1.2. Weymouth Equation

Another adaptation of the Bernoulli equation is the Weymouth equation (Eqs. 2, 3) arranged to solve for volumetric flowrate q (SCF/day) across a tubing section (King 2018). "H_e" is a pressure correction to the horizontal pipe flow model to account for hydrostatic head resulting from elevation difference.

$$q = 433.5 \times E_{eff} d^{2.667} \left(\frac{T_{sc}}{P_{sc}}\right) \left\{\frac{5280 \times [P_1^2 - exp(H_e)P_2^2]}{GZTL}\right\}^{0.5} \tag{2}$$

$$H_e = 0.375 \times G \left(\frac{z_1 - z_2}{TZ}\right) \tag{3}$$

Where

- E_{eff} = efficiency (tuning) factor for the tubing section, dimensionless
- d = inner diameter of the tubing, in
- T_{sc} = standard temperature, °R
- P_{sc} = standard pressure, psia
- P_1 = pressure at point 1 in the tubing, psia
- P_2 = pressure at point 2 in the tubing, psia
- G = specific gravity of gas ($=\frac{MW_g}{MW_{air}}$), dimensionless
- Z = compressibility factor, dimensionless
- T = average temperature of the tubing section, °R
- L = length of the tubing section along its axis, ft
- z_1 = elevation at point 1 along the section of tubing, ft
- z_2 = elevation at point 2 along the section of tubing, ft
- MW_g = molecular weight of the natural gas, lb/lb-mole
- MW_{air} = molecular weight of air, 28.97 lb/lb-mole

2.2.1.3. Cullender and Smith

Cullender and Smith (1956) developed a fast numerical algorithm for solving an equation for single-phase vertical gas flow in tubing with large temperature gradients. An algorithm was used here as described in Guo and Ghalambor (2012). The flow equation starts with the following form shown in Eq. 4:

$$\int_{P_{BHF}}^{P_{WHF}} \left[\frac{\frac{P}{ZT}}{0.001cos\theta \left(\frac{P}{ZT}\right)^2 + 0.6666\left(\frac{f q_{msc}^2}{d^5}\right)}\right] dp = 18.75GL \tag{4}$$

Where:

- P_{WHF} = flowing wellhead pressure, psia
- P_{BHF} = flowing bottomhole pressure, psia

- Z = Compressibility factor, dimensionless
- T = Temperature, °R
- θ = angle of tubing axis from vertical, radians
- G = specific gravity of gas ($=\frac{MW_g}{MW_{air}}$), dimensionless
- L= length of the tubing section along its axis, ft
- d = inner diameter of the tubing, in
- f = friction factor, dimensionless
- q_{msc}= gas flowrate, MMSCFD

If the integrant in Eq. 4 is denoted with symbol I, then:

$$I = \frac{\frac{P}{ZT}}{0.001cos\theta\left(\frac{P}{ZT}\right)^2 + 0.6666\left(\frac{f q_{msc}^2}{d^5}\right)} \tag{5}$$

And Eq. 5 becomes:

$$\int_{P_{BHF}}^{P_{WHF}} I\, dp = 18.75GL \tag{6}$$

Numerically integrating Eq. 6 over two half-heights requires evaluation of I at three conditions: I_{WHF}, I_{MF}, and I_{BHF}. Each requires P, Z, and T at their respective conditions. Numerical integration yields the following expressions:

$$P_{MF} = P_{WHF} + \frac{18.75GL}{I_{MF} + I_{WHF}} \tag{7}$$

$$P_{BHF} = P_{MF} + \frac{18.75GL}{I_{BHF} + I_{MF}} \tag{8}$$

P_{WHF} is given as a starting condition. Because I_{MF} is a function of P_{MF}, a Newton-Raphson iterative solution was used for P_{MF}. Once Eq. 7 was solved, then P_{MF} was substituted into Eq. 8 and P_{BHF} was solved iteratively.

To calculate the friction factor, *f*, in Eq. 5 above, the Swamee-Jain explicit formula (Eq. 9) was used as shown in King (2018):

$$f = \frac{0.25}{\left[log_{10}\left(\frac{1}{3.7} \times \frac{\epsilon}{d} + \frac{5.74}{Re^{0.9}}\right)\right]^2} \tag{9}$$

Where:

- ϵ = absolute roughness of the tubing, in
- d = inner diameter of the tubing, in
- Re=Reynolds number, dimensionless

Reynolds Number (Eq. 10) was calculated as shown in Chaudhry (2003):

$$Re = \frac{20{,}011 G q_{msc}}{\mu d} \tag{10}$$

Where

- G = specific gravity of gas ($=\frac{MW_g}{MW_{air}}$), dimensionless
- q_{msc}= gas flowrate at standard conditions, mmscfd
- μ = absolute viscosity of gas, centipoise
- d = inner diameter of the tubing, in

2.2.1.4. Gas Equation of State

Relationships among absolute pressure, absolute temperature, and gas density were determined through the real gas law:

$$\rho_g = \frac{P \times MW_g}{ZRT} \tag{11}$$

Where:

- ρ_g = gas density, lb/ft^3
- P = Pressure, psia
- MW_g = molecular weight of the gas, lb/lb-mole
- Z = compressibility factor, dimensionless
- R = gas constant, 10.7 (psi ft^3)/(lb-moles °R)
- T = Temperature, °R

The compressibility factor, Z, is a measure of deviation of real gas behavior from ideal gas law behavior. Z was calculated in this study by two methods.

First was an explicit correlation from Menon (2011) as shown in Eq. 12:

$$Z = \frac{1}{\left[1 + \left(\frac{P_{avg} \times 344{,}400 \times (10)^{1.785G}}{T_{avg}^{3.825}}\right)\right]} \tag{12}$$

Where:

- P_{avg}= Average gas pressure, psia

- T_{avg}= Average gas temperature, °R
- G= specific gravity of gas (=$\frac{MW_g}{MW_{air}}$), dimensionless

Second was the Hall-Yarborough equation, which requires an iterative solution that is described in Guo and Ghalambor (2012).

2.2.1.5. Gas Mixture Properties

The gas simulated in this study comprised a simple mixture with a majority methane (CH_4) and an assortment of minority components. A representative gas mixture formulation was chosen for use here, with mole% as shown in Table 2-1.

Table 2-1. Representative natural gas component mixture used in this study.

Component name	Formula	Mole fraction
Nitrogen	N_2	0.010
Oxygen	O_2	0.000
Carbon Dioxide	CO_2	0.005
Water	H_2O	0.000
Methane	CH_4	0.905
Ethane	C_2H_6	0.050
Propane	C_3H_8	0.030

Representative gas mixture properties such as *MW*, *G*, critical pressure (P_c), and critical Temperature, (T_c) were calculated using basic mole-weighted mixing rules as described in Guo and Ghalambor (2012). Table 2-2 lists the critical properties for each of the relevant gas mixture components as well as the mole-weighted mixture value (bottom row) calculated for further use in this analysis.

Table 2-2. Component critical properties and MW for natural gas components from Frick and Taylor (1962). Bottom row represents mixture value computed from simple mole-weighted mixing rule.

Component	Tc	Tc	Pc	MW
	[F]	[deg R]	[psia]	[lb/lb-mole]
Nitrogen	-232.8	227.2	492.4	28.02
Oxygen	-181.8	278.2	732	32.00
Carbon Dioxide	88	548	1071.6	44.01
Water	705.4	1165.4	3206	18.02
Methane	-117	343	673.3	16.04
Ethane	90	550	708	30.07
Propane	206.1	666.1	617.4	44.09
Mixture		362.9	673.5	17.84

Gas specific gravity (G) for the given mixture was calculated as shown in Eq. 13, where the molecular weight of air was taken as 28.97 lb/lb-mole (Guo and Ghalambor 2012):

$$G = \frac{MW_g}{MW_{air}} = \frac{17.84}{28.97} = 0.6159 \tag{13}$$

Further, the mass density of the gas mixture at standard conditions was calculated as shown in Eq. 14

$$\rho_{sc} = \frac{P_{sc} MW_g}{ZRT_{sc}} = 0.0471 \ {}^{lb}/_{ft^3} \tag{14}$$

Where:

- P_{sc} = 14. 7 psia
- MW_g = 17.84 lb/lb-mole
- Z = 1
- R = gas constant, 10.7 (psi ft^3)/(lb-mole °R)
- T_{sc} = 60+460 = 520 °R

Gas mixture absolute viscosity (μ) was estimated graphically from Frick and Taylor (1962) Figure 17-11 for gas gravity G = 0.62, temperature = 100°F, absolute pressure between 14.7 and 500 psia, resulting in μ = 0.012 centipoise. Note gas viscosity is used to compute the Reynolds number in Eq. 10 above.

2.2.2. Well and Reservoir Deliverability

A simple well deliverability model was developed from a commonly-used formula in underground gas storage facility design (Flanigan 1995) as expressed in Eq. 15:

$$Q_i = C_i[P_{RSI}^2 - P_{BHF}^2]^{n_i} \tag{15}$$

Where:

- Q_i= gas flowrate for well *i*, MMSCFD
- C_i = Deliverability constant for well *i*
- P_{RSI} = Reservoir shut-in pressure, psia
- P_{BHF} = Bottom hole flowing pressure, psia
- n_i = deliverability exponent for well *i*
- *i* = subscript denoting an individual well number

Deliverability for an entire field comprising "N" wells may then be evaluated by taking the sum of the individual wells as shown in Eq.16:

$$Q_{field} = \sum_{i=1}^{N} Q_i \tag{16}$$

Where:

- Q_{field}= gas flowrate for a given field with N wells, MMSCFD
- Q_i= gas flowrate for well *i*, MMSCFD
- *i* = subscript denoting an individual well number
- *N* = number of wells in a given field

Note this approach does not account for the features of the gathering system downstream of the wellhead(s) at an operator's facility. As such, field-level deliverability is defined here at the wellhead(s), not at the outlet of the facility.

2.3. Numerical Models

2.3.1. Sandia in-House Models

2.3.1.1. Darcy Model for Vertical Pipe Flow

The explicit formulation of the Darcy model shown in Eq. 1 was coded into an Excel workbook, which returns a pressure difference, ΔP, in psi. Inputs for mass rate of flow (*W*), specific volume of fluid ($\bar{V}$), and friction factor (*f*) were computed based on additional inputs.

Mass rate of flow (*W*) was evaluated using Eq. 17 :

$$W = \frac{\rho_{sc} q_{msc} \times 10^6}{24} \tag{17}$$

Where:

- W = mass rate of flow, lb/hr
- ρ_{sc} = mass density of gas at standard conditions, lb/ft^3 (see Eq. 14)
- q_{msc} = gas volumetric flowrate at standard conditions, mmscfd

Specific volume of fluid ($\bar{V}$), was estimated using Eq. 18:

$$\bar{V} = \frac{ZRT_{BHF}}{P_{BHF}MW_g} \tag{18}$$

Where:

- $\bar{V}$ = specific volume of fluid, ft^3/lb
- Z = compressibility at local P,T conditions, dimensionless (see Eq. 12)
- R = gas constant, 10.7 (psi ft^3)/(lb-mole °R)
- T_{BHF} = Bottomhole flowing temperature, °R
- P_{BHF} = Bottomhole flowing pressure, psia
- MW_g = molecular weight of the gas, lb/lb-mole

Friction factor (f) was evaluated using Eq. 9. Since q_{msc} was given as input, Re was evaluated as show in Eq. 10.

2.3.1.2. Weymouth Model for Vertical Pipe Flow

The Weymouth model was coded into an Excel workbook based on the explicit formulations shown in Eqs. 2 and 3, which returns a volumtric flowrate, q, in SCFD. The efficiency term "E_{eff}" was set to 1.0 as a starting point as suggested in King (2018). This parameter could be adjusted to match field data as it represents an emprical tuning factor. 333

2.3.1.3. Cullender-Smith Model for Vertical Pipe Flow

The Cullender-Smith approach shown in Eqs. 4 - 8 was programmed into an Excel workbook. The workbook was coupled with Visual Basic for Applications (VBA) coding to enable the iterative solutions required to solve the implicit equations. The compressibility factor Z was computed using the Hall-Yarborough solution from Guo and Ghalambor (2012).

2.3.2. Commercial Process Simulator (PSM) for Vertical Pipe Flow

Sandia utilized a commercial oil and gas process simulator model (PSM) to run comparison calculations on selected configurations for dry gas flow in vertical pipes. The purpose of these commercial model runs was to create comparison data to allow for verification that the Sandia models were calculating output (gas flowrates, pressure drops, gas flow velocities, gas density, Z-factor) for vertical pipe flow scenarios that were mathematically correct and matched well with an established commercial simulator. The decision to use Sandia-developed models as opposed to the commercial

model for the large matrix of runs ultimately executed in this study was based on two factors: (i) the commercial simulator did not have a pre-defined reservoir deliverability function, and (ii) setting up flexible, user-defined input and output was important for this work and easier for Sandia to implement using in-house codes rather than developing pre- and post-processors for the commercial PSM.

2.3.3. Combined Pipe and Well Flow Model

A combined pipe and well flow model was programmed into an Excel workbook that coupled the simple well deliverability model expressed in Eq. 15 with the Cullender-Smith vertical pipe flow model shown in Eqs. 4 - 8. A screenshot of the user interface page is shown in Figure 2-3. The model input required the following:

- Well Inner Diameter (in)
- Absolute Roughness (in)
- Well Depth (ft)
- Wellhead Flowing Pressure (psia)
- Wellhead Flowing Temperature (F)
- Bottomhole Temperature (F)
- Reservoir Shut-in Pressure (psia)
- Reservoir (well) Deliverability "C" (mmscfd)
- Reservoir (well) Exponent "n"(dimensionless)
- Gas volumetric flowrate, guess to start the iterations (mmscfd)
- Gas viscosity (cP)
- Gas Formulation Name (text field)
- Pseudocritical Pressure (psia)
- Pseudocritical Temperature (°R)
- Gas Specific Gravity (dimensionless)
- Gas Molecular Weight (lb/lbmole)
- Verification Output Flag (text field)

The screenshot in Figure 2-3 shows the input and output for 20 model runs in a given simulated field of 20 wells, all identical except for well number (row 4) a well-specific "C" or "n" (rows 12, 13) associated with the deliverability of the given well, and initial guess at the gas volumetric flowrate (row 14). Code input comprises the upper half of the screen (rows 4-22), while code output comprises the lower half of the screen (rows 27-39). Additional data output formats were available and selected by user flag (row 22).

	A	B	C	D	E	F	G	H	I	J	K	L	M	N	O	P	Q	R	S	T	U	V
1	**Cullender-Smith Solver**																					
2																						
3	**Input**																					
4	*Variable*	*Units*	*1*	*2*	*3*	*4*	*5*	*6*	*7*	*8*	*9*	*10*	*11*	*12*	*13*	*14*	*15*	*16*	*17*	*18*	*19*	*20*
5	Well Inner Diameter	in	2.441	2.441	2.441	2.441	2.441	2.441	2.441	2.441	2.441	2.441	2.441	2.441	2.441	2.441	2.441	2.441	2.441	2.441	2.441	2.441
6	Absolute Roughness	in	0.0006	0.0006	0.0006	0.0006	0.0006	0.0006	0.0006	0.0006	0.0006	0.0006	0.0006	0.0006	0.0006	0.0006	0.0006	0.0006	0.0006	0.0006	0.0006	0.0006
7	Well Depth	ft	1800	1800	1800	1800	1800	1800	1800	1800	1800	1800	1800	1800	1800	1800	1800	1800	1800	1800	1800	1800
8	Wellhead flowing pressure	psia	350	350	350	350	350	350	350	350	350	350	350	350	350	350	350	350	350	350	350	350
9	Wellhead flowing temperature	F	80	80	80	80	80	80	80	80	80	80	80	80	80	80	80	80	80	80	80	80
10	Bottomhole Temperature	F	98	98	98	98	98	98	98	98	98	98	98	98	98	98	98	98	98	98	98	98
11	Reservoir Shut-in Pressure	Psia	**400**	**400**	**400**	**400**	**400**	**400**	**400**	**400**	**400**	**400**	**400**	**400**	**400**	**400**	**400**	**400**	**400**	**400**	**400**	**400**
12	Reservoir Deliverability C		6.78E-05	4.46E-05	3.09E-05	2.75E-05	2.49E-05	2.32E-05	2.12E-05	1.90E-05	1.79E-05	1.67E-05	1.52E-05	1.37E-05	1.25E-05	1.04E-05	9.14E-06	8.10E-06	6.83E-06	5.67E-06	8.02E-06	8.10E-06
13	Reservoir exponent n		1	1	1	1	1	1	1	1	1	1	1	1	1	1	1	1	1	1	0.95	0.9
14	Gas volumetric flowrate (guess	mmscfd	1.8335	1.21436	0.8417	0.74976	0.67956	0.6318	0.57842	0.51713	0.48756	0.45565	0.41522	0.3731	0.34225	0.28266	0.24902	0.22103	0.1866	0.15485	0.13128	0.07954
15	Gas viscosity	cP	0.012	0.012	0.012	0.012	0.012	0.012	0.012	0.012	0.012	0.012	0.012	0.012	0.012	0.012	0.012	0.012	0.012	0.012	0.012	0.012
16	Gas Formulation Name		NG-4	NG-5	NG-6	NG-7	NG-8	NG-9	NG-10	NG-11	NG-12	NG-13	NG-14	NG-15	NG-16	NG-17	NG-18	NG-19	NG-20	NG-21	NG-22	NG-23
17	Pseudocritical Pressure	psia	673.541	673.541	673.541	673.541	673.541	673.541	673.541	673.541	673.541	673.541	673.541	673.541	673.541	673.541	673.541	673.541	673.541	673.541	673.541	673.541
18	Pseudocritical Temperature	R	362.911	362.911	362.911	362.911	362.911	362.911	362.911	362.911	362.911	362.911	362.911	362.911	362.911	362.911	362.911	362.911	362.911	362.911	362.911	362.911
19	Gas Specific Gravity	-	0.6159	0.6159	0.6159	0.6159	0.6159	0.6159	0.6159	0.6159	0.6159	0.6159	0.6159	0.6159	0.6159	0.6159	0.6159	0.6159	0.6159	0.6159	0.6159	0.6159
20	Molecular Weight	lb/lb-mole	17.8426	17.8426	17.8426	17.8426	17.8426	17.8426	17.8426	17.8426	17.8426	17.8426	17.8426	17.8426	17.8426	17.8426	17.8426	17.8426	17.8426	17.8426	17.8426	17.8426
21																						
22	Verification Output Flag		2	2	2	2	2	2	2	2	2	2	2	2	2	2	2	2	2	2	2	2
23																						
24			1.83	1.21	0.84	0.75	0.68	0.63	0.58	0.52	0.49	0.46	0.42	0.37	0.34	0.28	0.25	0.22	0.19	0.15	0.13	0.08
25	**Output**		(0.37)	(0.14)	(0.05)	(0.04)	(0.03)	(0.02)	(0.02)	(0.01)	(0.01)	(0.01)	(0.01)	(0.01)	(0.00)	(0.00)	(0.00)	(0.00)	(0.00)	(0.00)	-	-
26	Run ID																					
27	Calculated gas flowrate	mmscfd	1.460	1.076	0.789	0.711	0.650	0.609	0.560	0.503	0.476	0.446	0.408	0.367	0.338	0.280	0.248	0.220	0.186	0.154	0.131	0.080
28	P_{WHF}	psia	350	350	350	350	350	350	350	350	350	350	350	350	350	350	350	350	350	350	350	350
29	P_{BHF}	psia	372	369	367	366	366	366	366	365	365	365	365	365	365	365	365	364	364	364	364	364
30	Reservoir Pressure	psia	400	400	400	400	400	400	400	400	400	400	400	400	400	400	400	400	400	400	400	400
31	T_{WHF}	F	80	80	80	80	80	80	80	80	80	80	80	80	80	80	80	80	80	80	80	80
32	T_{BHF}	F	98	98	98	98	98	98	98	98	98	98	98	98	98	98	98	98	98	98	98	98
33	Reservoir C		6.78E-05	4.46E-05	3.09E-05	2.75E-05	2.49E-05	2.32E-05	2.12E-05	1.90E-05	1.79E-05	1.67E-05	1.52E-05	1.37E-05	1.25E-05	1.04E-05	9.14E-06	8.10E-06	6.83E-06	5.67E-06	8.02E-06	8.10E-06
34	Reservoir n		1	1	1	1	1	1	1	1	1	1	1	1	1	1	1	1	1	1	0.95	0.9
35	Well Internal Diameter	in	2.441	2.441	2.441	2.441	2.441	2.441	2.441	2.441	2.441	2.441	2.441	2.441	2.441	2.441	2.441	2.441	2.441	2.441	2.441	2.441
36	Friction Factor	-	0.01569	0.01605	0.0165	0.01667	0.01683	0.01695	0.01711	0.01732	0.01744	0.01758	0.01778	0.01803	0.01824	0.01875	0.0191	0.01947	0.02003	0.02069	0.02132	0.02356
37	Static Head	psi	15.8027	15.8027	15.8027	15.8027	15.8027	15.8027	15.8027	15.8027	15.8027	15.8027	15.8027	15.8027	15.8027	15.8027	15.8027	15.8027	15.8027	15.8027	15.8027	15.8027
38	Static Wellhead Pressure	psia	384.197	384.197	384.197	384.197	384.197	384.197	384.197	384.197	384.197	384.197	384.197	384.197	384.197	384.197	384.197	384.197	384.197	384.197	384.197	384.197
39	dP^2	psi^2	25107.6	25107.6	25107.6	25107.6	25107.6	25107.6	25107.6	25107.6	25107.6	25107.6	25107.6	25107.6	25107.6	25107.6	25107.6	25107.6	25107.6	25107.6	25107.6	25107.6

Figure 2-3. Screenshot of combined pipe and well flow model showing 20 model runs for a given well field.

This page left blank

3. MODEL VERIFICATION AND VALIDATION

Model verification was performed to assure that the numerical models developed here solved the basic mathematical problems correctly. Model validation was performed to assess how well the numerical models simulated real-world systems.

3.1. Vertical Pipe Flow Model Verification

3.1.1. Verification Cases

Two simple cases were set up as summarized in in Table 3-1 for the purpose of verifying performance of the Sandia in-house vertical pipe flow numerical models against the commercial process simulator model. Case 1 was run for a 2,000 ft. vertical pipe with 100 psi pressure difference imposed, and Case 2 was run for a 6,000 ft. vertical pipe with 500 psi pressure difference imposed.

Table 3-1. Summary of test cases for vertical pipe flow verification

Case Number	1	2
Pipe Length [ft]	2,000	6,000
Pressure Difference [psi]	100	500
Pipe Roughness [in]	0.0006	0.0006
Gas Viscosity [cp]	0.012	0.012
Gas Gravity [-]	0.62	0.62

3.1.2. Verification Results

Model results for the two verification cases identified above were compared for selected key output variables including volumetric flowrate [MMSCFD], mass flowrate [lb/hr], and gas velocity at the wellhead (ft/sec). Results for Case 1 are shown in Figure 3-1 through Figure 3-3, and results for Case 2 are shown in Figure 3-4 through Figure 3-6. Each column chart shows a particular analysis variable as a function of model type (indicated in legend), and pipe inner diameter, listed on the horizontal axis. For a given analysis variable and pipe inner diameter, the models tend to compare closely, though flowrate for the Weymouth model is consistently lower than the others. For Case 1, flowrates (volumetric and mass) for the Darcy and Cullender-Smith compare to within 1% of the PSM, and are between 13-17% lower for the Weymouth model. Case 1 gas velocity at the wellhead is 10-17% higher than the PSM for Darcy and Cullender-Smith, while a little closer for Weymouth. For Case 2, results are similarly agreeable with the PSM, where Darcy and Cullender-Smith agree with the PSM within 3% for flowrates, and Weymouth flowrate is about 10-14% lower than the PSM. Case 2 gas velocity at the wellhead for all models, all tubing diameters, compare within 7% of the PSM.

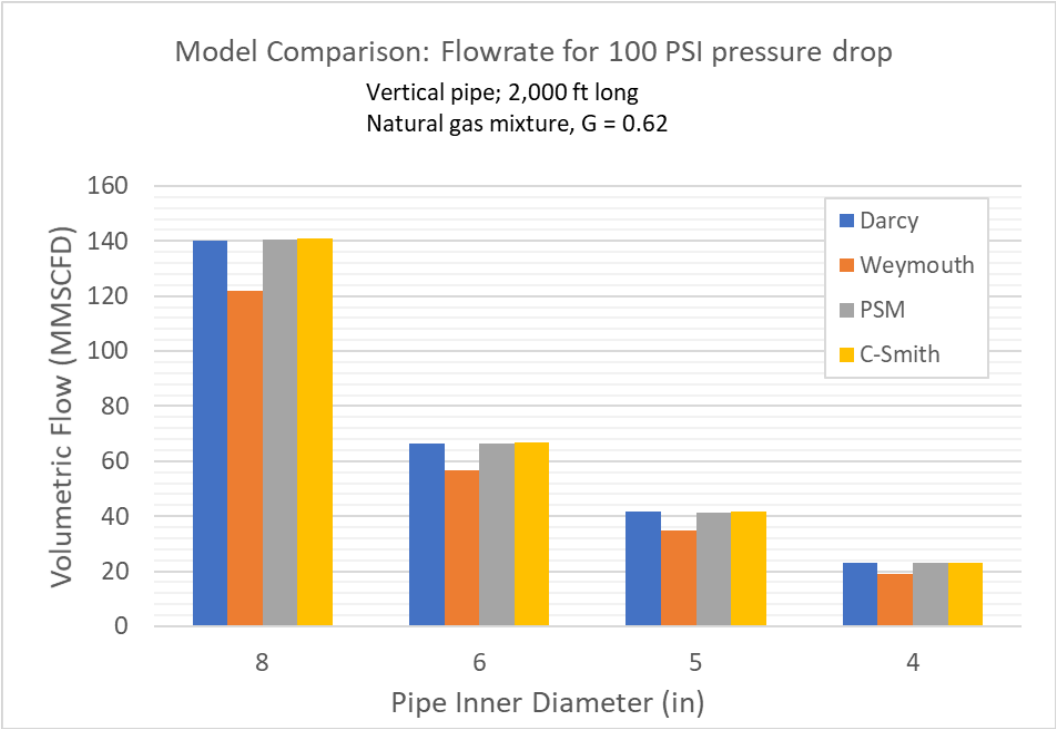

Figure 3-1. Case 1 model verification results, volumetric flowrate with pipe inner diameter.

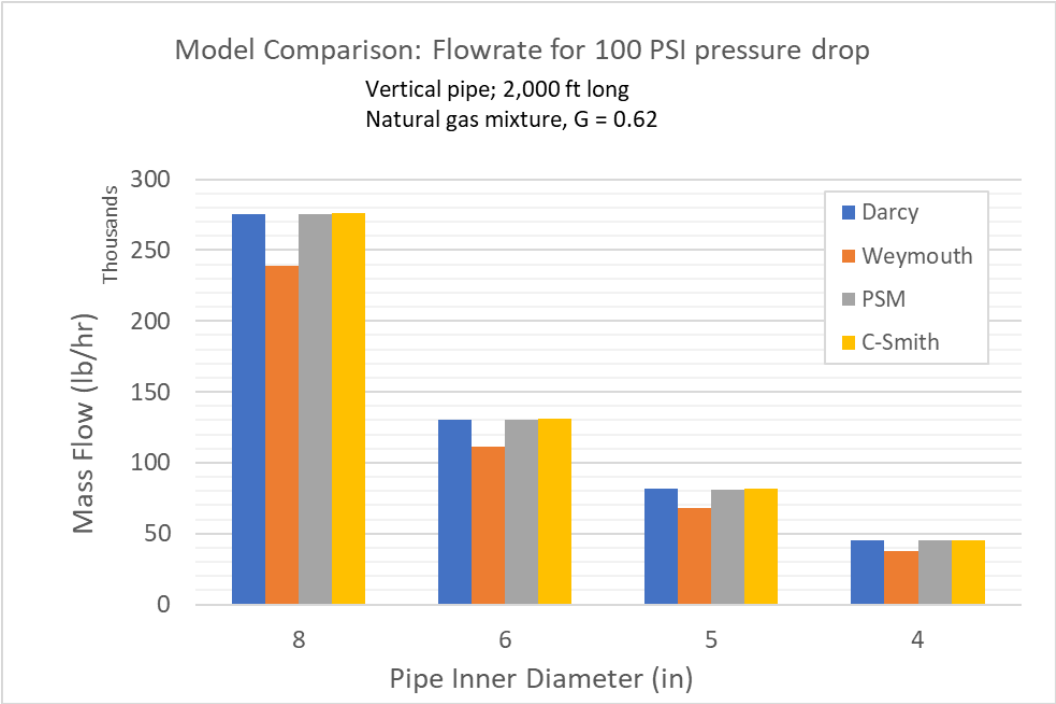

Figure 3-2. Case 1 model verification results, mass flowrate with pipe inner diameter.

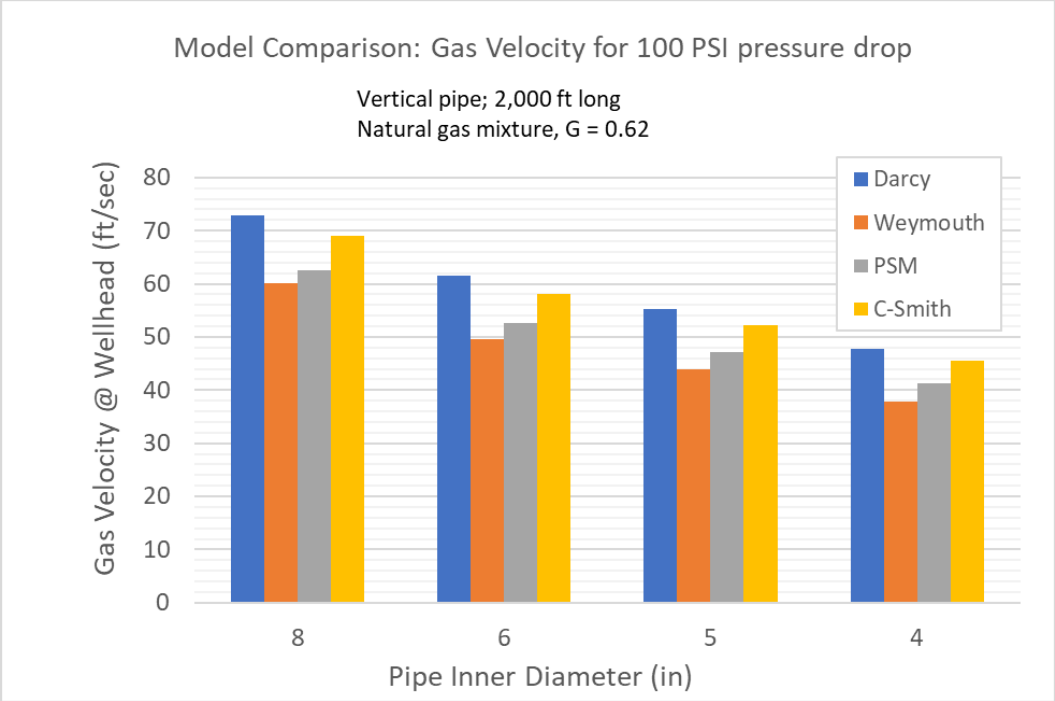

Figure 3-3. Case 1 model verification results, gas velocity at wellhead with pipe inner diameter.

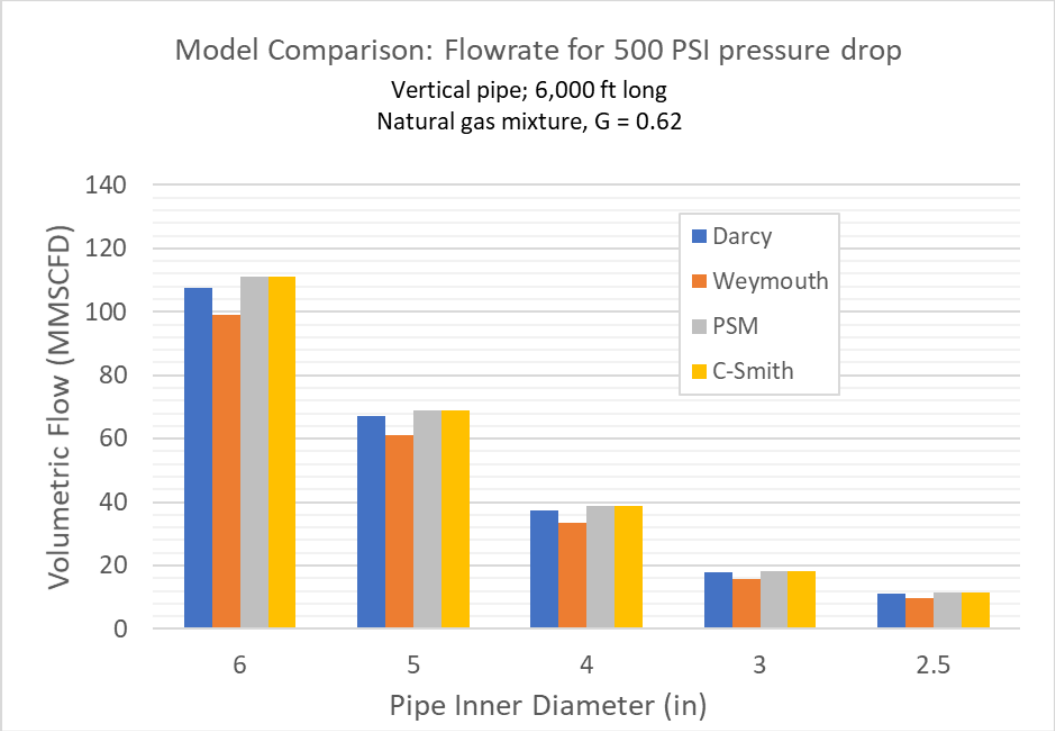

Figure 3-4. Case 2 model verification results, volumetric flowrate with pipe inner diameter

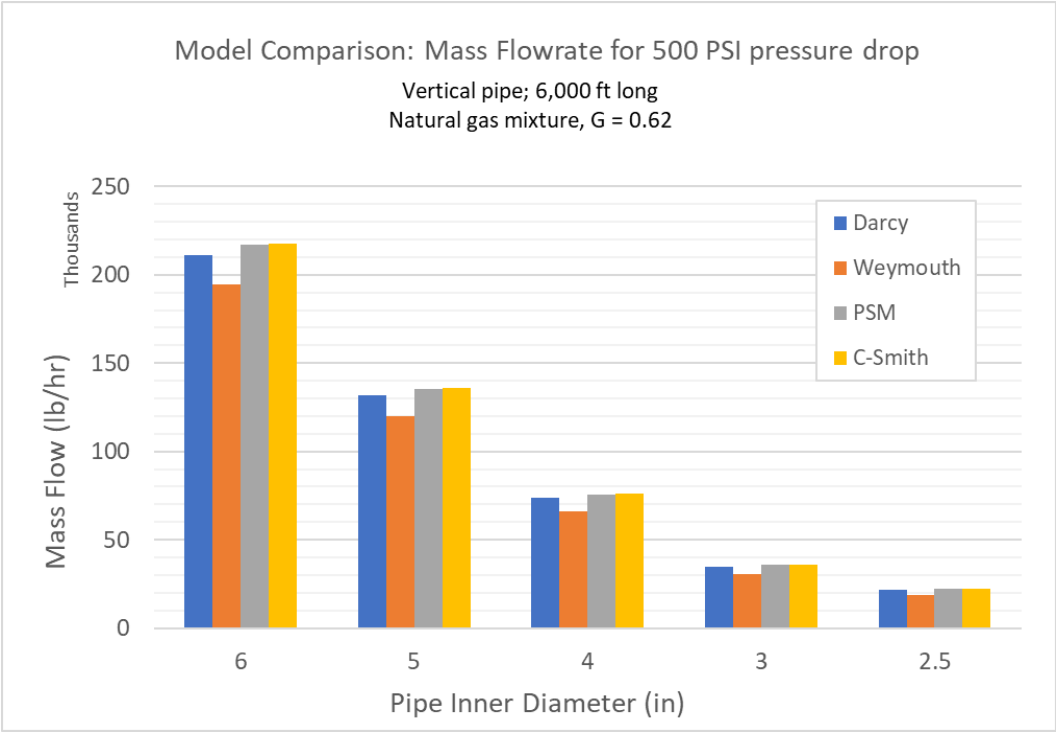

Figure 3-5. Case 2 model verification results, mass flowrate with pipe inner diameter

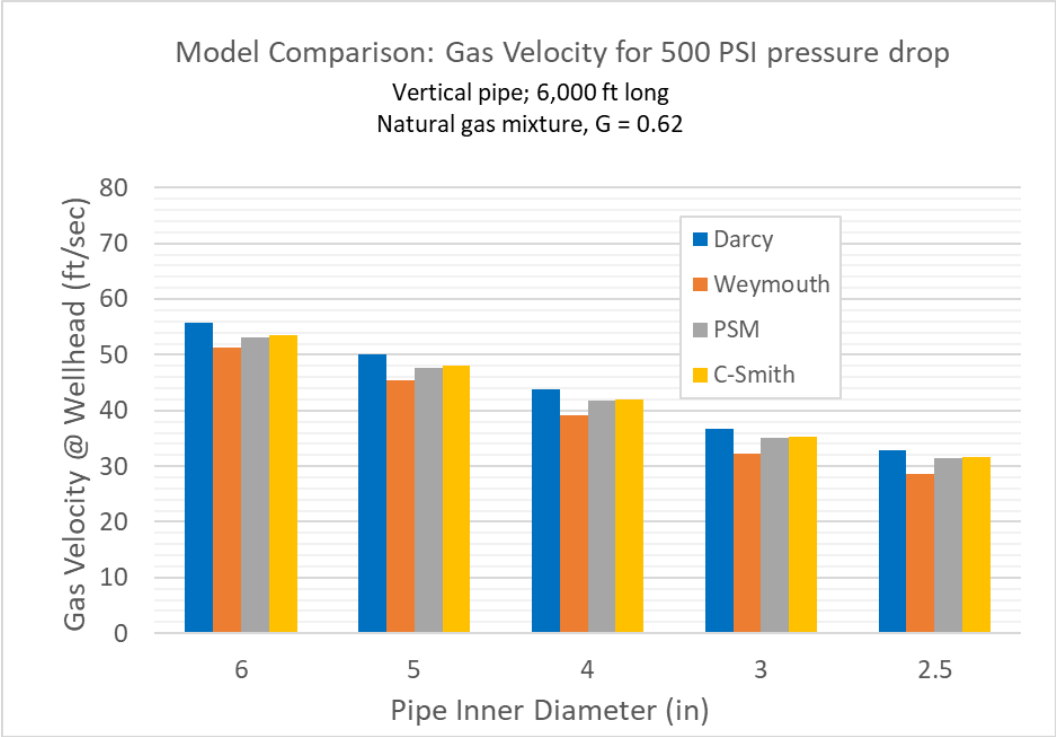

Figure 3-6. Case 2 model verification results, gas velocity at wellhead with pipe inner diameter

Recall the main purpose of this modeling study is to understand the effects of reducing tubing inner diameter on flowrate. To this end, all of the numerical models show nearly the same level of relative reduction in volumetric flowrate with tubing inner diameter, as illustrated in Figure 3-7, and could potentially all be used moving forward, expecting nearly indistinguishable results as a function of model choice.

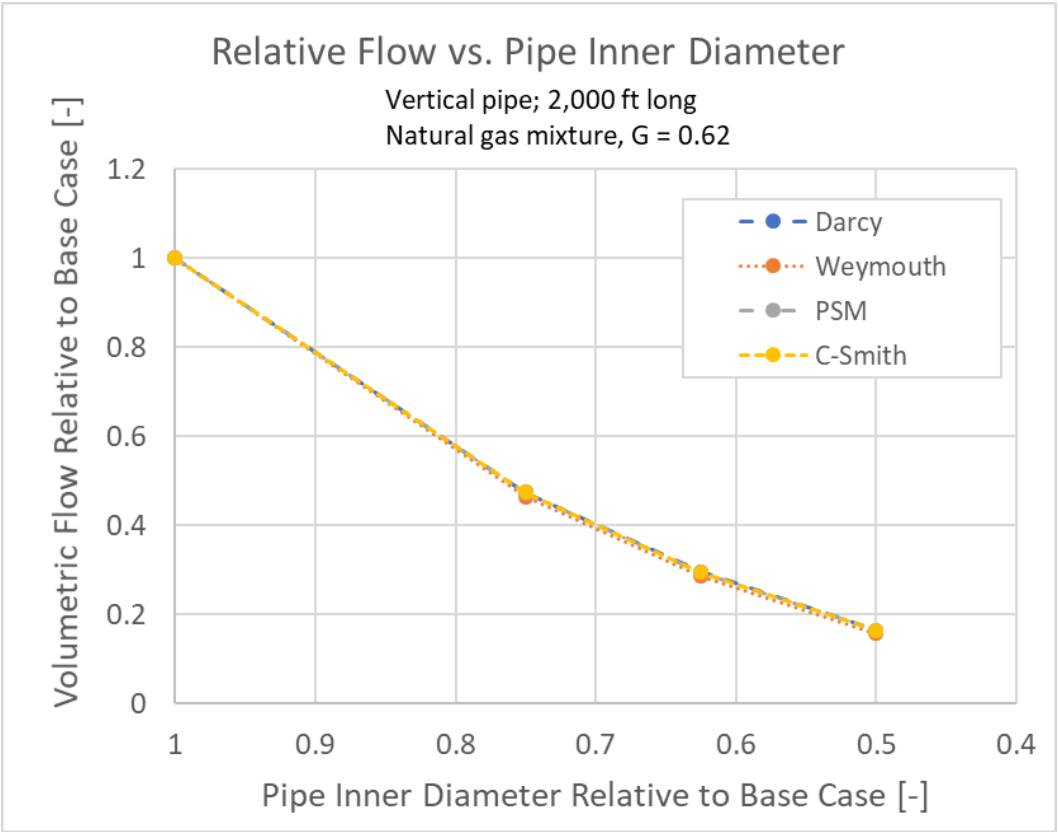

Figure 3-7. Case 1 relative changes in volumetric flow with reductions in pipe inner diameter.

3.1.3. Summary Comments on Verification Results

The model verification results show that the vertical pipe flow models developed from the Darcy, Weymouth, and Cullender-Smith equations and coded by Sandia into Excel workbooks return flowrates and gas velocities that are comparable to a commercial oil & gas process simulator model (PSM). While some model-to-model differences appear, like the Weymouth model flowrates and gas velocities sitting a little lower than the rest, in the judgement of the authors, the models compare well enough for the purposes of this work, which is to show relative effects of tubing size reductions on flowrates. To this end, when comparing each models' prediction of relative reduction in flowrate for a given pipe size reduction, the models are nearly indistinguishable as shown in Figure 3-7 and the ultimate results of this study do not depend on the choice of vertical pipe flow model among the options investigated.

3.2. Combined Pipe and Well Flow Model Validation

The combined pipe and well flow numerical model from section 2.3.3 was run with field data made available to Sandia to validate the model's ability to predict flowrates and pressure drops against actual field results. This step is important to building confidence in the numerical model's ability to predict real system behavior due to operational changes such as reducing tubing diameter or changing wellhead or reservoir pressures.

Well test data for Field "A" were provided that included flowing wellhead pressures, reservoir shut-in pressures, well deliverability parameters C and n, and well inner diameters for four wells, each tested at several flowing wellhead pressures for 4 wells comprising 13 tests. No data on gas gravity, well depth or roughness were given. The given data were imported into the combined model and some trial runs were implemented to find gravity, depth and roughness ranges that returned model output that were comparable to the observed field pressures and flowrates. Three different internal well diameters, ID = 3.476, 2.992, and 2.441 inches were represented in this group.

A comparison of the field data and model output is shown in Figure 3-8. Field data are shown in open symbols connected by dashed lines, while model results are shown in solid symbols connected by solid lines. The model-calculated volumetric gas flowrate compares to within 10% of the field data values for 10 of the 13 points compared, and within 10-30% for the other three points compared.

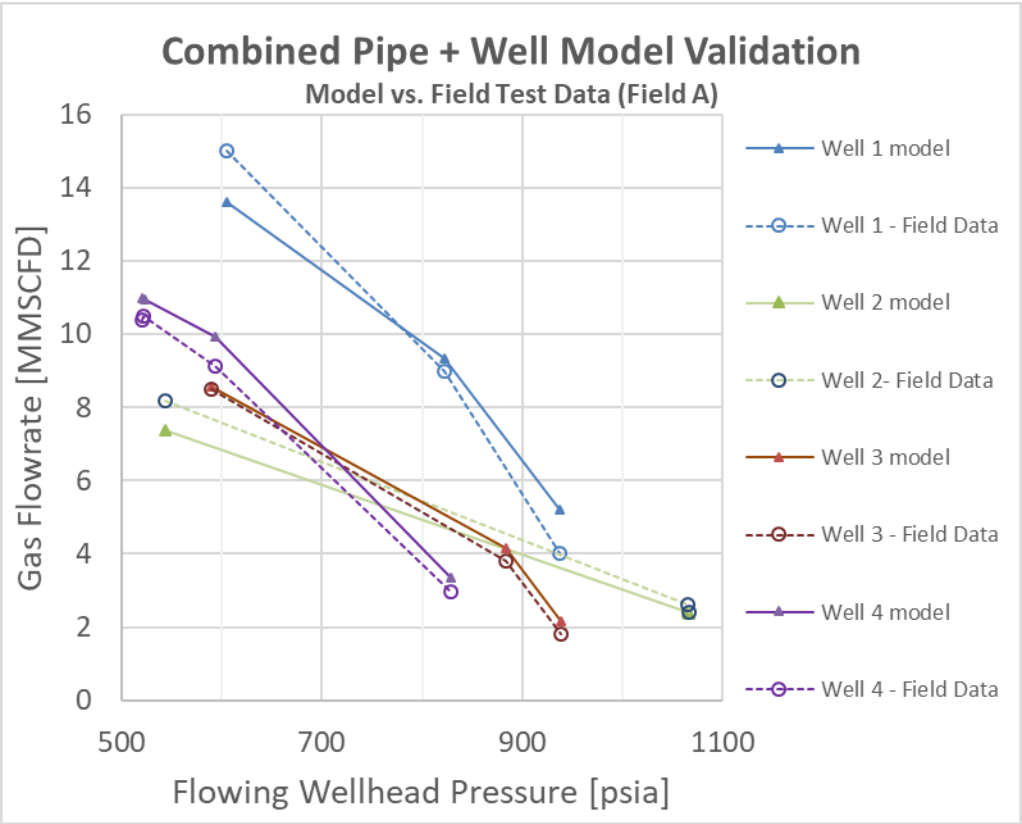

Figure 3-8. Model overlay with field data for four wells to validate model performance.

3.2.1. Summary Comments on Combined Model Validation

The field data-numerical model comparison shown above in Figure 3-8 indicates that for most conditions, the model was able to predict flowrate within 10% of what was observed in the field, and for all cases considered, within 30% of what was observed. The authors judge this as sufficient performance to meet the objectives of the work, which is to evaluate the effects of reduced tubing diameter on volumetric flowrate. The well depths, flowrates, and internal diameters in this example are consistent with the parameter range explored in this study.

This page left blank

4. SIMULATION CASES

This section outlines the simulation cases that were explored in this work. Simulation cases represent potential outcomes, in the form of deliverability reductions within a field, that result from reductions in tubing diameters. A field, as defined here, comprises a single underground gas storage reservoir and numerous wells under control of a single operator. The wells connect a reservoir to the surface piping, and deliverability of the field is ultimately determined by taking the sum of deliverability over all of the wells in the field (recall Eq. 16). Reductions in tubing size will occur at the well level, so the realization of the change in tubing diameters appears in the well equations, creating a tubing effect. In addition to the tubing effect, each well in a field can exhibit its own unique deliverability as controlled by the local porosity, permeability, formation thickness, and interface properties where the bottom of the well makes direct contact with the reservoir through the completion zone, quantified by parameters "C" and "n" from Eq. 15. Such well-to-well differences are common and are considered here in the overall configuration of simulation cases.

4.1. Deliverability within a Field

Deliverability differences among wells within a field are possible in spite of sharing relatively uniform boundary conditions like reservoir shut-in pressure, wellhead flowing pressure, and well dimensions including depth and inner diameter. Examples of the range of well deliverabilities in real depleted reservoir storage fields are shown in Figure 4-1 through Figure 4-4. The relative well deliverabilities were drawn from actual historical well test data from several storage fields in North America, though the average flowrates and associated depths and pressures were adjusted by the authors for the purpose of fitting with the current study. Deliverability distribution for Field A, shown in Figure 4-1, is the same field as examined in the combined model validation exercise in section 3.2, run at uniform boundary conditions here across all wells with dP^2 = 500,000 psi^2.

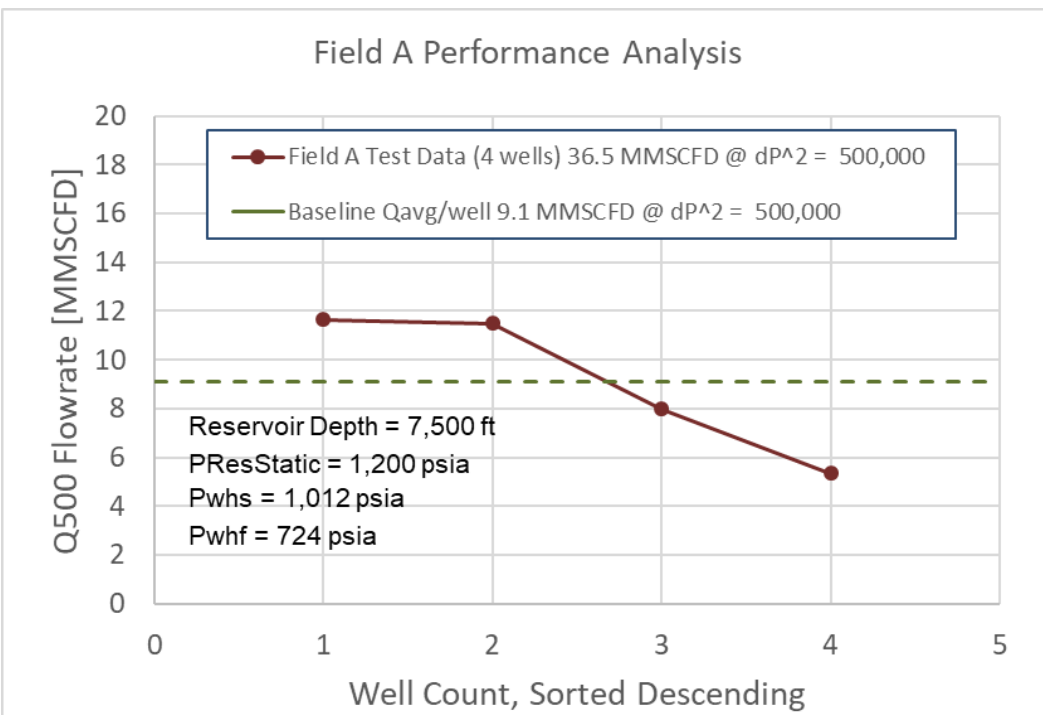

Figure 4-1. Deliverability distribution for field "A" comprising 4 wells with $Q_{avg/well}$ = 9.1 MMSCFD @ dP^2 = 500,000 psi^2.

Three other fields with many more wells are shown in Figure 4-2 through Figure 4-4. The blue points on each figure represent the deliverability of each individual well given the dP^2 indicated on each figure. A field-level $Q_{avg/well}$ is also given and shown as a dashed green line. The important takeaway from these figures is that diferent wells within a given field can exhibit notably different flowrates, with some much higher, and some much lower than the average. For example, in Field C, the highest-delivering well at 2.1 MMSCFD is about 4× the average at 0.5 MMSCFD. In the same field, there are wells that produce as little as 0.05 MMSCFD or about 1/10× the field average per well.

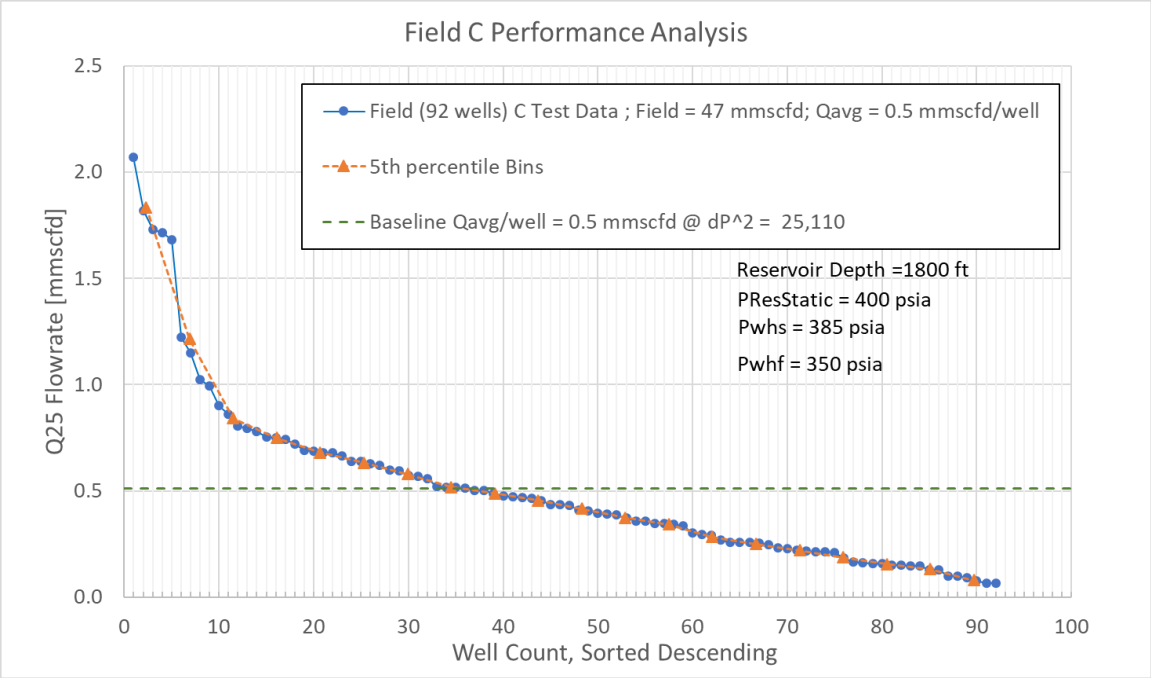

Figure 4-2. Deliverability distribution for field "C" comprising 92 wells based on field data scaled by the authors to yield a Qavg/well = 0.5 MMSCFD.

Field "G" in Figure 4-3 shows a tighter and more linear distribution of flowrates around the avererage. The highest-delivering well at 4.4 MMSCFD is 1.8× the average at 2.4 MMSCFD, while the lowest delivering well in that field sits at 0.5 MMSCFD, about 1/5 the average per well. Another example, Field "D" in Figure 4-4 shows a distrbution similar to Field C, though there of some very low-end wells delivering at less than 0.1 MMSCFD. The implications of these different distrbutions will come clearer as the analysis results are presented. Low-deliverability wells tend to be limted by local reservoir/well interface characteristics, and will tend to show less sensitivity to changes in tubing diameter. High-deliverability wells tend to be limited by tubing size, and can show more marked sensitivity to any new flow restrictions such as reduced tubing size.

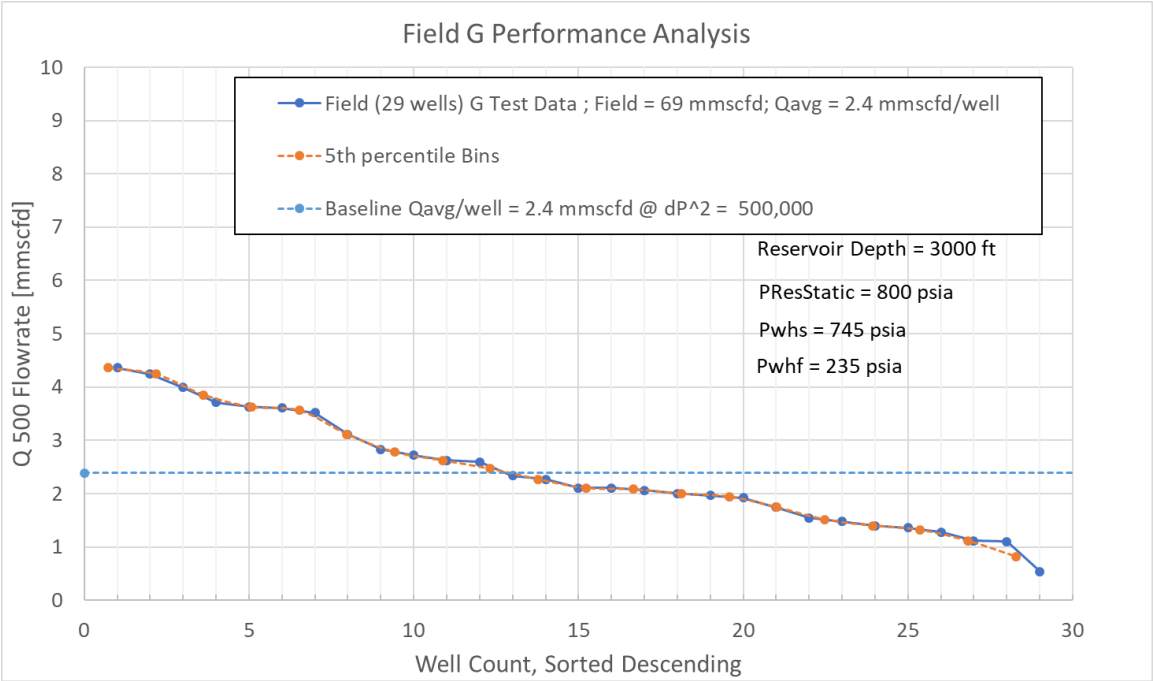

Figure 4-3. Deliverability distribution for field "G" comprising 29 wells based on field data scaled by the authors to yield a $Q_{avg/well}$ = 2.4 MMSCFD.

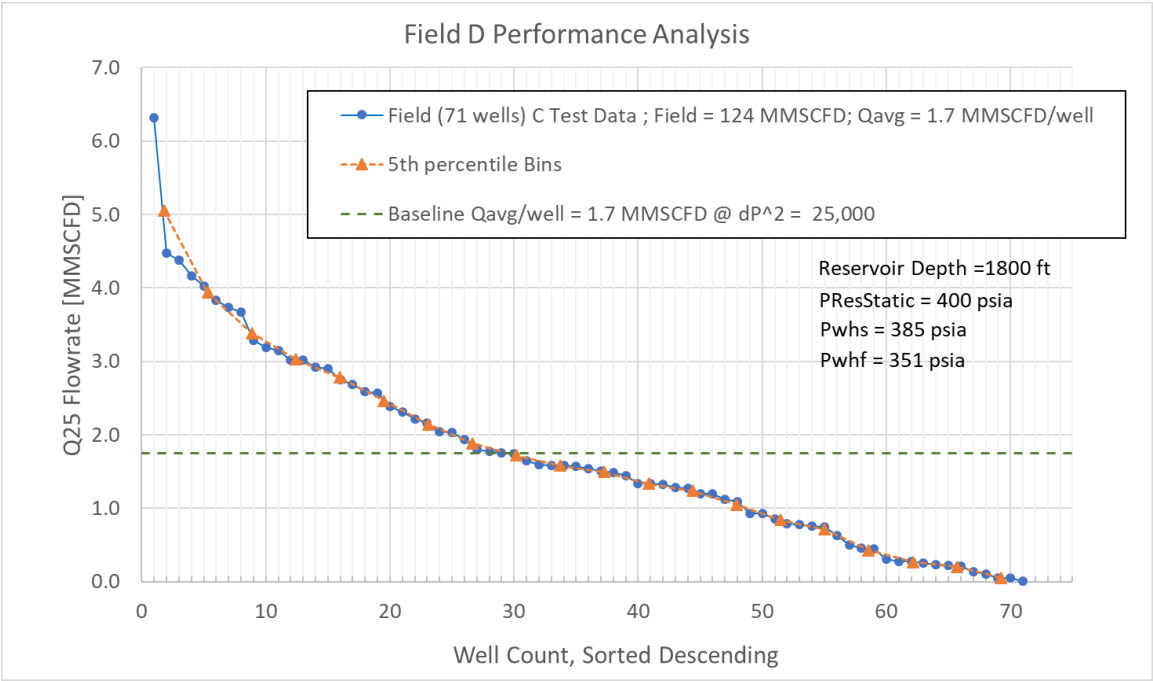

Figure 4-4. Deliverability distribution for field "D" comprising 71 wells based on field data scaled by the authors to yield a $Q_{avg/well}$ = 1.7 MMSCFD.

4.2. Fields, Wells, and Working Gas Capacities Across the U.S.

The 2016-2017 Survey of Underground Storage of Natural Gas in the United States and Canada (AGA 2017), published by the American Gas Association (AGA) was used as background for this analysis. According to the AGA data, as of 2017 there were 359 aquifer and depleted reservoir storage fields in the U.S. comprising 13,909 wells and 4.13×10^6 MMSCF (4.13 TCF) of working gas capacity. The data were subdivided into average deliverability bins, denoted as $Q_{avg/well}$, computed by taking the stated Working Gas Capacity for each field and dividing it by the number of wells in that field and then by 90 (days) for an estimate of average MMSCFD/well for a given field that would be required to deliver the working gas capacity of that field to a customer over a 90-day period, which is a typical duration of a peak demand contract period for a facility operator. A graphical representation of these data is given in Figure 4-5, where the horizontal axis represents $Q_{avg/well}$ bins from 0.5 up to the maximum of 46.5 MMSCFD.

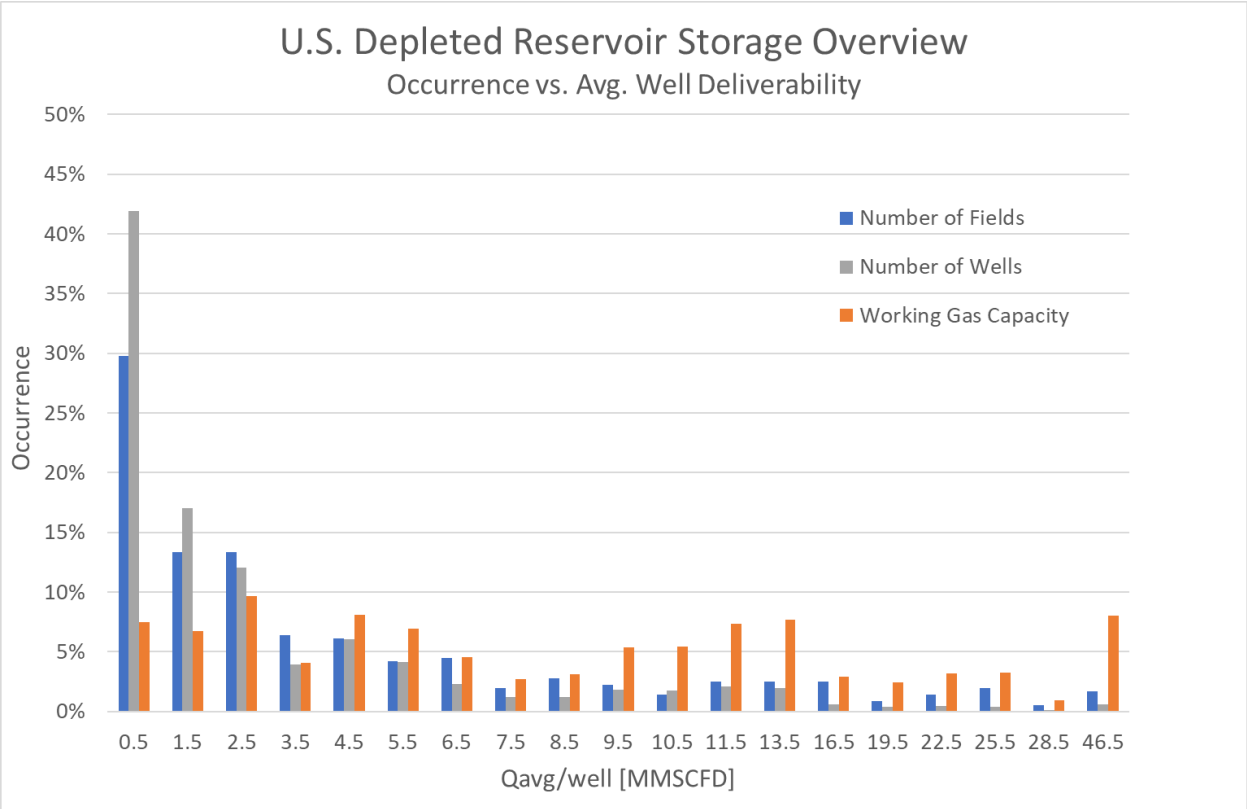

Figure 4-5. Overview of U.S. Depleted Reservoir Storage showing relative occurrence of number of fields, number of wells, and working gas capacity versus average deliverability per well for all reported fields in 2016-2017. Data from AGA (2017).

4.3. Simulation Cases

The scope of this study is to simulate possible outcomes for tubing reductions over most of the expected pressure, depth, and deliverability ranges observed in U.S. gas reservoir storage. There may be outlier cases, but this work is intended to give insight for the effects on most wells in most fields for most operators. As such, simulation cases were developed around the occurrence data defined from the AGA report and illustrated in Figure 4-5. Two fields, with deliverability distributions modeled after field "C" with a distribution shaped like a hockey stick, and field "G" with a nearly

linear distribution, both introduced in section 4.1, were simulated through a selected range of average deliverability bins, as illustrated in Figure 4-6. For a given deliverability bin, the average reservoir depth and static reservoir pressure were determined from representative values out of the AGA data that corresponded to those bins.

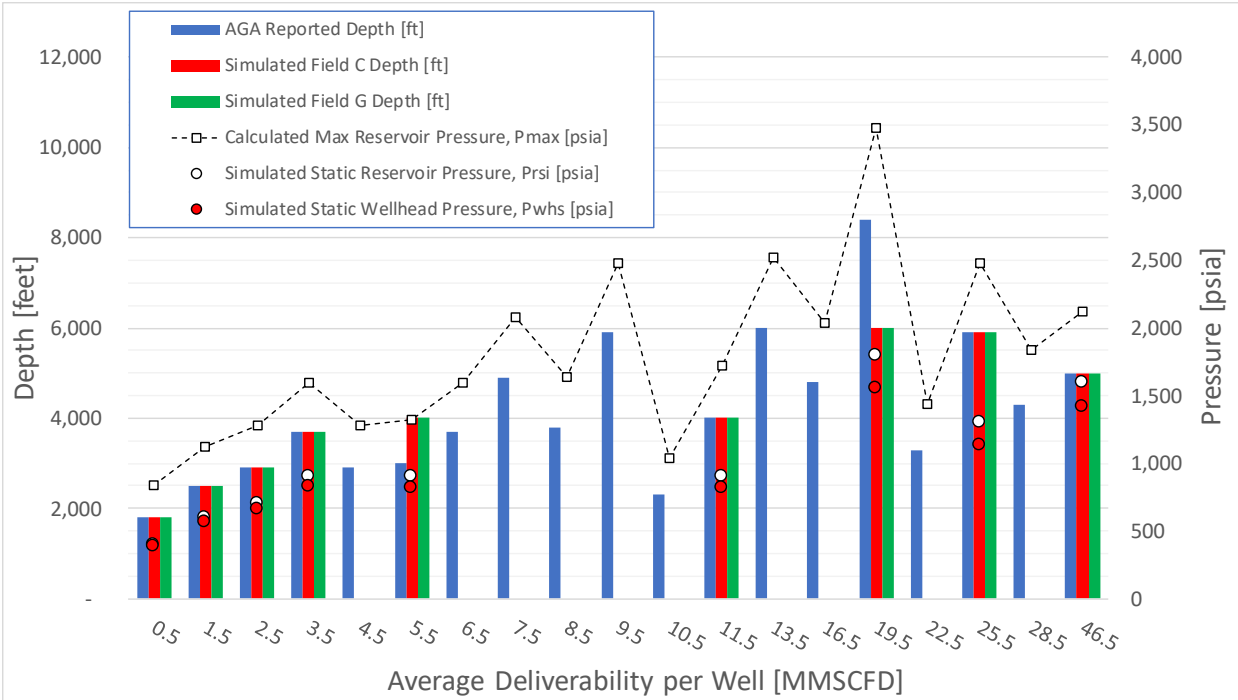

Figure 4-6. Overview of simulation cases (red and green bars) run in association with the AGA data (blue bars) on average deliverability per well in U.S. gas storage fields.

To determine representative depth for a given deliverability bin, a weighted average was computed from the AGA data by taking each well and multiplying it by the depth of the field it is in and then dividing by the total number of wells in that bin. To determine maximum reservoir pressure, the AGA data were plotted as pressure versus depth in Figure 4-7, and a straight line was fitted to the data yielding the best fit equation shown on the plot. From there, a simple equation for maximum reservoir pressure was derived as shown in Eq. 19:

$$P_{max} = 0.4 \times D + 120 \tag{19}$$

Where:

- P_{max} = maximum reservoir pressure, psia
- D = reservoir depth, ft

Maximum reservoir pressure must be converted to a static reservoir shut-in pressure relevant to a field operator for meeting deliverability requirements throughout the duration of a typical contract. This static reservoir pressure will be used in modeling to represent the P_{RSI} denoted in the well deliverability equation (Eq. 15) and serves as direct input to the combined pipe and well flow model. The full pressure, P_{max}, may only be available to the operator on the first day of drawdown when the reservoir is full. A more practical and conservative shut-in pressure is needed that represents what is achievable when the working gas inventory has been largely exhausted and mainly cushion gas remains.

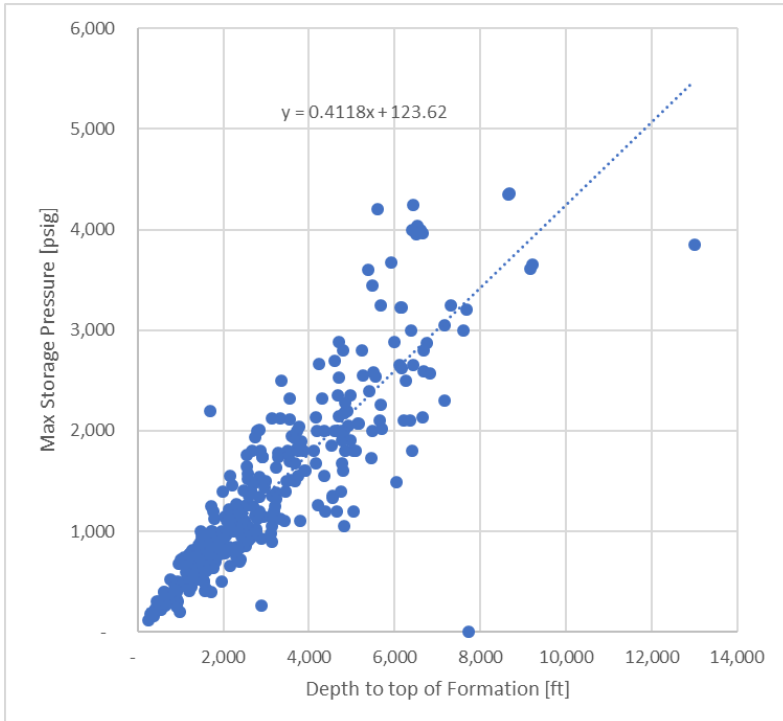

Figure 4-7. Plot of P_{max} versus D as interpreted from AGA (2017). Linear fit equation is shown on plot.

The authors assumed that about half of the total inventory in a given reservoir is working gas (V_{wg}), while the other half is cushion gas (V_{cg}), consistent with the range of typical cushion gas (40-70% of total reservoir capacity) cited in Flanigan (1995). In addition, according to an industry contact, deliverability guarantees are typically specified to about 20-30% (X) of working gas inventory, so a pressure correction to P_{RSI} could be applied as $(1/(1-X))$. Adding one more consideration, a real gas reservoir may not drain evenly and may leave gas held up in poorly-drained areas due to an efficiency factor we will call Y. The effect would be a slightly reduced pressure than expected at the wellhead, say $Y = 0.85$. Taking these three considerations, the resulting P_{RSI} was computed as follows:

$$P_{RSI} = P_{max}\left(\frac{V_{cg}}{V_{wg} + V_{cg}}\right)\left(\frac{1}{1-X}\right)Y \tag{20}$$

Where:

- P_{max} = maximum reservoir pressure, psia (see Eq. 19
- V_{cg} = Volume of cushion gas, MMSCF
- V_{wg} = Volume of working gas, MMSCF
- X = deliverability guarantee parameter, volume fraction (0.2 used here)
- Y = Drainage efficiency factor, (0.85 used here)

For the assumptions taken here, $P_{RSI} = P_{max} \times 0.53$. As used in the modeling exercise, P_{RSI} was then rounded to the nearest 100 psi.

Other parameter settings included:

- ϵ = 0.0006 in
- T_{WHF} = 80°F
- $T_{BHF} = T_{WHF}$ + reservoir depth (ft) × 0.01 deg F/ft

4.3.1. Run Matrices

The run matrices for this modeling study are given in Table 4-1 through Table 4-4. Taking Table 4-1 as a starting point, for a given field of wells, Field C (hockey stick distribution) in this case, the model was run for a selected $Q_{avg/well}$ three times: once for the baseline well inner diameter (Base ID), and then two more times for liner sizes (Liner 1 ID, Liner 2 ID) that would potentially fit inside the baseline well. Liner sizes correspond to those listed in a readily-available commercial catalog (USS 2014). While the largest liner that would fit into an existing production casing would be the logical choice for an operator, many factors associated with years of service may lead to deformation of the production casing to create an effective ID that is smaller than the nominal ID. As such, there may be a practical need in the field to use a smaller liner size than anticipated simply by nominal ID of the production casing. Additional model runs at a second liner size also provide a clearer picture of the relationships between well diameter and deliverability for relatively low effort once the model is running.

Seven $Q_{avg/well}$ bins, from 0.5 through 19.5 MMSCFD, were modeled in this fashion. For Field C, the maximum $Q_{avg/well}$ bin at Base ID = 4.95" that would be plausible given the likely operational conditions (Depth, P_{RSI}, P_{WHF}) was $Q_{avg/well}$ = 19.5 MMSCFD. From there, a larger baseline production casing size of Base ID = 6.276" was required. As such, another series of four $Q_{avg/well}$ bins was run with the larger Base ID of 6.276", represented by the bottom four rows in Table 4-1. A similar process was followed using Field G (linear distribution), as summarized in Table 4-2.

An additional series was constructed to explore the effects of reservoir/well depth on well deliverability for a few selected configurations as summarized in Table 4-3. Reviewing Table 4-3 exploring depth effects, for the 5.5" OD (4.95" ID) base case, two $Q_{avg/well}$ bins were simulated, namely 0.5 and 3.5 MMSCFD. For the 7" OD base case (6.276" ID), $Q_{avg/well}$ bins of 25.5 and 46.5 MMSCFD were simulated. Modeling results for all of these cases are discussed below in Chapter 5.

A final series was run to simulate effects of reservoir shut-in pressure (P_{RSI}) for selected configurations as summarized in Table 4-4. For the 5.5" OD (4.95" ID) base case, two $Q_{avg/well}$ bins were simulated, namely 3.5 and 11.5 MMSCFD, with four pressures simulated for each case from P_{max} down to a practical minimum of 900 psi. This distinction is relevant because a reservoir is potentially operated over a wide range of pressures from effectively full inventory at P_{max} to effectively empty at about half P_{max} with only cushion gas. Such pressure differences could, in turn, affect the sensitivity of the reservoir deliverability to liner additions. Modeling results for all of these cases are presented in section 5.

Table 4-1. Run matrix for Field C (hockey stick distribution) across $Q_{avg/well}$ bins for 5.5 and 7-in OD base casing size.

Qavg/well [MMSCFD]	Depth [ft]	P_{RSI} [psia]	P_{WHS}^2-P_{WHF}^2 [psi^2]	Base OD [in]	Base ID [in]	Liner 1 OD [in]	Liner 1 ID [in]	Liner 2 OD [in]	Liner 2 ID [in]
0.5	1,800	400	25,000	5.5	4.95	3.5	2.992	2.875	2.441
1.5	2,500	600	100,000	5.5	4.95	3.5	2.992	2.875	2.441
2.5	2,900	700	250,000	5.5	4.95	3.5	2.992	2.875	2.441
3.5	3,700	900	250,000	5.5	4.95	3.5	2.992	2.875	2.441
5.5	4,000	900	500,000	5.5	4.95	3.5	2.992	2.875	2.441
11.5	4,000	900	500,000	5.5	4.95	3.5	2.992	2.875	2.441
19.5	6,000	1,800	1,000,000	5.5	4.95	3.5	2.992	2.875	2.441
3.5	3,700	900	250,000	7.0	6.276	4.5	3.958	4.0	3.476
11.5	4,000	900	500,000	7.0	6.276	4.5	3.958	4.0	3.476
25.5	5,900	1,300	1,000,000	7.0	6.276	4.5	3.958	4.0	3.476
46.5	5,000	1,600	1,200,000	7.0	6.276	4.5	3.958	4.0	3.476

Table 4-2. Run matrix for field G (linear distribution) across $Q_{avg/well}$ bins for 5.5 and 7-in OD base casing size.

Field G Run Matrix									
Qavg/well [MMSCFD]	Depth [ft]	P_{RSI} [psia]	P_{WHS}^2-P_{WHF}^2 [psi^2]	Base OD [in]	Base ID [in]	Liner 1 OD [in]	Liner 1 ID [in]	Liner 2 OD [in]	Liner 2 ID [in]
0.5	1,800	400	25,000	5.5	4.95	3.5	2.992	2.875	2.441
1.5	2,500	600	100,000	5.5	4.95	3.5	2.992	2.875	2.441
11.5	4,000	900	500,000	5.5	4.95	3.5	2.992	2.875	2.441
19.5	6,000	1,800	1,000,000	5.5	4.95	3.5	2.992	2.875	2.441
3.5	3,700	900	250,000	7.0	6.276	4.5	3.958	4.0	3.476
11.5	4,000	900	500,000	7.0	6.276	4.5	3.958	4.0	3.476
25.5	5,900	1,300	1,000,000	7.0	6.276	4.5	3.958	4.0	3.476
46.6	5,000	1,600	1,200,000	7.0	6.276	4.5	3.958	4.0	3.476

Table 4-3. Run matrix for Field C (hockey stick distribution) across selected depths and $Q_{avg/well}$ bins for 5.5 and 7-in OD base casing size.

Qavg/well [MMSCFD]	Depth [ft]	P_{RSI} [psia]	P_{WHS}^2-P_{WHF}^2 [psi^2]	Base OD [in]	Base ID [in]	Liner 1 OD [in]	Liner 1 ID [in]	Liner 2 OD [in]	Liner 2 ID [in]
0.5	1,800	400	25,000	5.5	4.95	3.5	2.992	2.875	2.441
0.5	4,000	400	25,000	5.5	4.95	3.5	2.992	2.875	2.441
0.5	6,000	400	25,000	5.5	4.95	3.5	2.992	2.875	2.441
3.5	2,000	900	250,000.0	5.5	4.95	3.5	2.992	2.875	2.441
3.5	3,700	900	250,000.0	5.5	4.95	3.5	2.992	2.875	2.441
3.5	6,000	900	250,000.0	5.5	4.95	3.5	2.992	2.875	2.441
25.5	4,000	1,300	500,000	7	6.276	4.5	3.958	4.0	3.476
25.5	5,900	1,300	500,000	7	6.276	4.5	3.958	4.0	3.476
25.5	7,000	1,300	500,000	7	6.276	4.5	3.958	4.0	3.476
46.5	4,000	1,600	1,200,000	7	6.276	4.5	3.958	4.0	3.476
46.5	5,000	1,600	1,200,000	7	6.276	4.5	3.958	4.0	3.476

Table 4-4. Run matrix for Field C (hockey stick distribution) across selected P_{RSI} and $Q_{avg/well}$ bins for 5.5-in OD base casing.

Qavg/well [MMSCFD]	Depth [ft]	P_{RSI} [psia]	P_{WHS}^2-P_{WHF}^2 [psi^2]	Base OD [in]	Base ID [in]	Liner 1 OD [in]	Liner 1 ID [in]	Liner 2 OD [in]	Liner 2 ID [in]
3.5	3,700	900	250,000	5.5	4.95	3.5	2.992	2.875	2.441
3.5	3,700	1,200	250,000	5.5	4.95	3.5	2.992	2.875	2.441
3.5	3,700	1,500	250,000	5.5	4.95	3.5	2.992	2.875	2.441
3.5	3,700	1,600	250,000	5.5	4.95	3.5	2.992	2.875	2.441
11.5	4,000	900	500,000	5.5	4.95	3.5	2.992	2.875	2.441
11.5	4,000	1,200	500,000	5.5	4.95	3.5	2.992	2.875	2.441
11.5	4,000	1,500	500,000	5.5	4.95	3.5	2.992	2.875	2.441
11.5	4,000	1,720	500,000	5.5	4.95	3.5	2.992	2.875	2.441

This page left blank

5. MODELING RESULTS

Results from the combined pipe and well flow model runs for the simulation cases listed in Table 4-1 through Table 4-2 are summarized here. A given figure generally represents the results from 60 model realizations for a given field: 20 well percentile bins × 3 well inner diameters (base ID, liner 1, liner2).

5.1. Field C (Hockey Stick Distribution) Results Across Selected $Q_{avg/well}$ Bins

Gas flowrate distributions for selected $Q_{avg/well}$ bins are illustrated below as modeled for Field C. Individual points on the figure represent the flowrate associated with each 5th percentile of wells in a given field, sorted descending. The values shown for the field in the figure legend represent the flowrates numerically integrated over a hypothetical field of 100 wells. Percent reductions in deliverability are thus compared against the baseline for the entire field. While selected results are shown here to illustrate important features of the analysis, results for all simulation cases listed in Table 4-1 are given in 0. Model results for fields with baseline wells measuring 4.95" ID (5/5" OD) appear in Figure 5-1 through Figure 5-4. Results for fields with baseline wells measuring 6.276" ID (7" OD) appear in Figure 5-6 through Figure 5-7.

The first figure, Figure 5-1, is described in detail as an example. Field C was simulated here using a "Q25" pressure difference. This Q25 shorthand denotes the difference in squares of the wellhead pressures at static and flowing conditions, shown in the P_{WHS}^2-P_{WHF}^2 column in Table 4-1. The thousands are dropped in the shorthand, so that if P_{WHS}^2-P_{WHF}^2 = 25,000 psi^2, the corresponding notation is Q25. Individual well deliverabilities for the given conditions are shown as points on the figure, sorted descending. Points under a given well diameter case (Base, Liner 1, Liner 2) are connected by simple straight line connectors. The $Q_{avg/well}$ for the baseline case is shown on each figure as a horizontal dashed green line. For Figure 5-1, the associated $Q_{avg/well}$ = 0.5 MMSCFD, and is visible in the placement of the dashed green line as well as listed in the figure legend.

With a baseline ID = 4.95", the deliverability distribution of this field at Q25 is represented by the series of green points and connectors. For a field with 100 wells, the simulated baseline deliverability for the entire field computed by numerical integration was 52.1 MMSCFD, as indicated in the legend. If a liner with ID = 2.992" is inserted in every well and the field is operated with the same Q25 pressure conditions, the deliverability distribution is represented by the series of blue points and connectors immediately below the green baseline series. The downward shift at the well level indicates the degree to which the individual well deliverability was affected by the reduction in ID by adding a liner of indicated size. The higher-deliverability wells are affected to a larger degree, both in absolute and relative terms, than the lower-deliverability wells. Numerically integrating across 100 wells with the 2.992" liner yields 50.6 MMSCFD, a 3% reduction from the baseline, as indicated in the figure legend. Repeating the process for a slightly smaller liner with ID = 2.441" yields the brown series and results in a 48.5 MMSCFD deliverability for the field for a 7% reduction against the baseline field at ID = 4.95". The subsequent figures, Figure 5-2, Figure 5-3, etc., show the deliverability effects on incrementally increasing $Q_{avg/well}$ bins. The magnitude of deliverability reduction due to liners increases considerably with increasing $Q_{avg/well}$. As the series of figures shows, while the 2.992 and 2.441" liners may only reduce the field deliverability by 3% and 7% respectively for $Q_{avg/well}$ = 0.5 MMSCFD, these deliverability reductions increase to 42% and 58% for $Q_{avg/well}$ = 19.5 MMSCFD shown in Figure 5-4.

Figure 5-5 through Figure 5-7 show the impacts of liner additions for a larger baseline well ID = 6.276" (OD = 7"). A similar pattern is observed, with the higher-deliverability wells in the higher-deliverability bins affected more than the lower-deliverability wells.

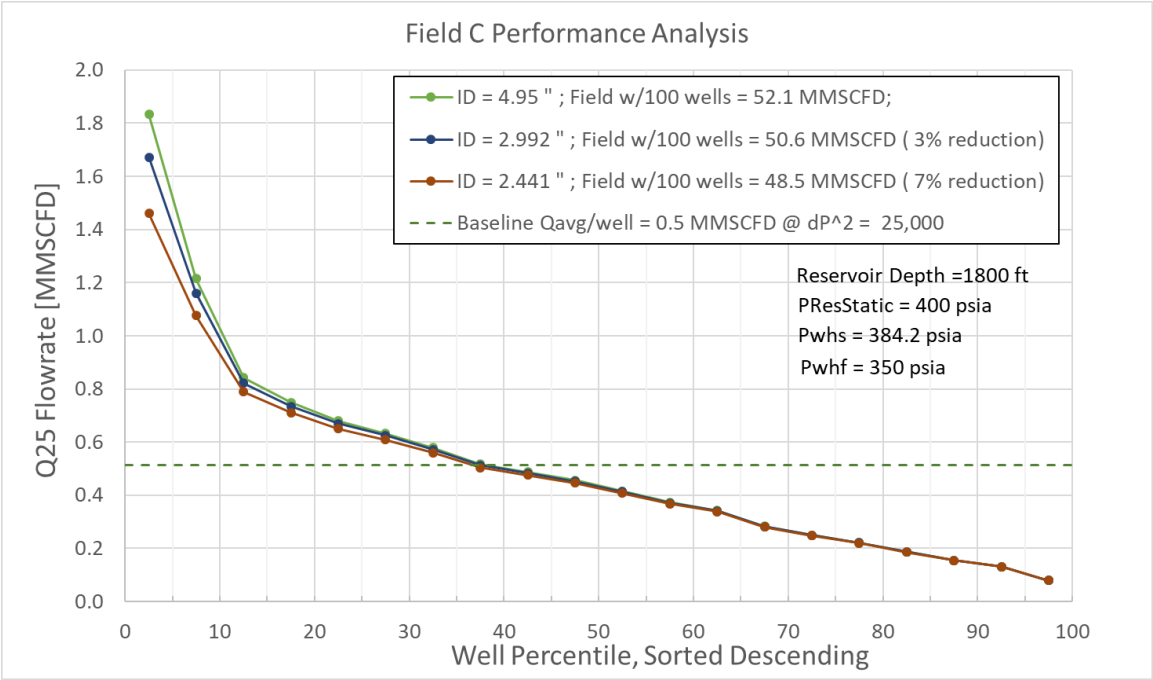

Figure 5-1. Q25 flowrates for Field C wells with baseline $Q_{avg/well}$ = 0.5 MMSCFD in 4.95" ID wells showing reductions at two liner sizes, 2.992 and 2.441".

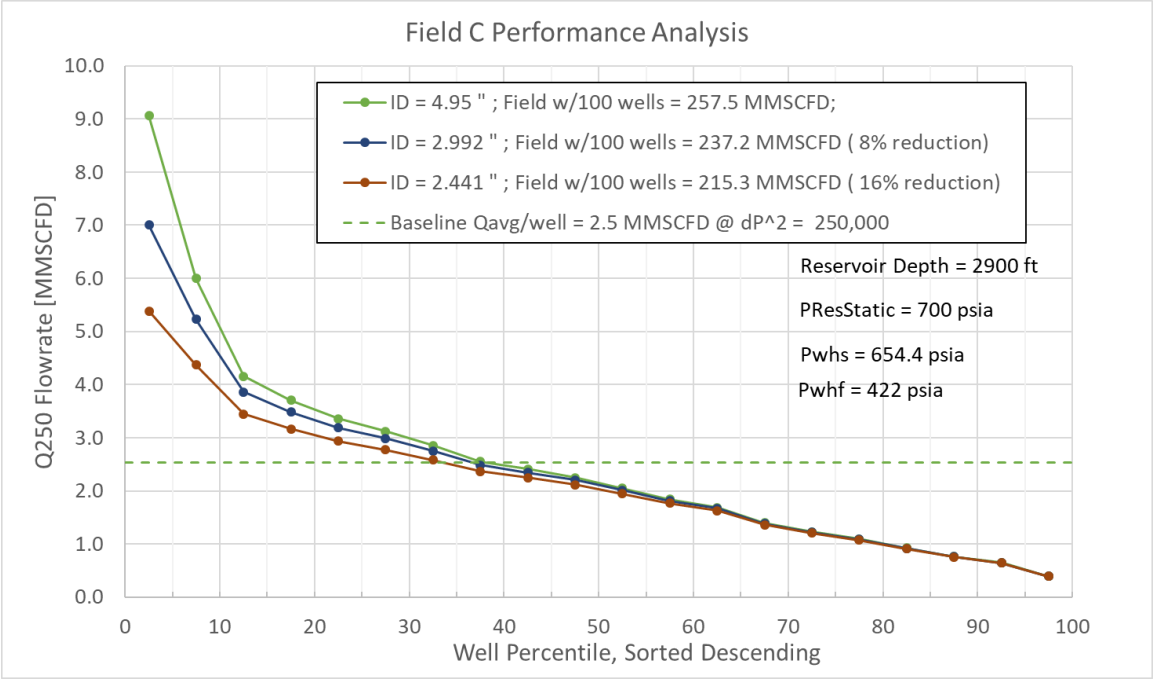

Figure 5-2. Q250 flowrates for Field C wells with baseline $Q_{avg/well}$ = 2.5 MMSCFD in 4.95" ID wells showing reductions at two liner sizes, 2.992 and 2.441".

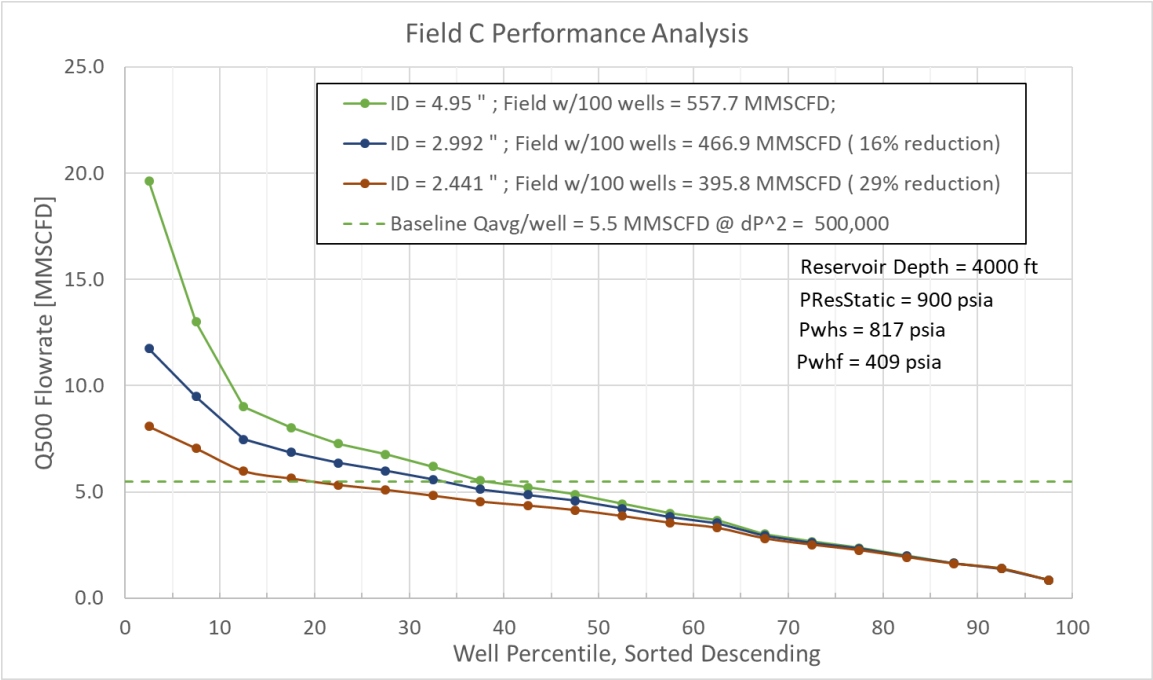

Figure 5-3. Q500 flowrates for Field C wells with baseline $Q_{avg/well}$ = 5.5 MMSCFD in 4.95" ID wells showing reductions at two liner sizes, 2.992 and 2.441".

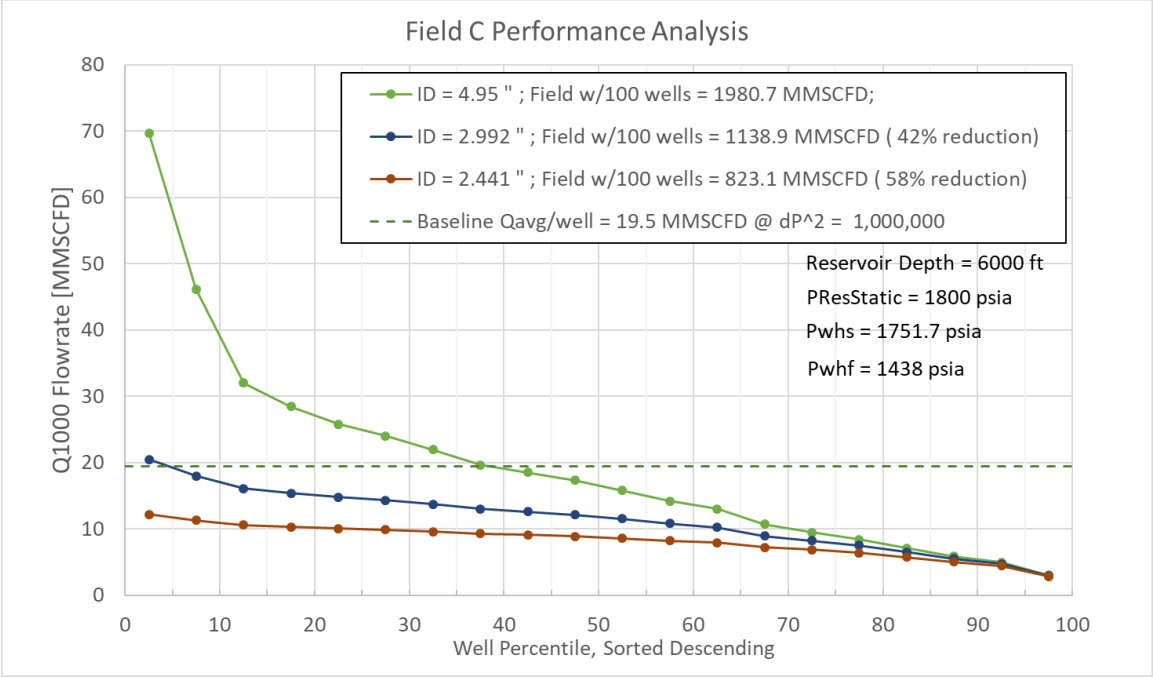

Figure 5-4. Q1000 flowrates for Field C wells with baseline $Q_{avg/well}$ = 19.5 MMSCFD in 4.95" ID wells showing reductions at two liner sizes, 2.992 and 2.441".

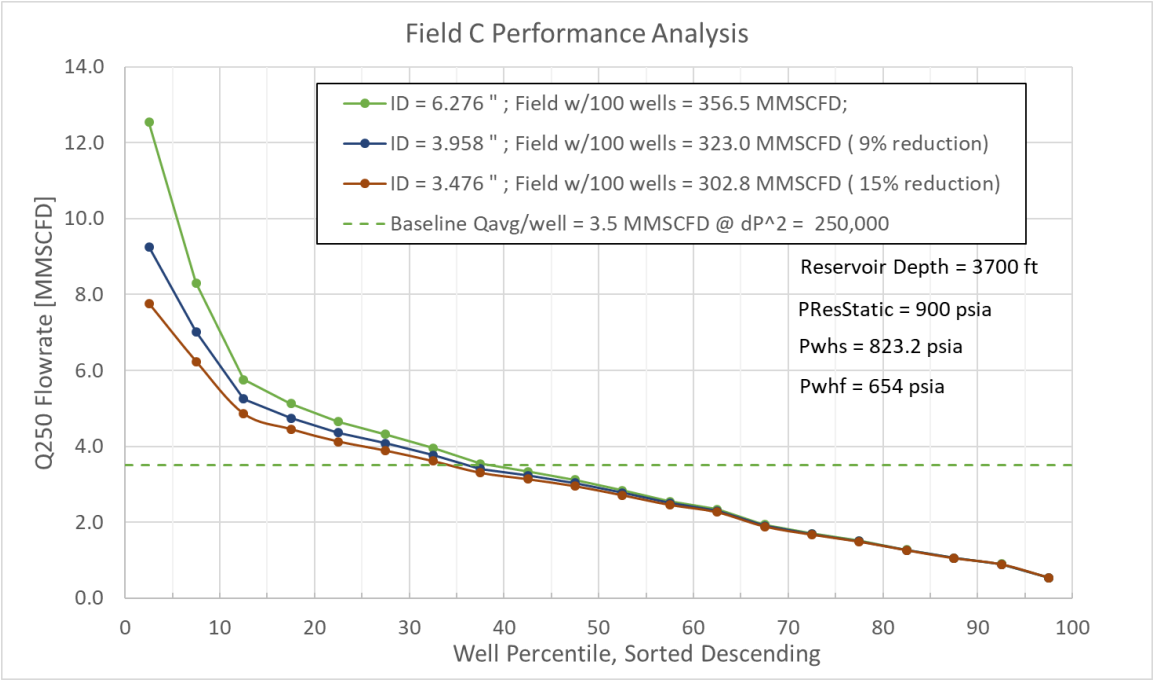

Figure 5-5. Q250 flowrates for Field C wells with baseline $Q_{avg/well}$ = 3.5 MMSCFD in 6.276" ID wells showing reductions at two liner sizes, 3.958 and 3.476".

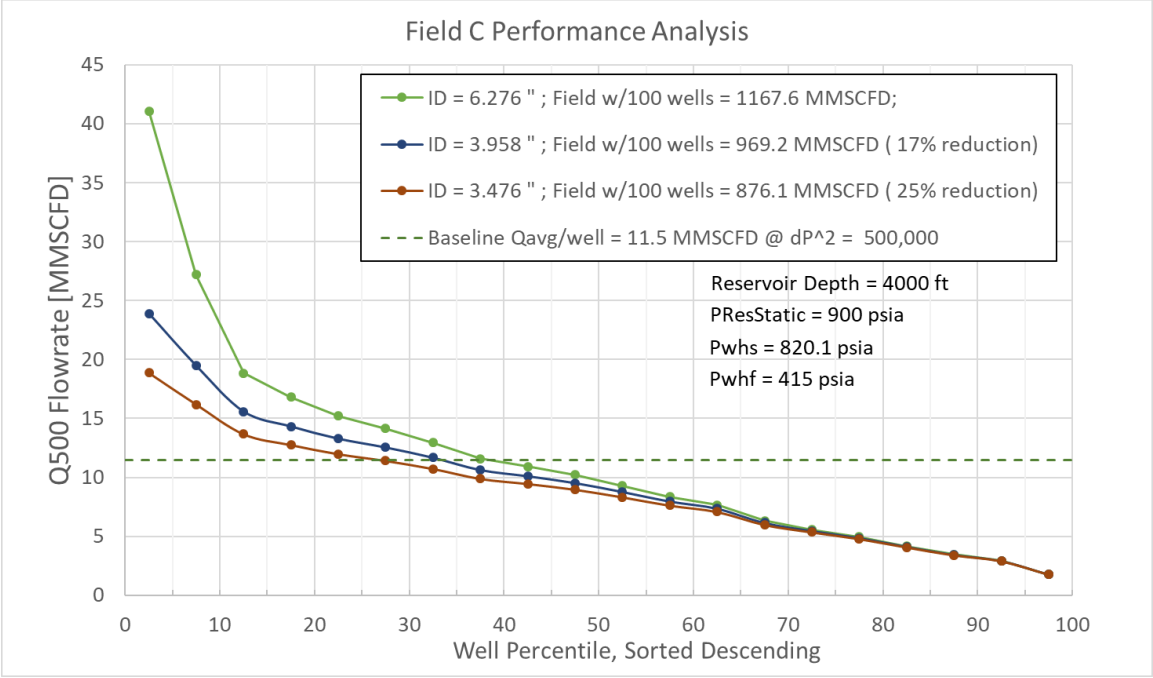

Figure 5-6. Q500 flowrates for Field C wells with baseline $Q_{avg/well}$ = 11.5 MMSCFD in 6.276" ID wells showing reductions at two liner sizes, 3.958 and 3.476".

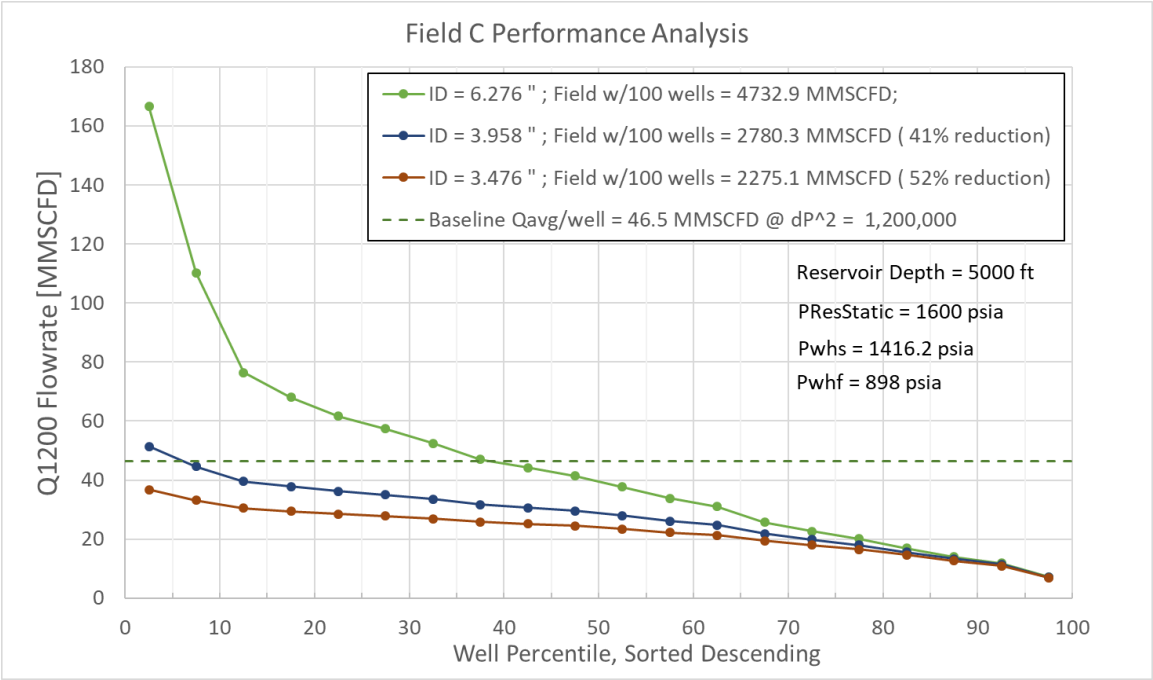

Figure 5-7. Q1200 flowrates for Field C wells with baseline $Q_{avg/well}$ = 46.5 MMSCFD in 6.276" ID wells showing reductions at two liner sizes, 3.958 and 3.476".

A summary of liner effects on field-level reductions in deliverability for Field C (hockey-stick distribution) is given in Figure 5-8 based on the run matrix outlined in Table 4-1. Tabular output for all of these runs are given in 0. Reviewing Figure 5-8, as field-level $Q_{avg/well}$ increased, the associated reductions in field-level deliverability also increased with incrementally smaller liners. For the base case ID = 4.95" (OD = 5.5") represented by the yellow and blue series on the upper left section of the plot, field-level deliverability reductions ranged from 3% to 42% for Liner 1 (ID = 2.992") and from 7% to 58% for Liner 2 (2.441"). When reviewing the results for the larger diameter wells with base case ID = 6.276" (OD = 7") represented by the red and orange series, field-level deliverability reductions ranged from 5% to 41% for Liner 1 (ID = 3.958") and from 8% to 52% for Liner 2 (ID =3.476"). At a given $Q_{avg/well}$, a smaller base ID was associated with more significant reductions in deliverability with liners. If we take $Q_{avg/well}$ = 3.5 MMSCFD as an example, the reductions due to liner for the base ID 4.95" case are 14-25%, while the reductions due to liner for the base ID = 6.276" case are 5-8%. Note the base case ID = 4.95" (OD = 5.5") field-level simulations were not run for $Q_{avg/well}$ bins > 19.5 MMSCFD because the base configuration could not support the highest-delivery wells in the hockey stick distribution. The pipe friction pressure drops in these wells were simply too high to support those base flowrate levels.

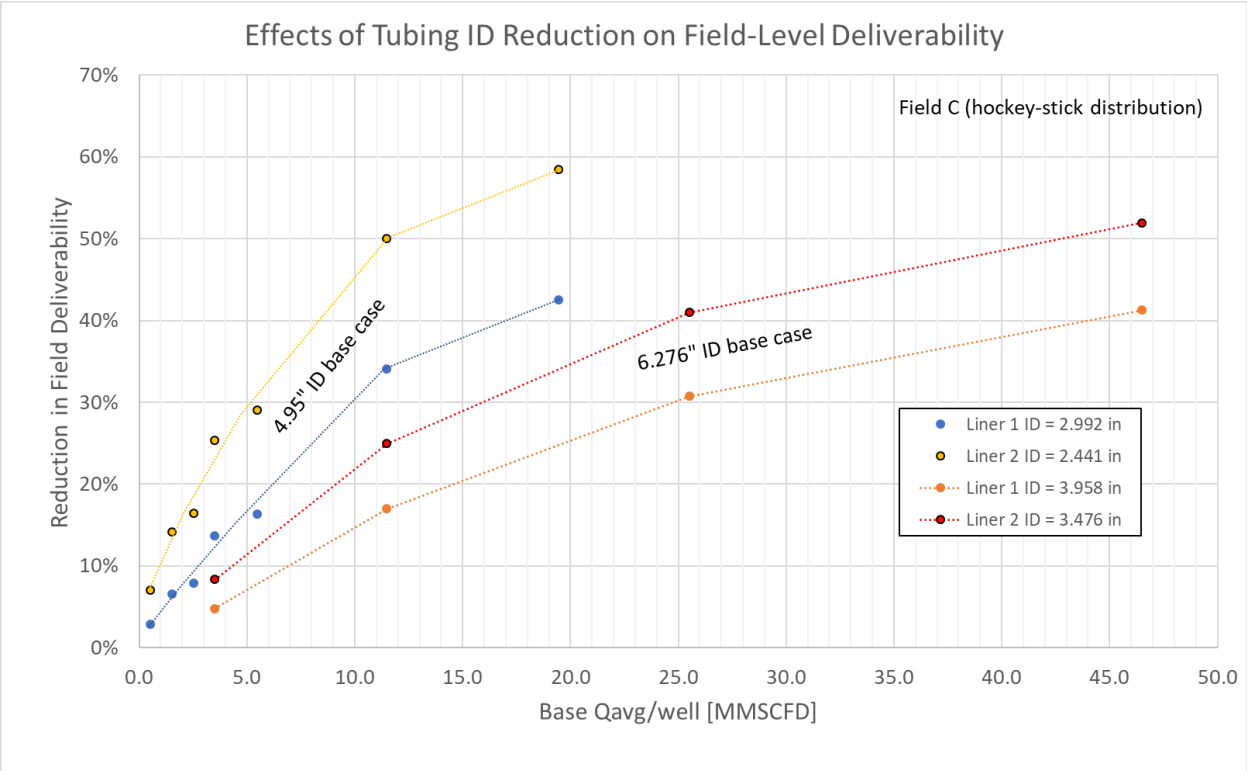

Figure 5-8. Summary results for Field C (hockey-stick distribution) for all $Q_{avg/well}$ and liners run against base case production casing ID = 4.95" and 6.276".

5.2. Field G (Linear Distribution) Results Across Selected $Q_{avg/well}$ Bins

Gas flowrate distributions for selected $Q_{avg/well}$ bins are illustrated below as modeled for Field G, which has a nearly linear distribution in well deliverability. While selected results are shown here for illustration, the complete results for the run matrix show in Table 4-2 are given in Appendix B. The effects of decreasing ID on deliverability follows the same general pattern as seen above for the Field C (hockey stick) distribution. Higher deliverability wells and higher deliverability bins are affected more than lower deliverability wells and bins, though the magnitude of tubing-induced reductions for the linear field is not as pronounced as for the hockey stick field. Some particular cases are discussed below.

The general effects of increasing $Q_{avg/well}$ in Field G is illustrated by comparing Figure 5-9 and Figure 5-10 for a baseline well ID = 4.95" (OD = 5.5"). The $Q_{avg/well}$ = 0.5 MMSCFD case in Figure 5-9 only sees 1% and 4% reductions in deliverability at the field level with addition of 2.992" and 2.441" liners, while the $Q_{avg/well}$ = 11.5 MMSCFD case in Figure 5-10 sees 28% and 46% reductions for the same liner sizes. Moving up to larger casing with baseline well ID = 6.276 at the same $Q_{avg/well}$ = 11.5 MMSCFD indicates that the effects of tubing size reductions are less severe at the field level, showing 11% and 19% reductions for liners with 3.958 and 3.476" ID, respectively, as shown in Figure 5-11. The field simulated in Figure 5-9 can be characterized as reservoir-limited, and its deliverability is relatively insensitive to incremental reductions in tubing size. In contrast, the field simulated in Figure 5-10 is tubing-limited and shows pronounced reductions in deliverability with tubing size reductions.

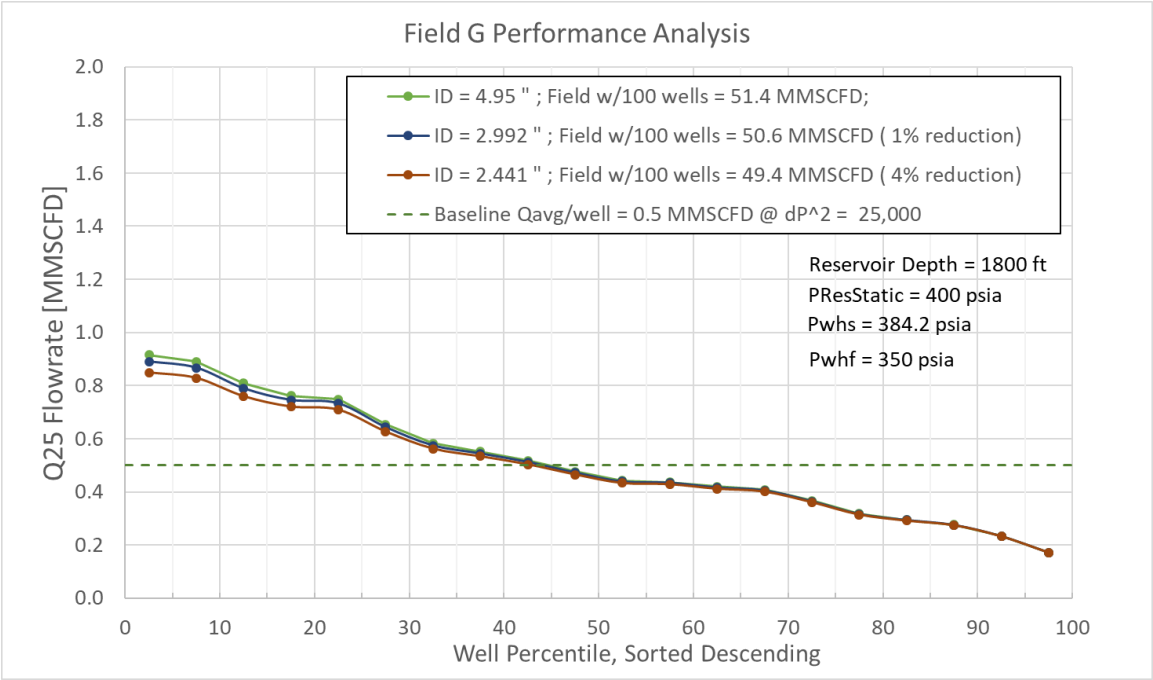

Figure 5-9. Q25 flowrates for Field G wells with baseline $Q_{avg/well}$ = 0.5 MMSCFD in 4.95" ID wells showing reductions at two liner sizes, 2.992 and 2.441".

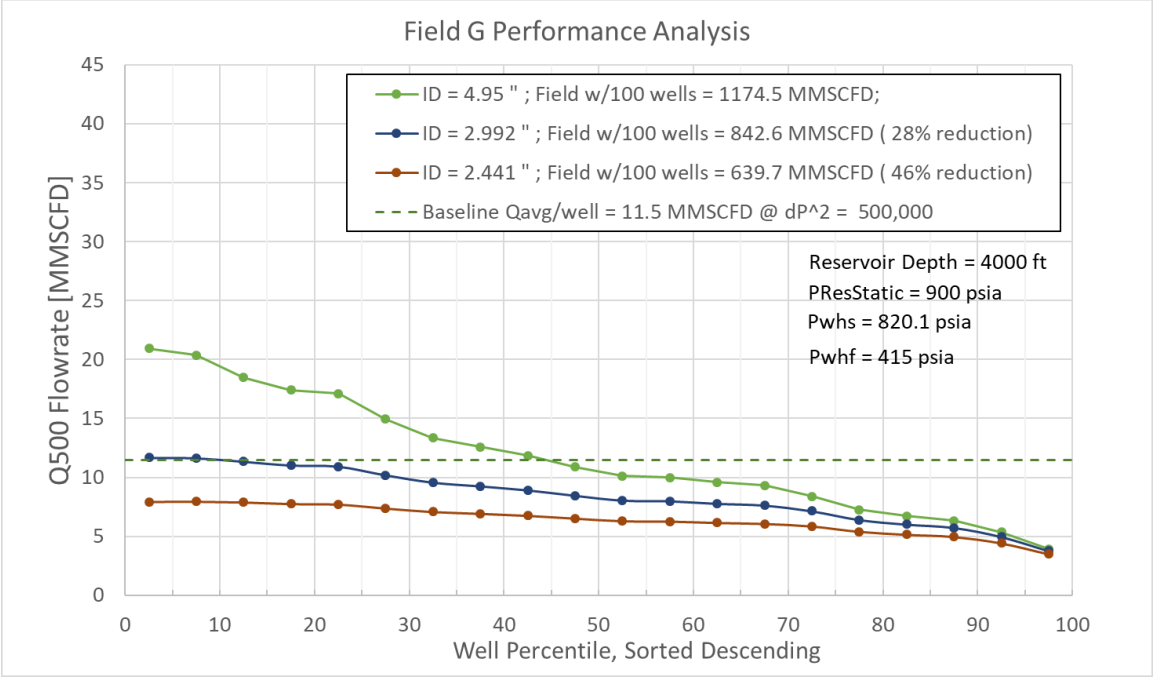

Figure 5-10. Q500 flowrates for Field G wells with baseline $Q_{avg/well}$ = 11.5 MMSCFD in 4.95" ID wells showing reductions at two liner sizes, 2.992 and 2.441".

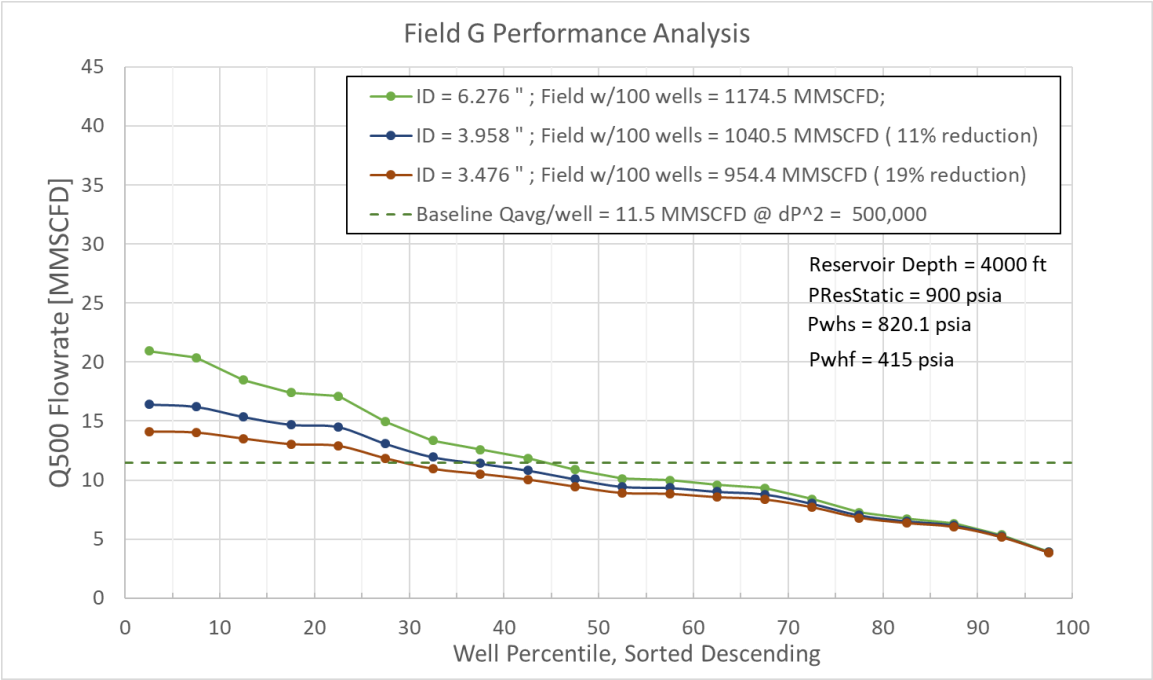

Figure 5-11. Q500 flowrates for Field G wells with baseline $Q_{avg/well}$ = 11.5 MMSCFD in 6.276" ID wells showing reductions at two liner sizes, 3.958 and 3.476".

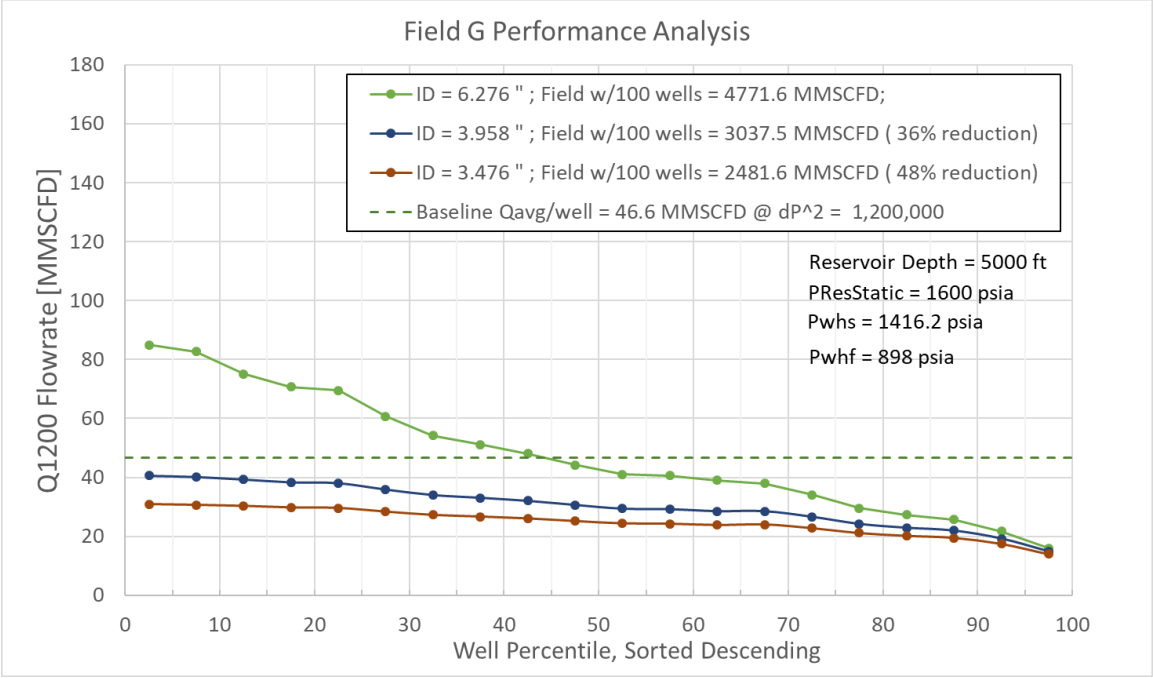

Figure 5-12. Q1200 flowrates for Field G wells with baseline $Q_{avg/well}$ = 46.5 MMSCFD in 6.276" ID wells showing reductions at two liner sizes, 3.958 and 3.476".

A summary figure showing liner effects on field-level deliverability for Field G (linear distribution) is shown in Figure 5-13 based on the run matrix outlined in Table 4-2. As field-level $Q_{avg/well}$ increased, the associated reductions in field-level deliverability also increased with incrementally smaller liners. Assuming a base case ID = 4.95" (OD = 5.5") represented by the green and purple series in the upper left of the plot, field-level deliverability reductions ranged from 1% to 38% for Liner 1 (ID = 2.992") and from 4% to 55% for Liner 2 (2.441"). Moving to a larger base case ID = 6.276" (OD = 7"), field-level deliverability reductions ranged from 2% to 36% for Liner 1 (ID = 3.958") and from 5% to 48% for Liner 2 (ID =3.476"). At a given $Q_{avg/well}$, a smaller base ID was associated with more significant reductions in deliverability with liners. If we take $Q_{avg/well}$ = 11.5 MMSCFD as an example, the reductions due to liner for the base ID 4.95" case are 28-46%, while the reductions due to liner for the base ID = 6.276" case are 11-19%.

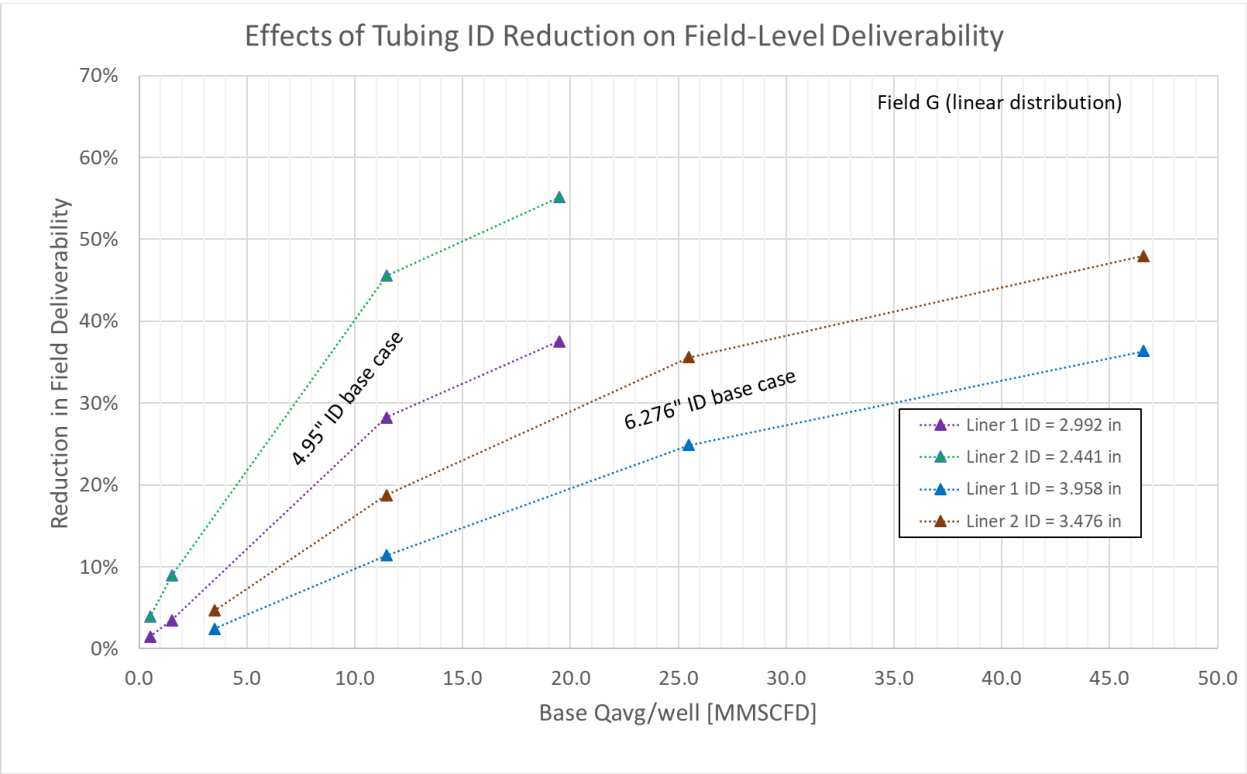

Figure 5-13. Summary results for Field G (linear distribution) for all $Q_{avg/well}$ and liners run against base case production casing ID = 4.95" and 6.276".

5.3. Field C vs. G Comparison

Several direct comparisons may be drawn to illustrate the effects of well deliverability distribution (i.e. hockey stick vs. linear) on field-level deliverability in selected $Q_{avg/well}$ bins. Generally speaking, the high outlier wells, which form the "blade" of the hockey stick, are more susceptible to deliverability losses than the rest of the wells in the field with the addition of a liner. As such, when comparing fields that have the same $Q_{avg/well}$, those with the hockey stick shape shown in Field C exhibit greater reductions in field-level deliverability than the more linear Field G. This effect is observed by comparing Figure 5-14 vs. Figure 5-15, where both figures show field-level well deliverability at $Q_{avg/well}$ = 3.5 MMSCFD, but the effects of adding liner are greater for the most productive wells on the extreme left side of each figure. Upon numerical integration across all wells in each of these fields, Field C experiences greater reductions (5% and 8% for Liners 1 and 2, respectively) than Field G (2%

and 5%). Figure 5-16 provides a side-by-side view of deliverability reductions for Field C vs. Field G across multiple $Q_{avg/well}$ bins and base ID = 4.95" and 6.276" for the addition of Liner 1. In every case, Field C saw slightly more reduction in field-level deliverability than Field G, indicated by a slight upward shift from each series "G" to each series "C".

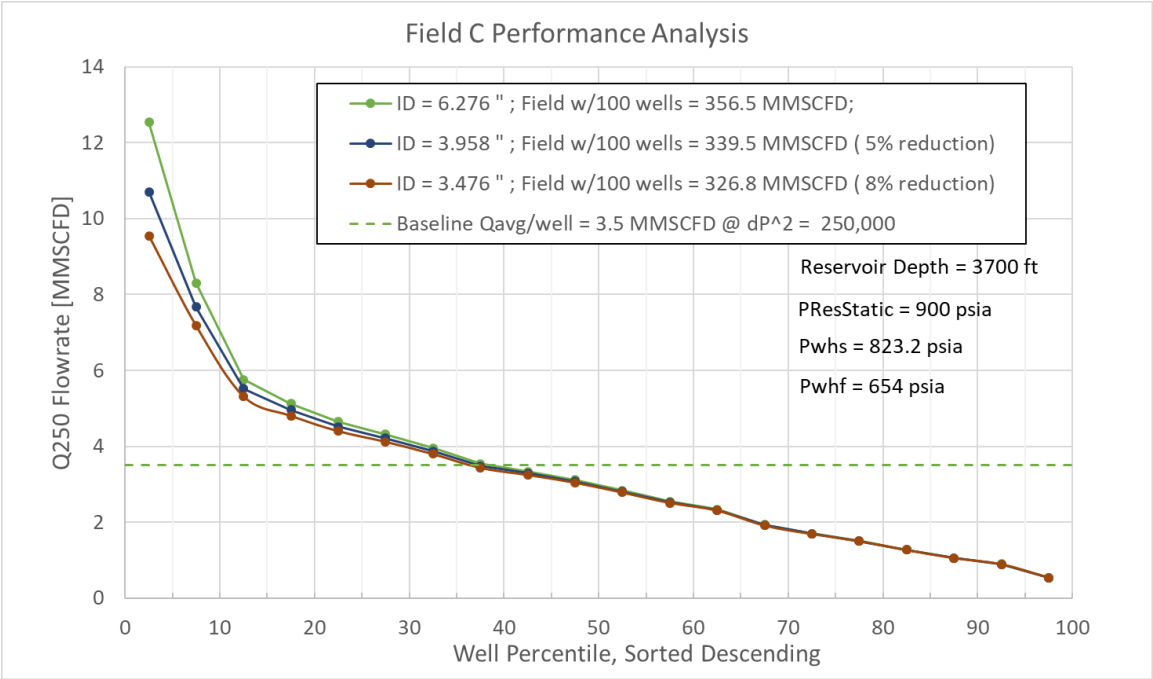

Figure 5-14. Q250 flowrates for Field C wells with baseline $Q_{avg/well}$ = 3.5 MMSCFD in 6.276" ID wells showing reductions at two liner sizes, 3.958 and 3.476".

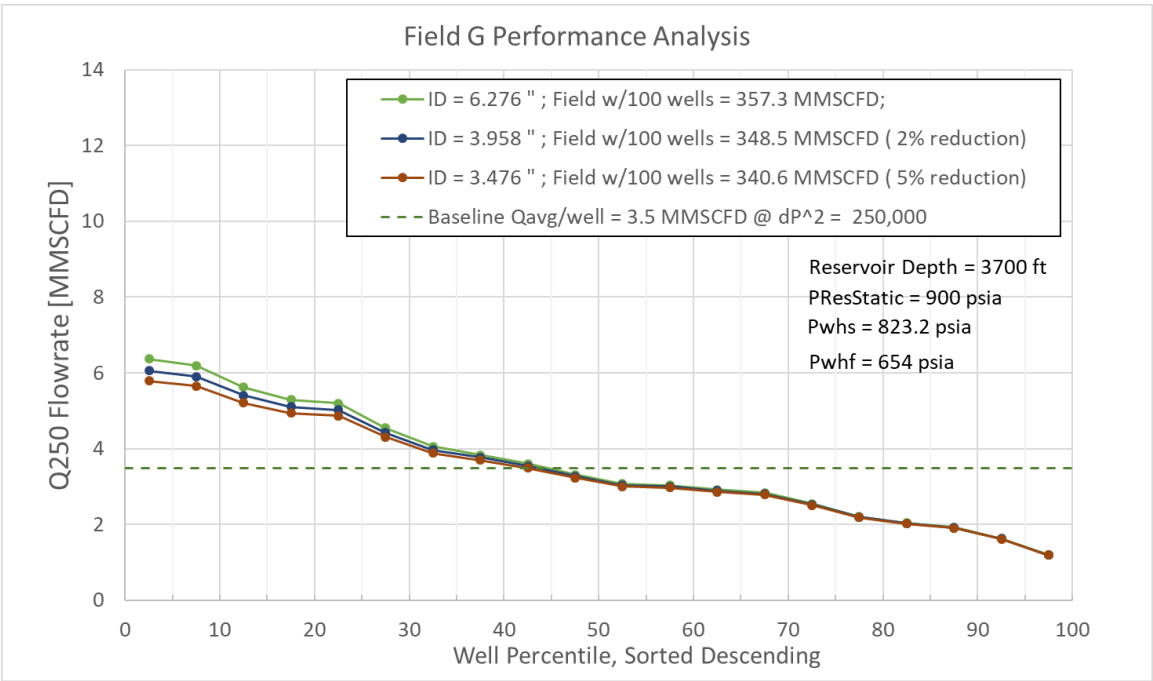

Figure 5-15. Q250 flowrates for Field G wells with baseline $Q_{avg/well}$ = 3.5 MMSCFD in 6.276" ID wells showing reductions at two liner sizes, 3.958 and 3.476".

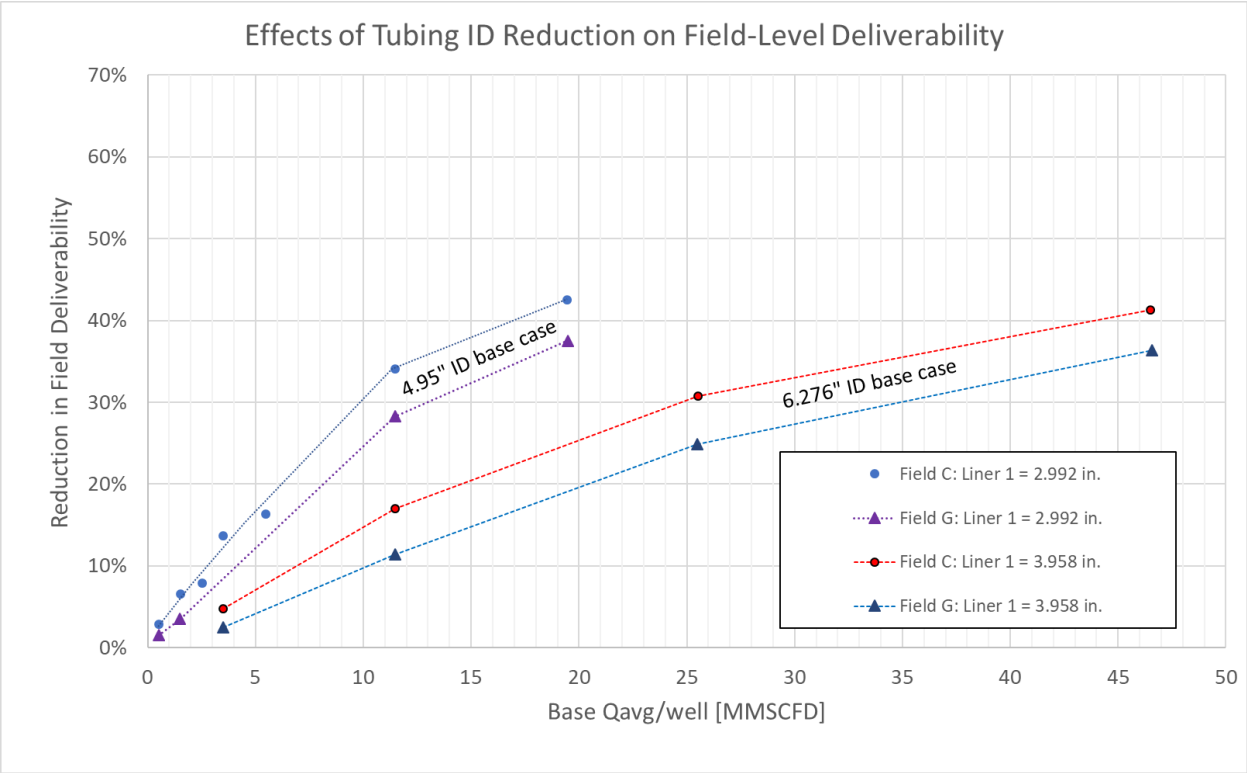

Figure 5-16. Summary results for Field C (hockey stick distribution) and Field G (linear distribution) for all $Q_{avg/well}$ bins and with Liner 1 run against base case production casing ID = 4.95" and 6.276".

5.4. Effects of Depth and Liners on Deliverability for Field C

The effects of well depth coupled with tubing ID reductions in Field C outlined in the run matrix in Table 4-3 are shown in Figure 5-17 through Figure 5-20. For each selected $Q_{avg/well}$ bin, three depth cases were run. The reservoir deliverability coefficients (C, n) were tuned to yield the given $Q_{avg/well}$ for the base case at each depth and then the effects of liners were computed. Deliverability reductions due to liners grow more pronounced with deeper wells. For example, for $Q_{avg/well}$ = 3.5 MMSCFD in Figure 5-18, the effects of adding Liner 1 (ID = 2.992") was a 9% field deliverability reduction for a 2,000 ft well, 14% for a 3,700 ft well, and 17% for a 6,000 ft well. This is conceptually consistent with the basic equations for steady pipe flow that indicate flowrate is inversely proportional to the square root of pipe length (recall Weymouth, Eq. 2), such that an increase in pipe length, holding all other terms the same, will decrease the flowrate. While not explicitly modeled here, deliverabillity impacts of liners in directionally drilled wells could potentially be greater than indicated in the modeling results presented here because the length of tubing is greater than a vertical well for a given reservoir depth.

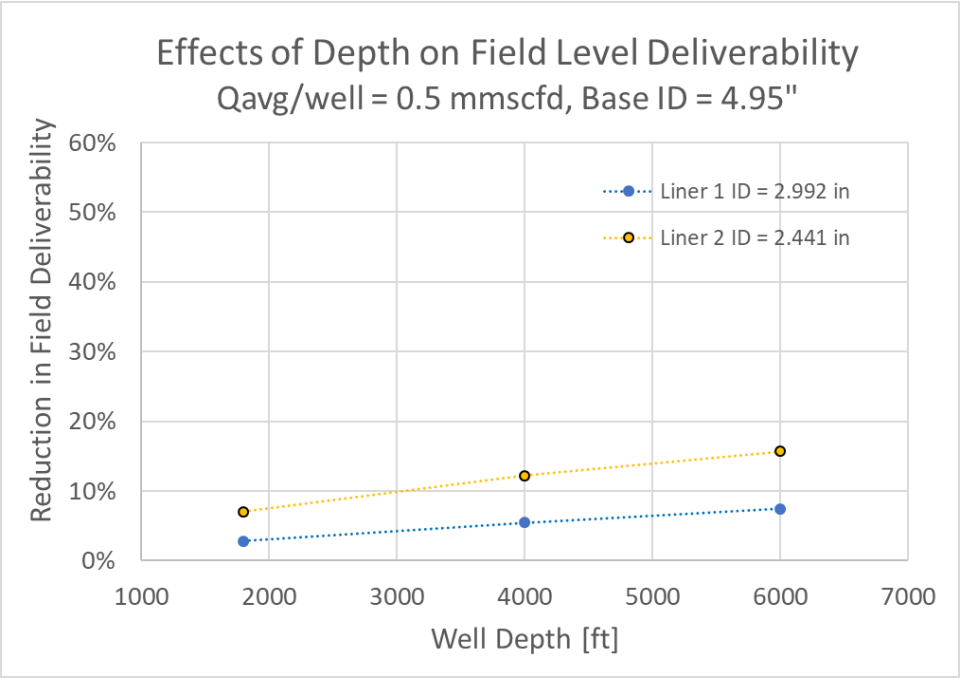

Figure 5-17. Field-level reductions in deliverability with well depth for baseline $Q_{avg/well}$ = 0.5 MMSCFD in 4.95" ID wells in Field C (hockey stick distribution) showing reductions at two liner sizes, 2.992 and 2.441".

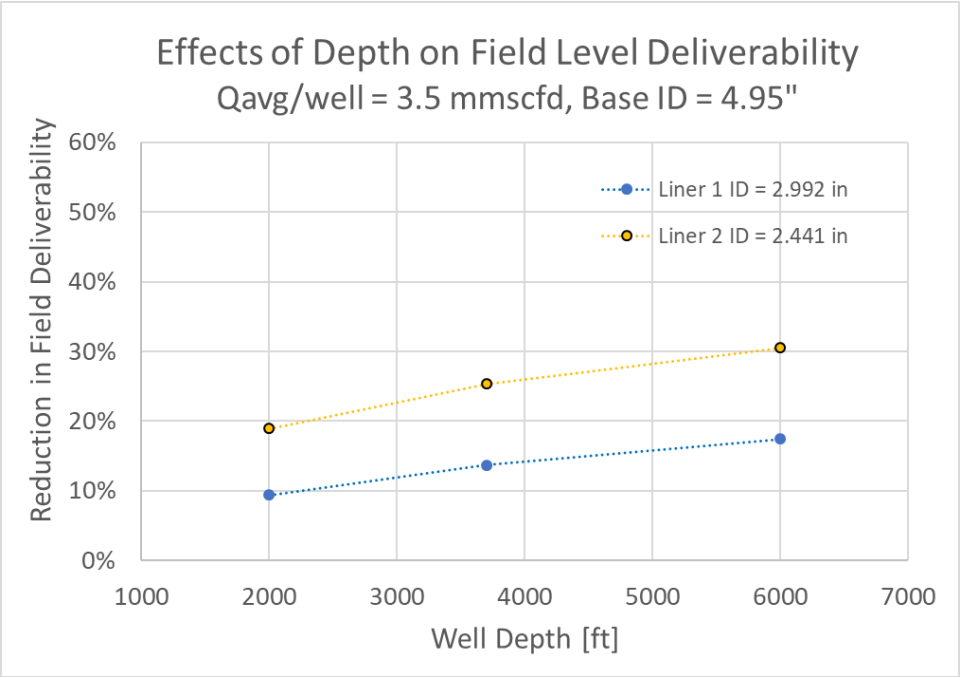

Figure 5-18. Field-level reductions in deliverability with well depth for baseline $Q_{avg/well}$ = 3.5 MMSCFD in 4.95" ID wells in Field C (hockey stick distribution) showing reductions at two liner sizes, 2.992 and 2.441".

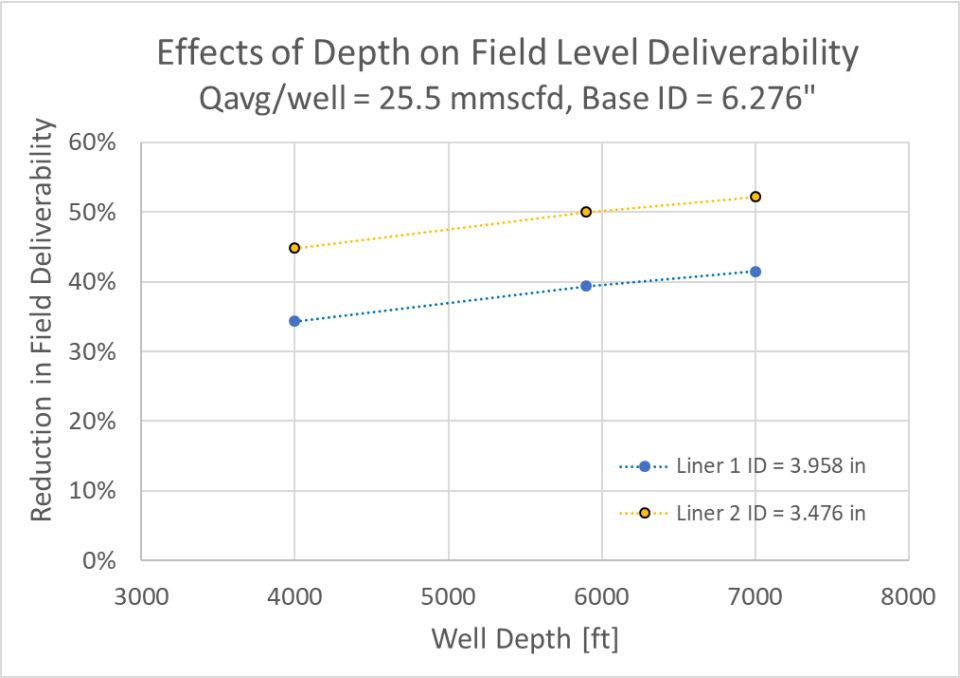

Figure 5-19. Field-level reductions in deliverability with well depth for baseline $Q_{avg/well}$ = 25.5 MMSCFD in 6.276" ID wells in Field C (hockey stick distribution) showing reductions at two liner sizes, 3.958 and 3.476".

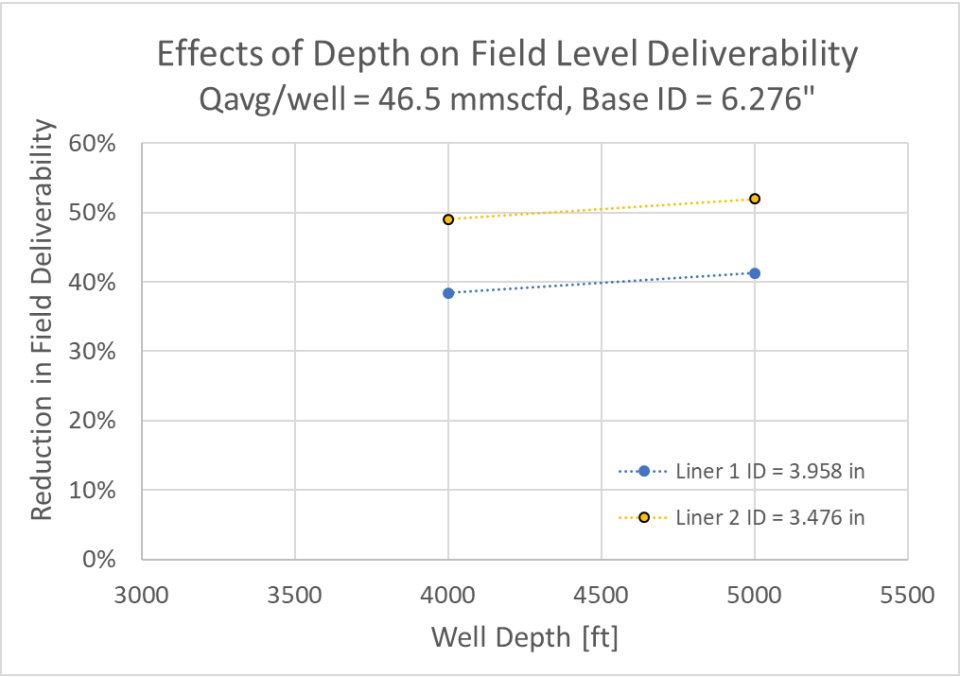

Figure 5-20. Field-level reductions in deliverability with well depth for baseline $Q_{avg/well}$ = 46.5 MMSCFD in 6.276" ID wells in Field C (hockey stick distribution) showing reductions at two liner sizes, 3.958 and 3.476".

5.5. Effects of Reservoir Shut-In Pressure on Deliverability for Field C

The effects of reservoir shut-in pressure (P_{RSI}) coupled with tubing ID reductions were explored for selected cases in Field C according to the run matrix in Table 4-4, with the results summarized in Table 5-1 below. For each selected $Q_{avg/well}$ bin, four P_{RSI} cases were run to simulate the effects of adding liners to reservoirs that are operated at a range of reservoir shut-in pressures from full inventory condition where $P_{RSI} = P_{max}$ down to about 20% of working inventory, estimated here at 900 psia. Note the P_{WHS}^2-P_{WHF}^2 term that drives flowrate remains constant in this matrix. P_{RSI} has an effect on deliverability reductions from liners, causing slightly greater deliverability reductions with lower P_{RSI}. For example, in the Q_{avg} = 3.5 MMSCFD series, adding Liner 1 results in deliverability reductions from base case by 14% for P_{RSI} = 900 psia as compared to 10% for P_{RSI} = 1,600 psia. Similar results are seen for Liner 2 with reductions ranging from 25% at P_{RSI} = 900 to 22% at P_{RSI} = 1,600 psia. A similar pattern is observed when looking at the Q_{avg} = 11.5 MMSCFD deliverability bin. While the dP^2 term and flowrates in these simulations are the same across the four P_{RSI} cases simulated, the lower flowing pressures associated with lower P_{RSI} cases induce higher velocities inside the well with resultant higher pressure drops due to friction that ultimately lead to greater losses in deliverability than at higher P_{RSI}.

Table 5-1. Summary of field-level reductions in deliverability for Field C with liner size and reservoir shut-in pressure for base well ID = 4.95".

P_{RSI} Series Field C				Base ID = 4.95 in	
Qavg/well [MMSCFD]	Depth [ft]	P_{RSI} [psia]	P_{WHS}^2-P_{WHF}^2 [psi^2]	Liner 1 ID = 2.992 in % Reduction	Liner 2 ID = 2.441 in % Reduction
3.5	3,700	900	250,000	14%	25%
3.5	3,700	1200	250,000	12%	24%
3.5	3,700	1500	250,000	11%	23%
3.5	3,700	1600	250,000	10%	22%
11.5	4,000	900	500,000	34%	50%
11.5	4,000	1200	500,000	33%	49%
11.5	4,000	1500	500,000	32%	48%
11.5	4,000	1720	500,000	31%	48%

5.6. Comparison Across Multiple Bins, Fields

A summary plot that aggregates field deliverability results from all of the simulations listed in Table 4-1 and Table 4-2 is given in Figure 5-21. The x-axis represents $Q_{avg/well}$, and the y-axis represents the reduction in field deliverability due to liner additions as a percentage of the base deliverability. Each series on the plot represents a field, either C (hockey-stick) or G (linear), evaluated over multiple $Q_{avg/well}$ bins. The line segment connectors are notional, added to guide the eye to the next point in the series, and do not represent a mathematical curve fit.

One of the first general observations of the data presented in this way is that the reduction in field deliverability increases with $Q_{avg/well}$ for every series examined. This is a reflection of the fact that higher flowrate wells are more subject to tubing limitations, amplified as successively smaller liners are introduced. Conversely, lower flowrate wells are more typically reservoir-limited, and are consequently less sensitive to introduction of liners. Deliverability is also clearly affected by the base case well ID,

as illustrated by the groupings visible in the figure with the 4.95-in ID (5.5-in OD) base case showing categorically greater reductions in deliverability with liners than the 6.276-in ID (7-in OD) base case.

Another observation that has been consistent across this report is that the linear field G deliverability is less affected than the hockey-stick field C for the same boundary conditions (P_{WHS}^2-P_{WHF}^2, P_{RSI}) with tubing size reductions: for every Field G series there is a corresponding Field C series that is shifted upward. The greater sensitivity of the highest deliverability wells (blade of the hockey stick) from Field C drive this effect at the well- and field-levels.

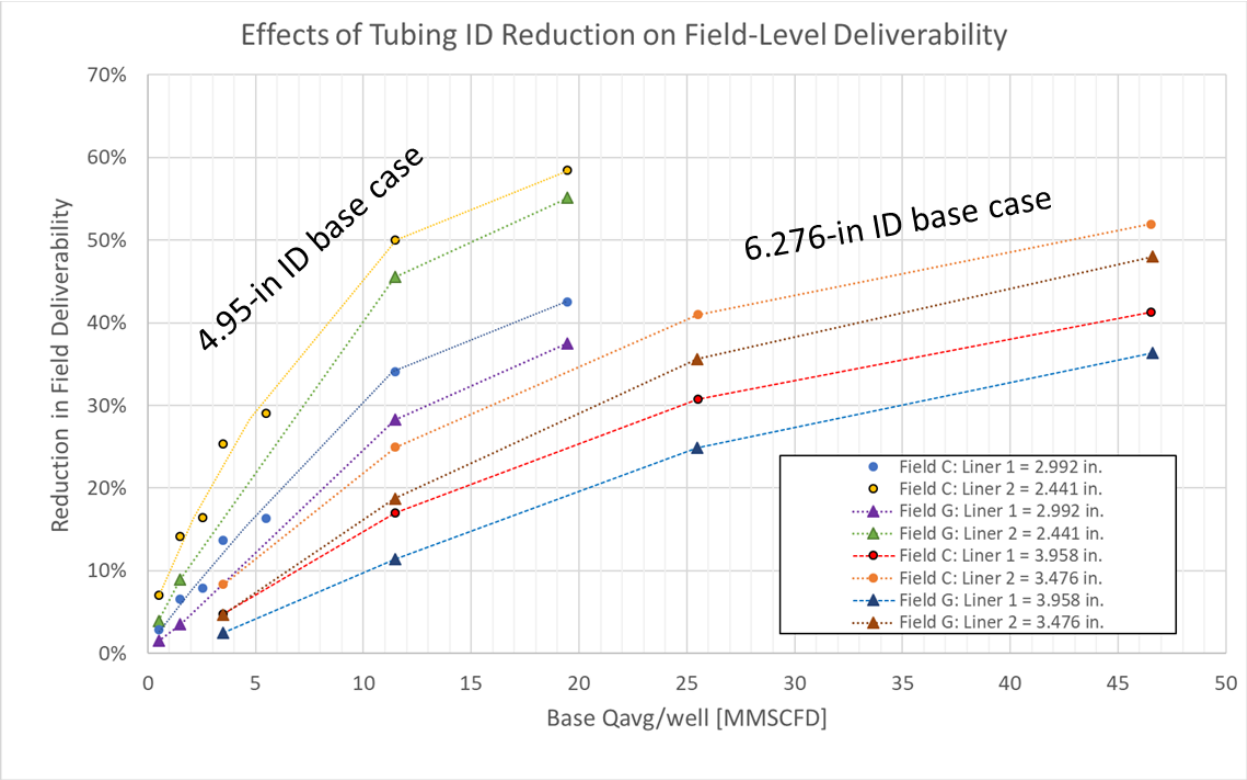

Figure 5-21. Summary plot of field deliverability across a broad range of $Q_{avg/well}$ bins for 4.95" and 6.276" ID base case wells with the addition of liners.

5.7. Interpretation for U.S. Depleted Reservoir Storage

The results of this modeling study illustrate several basic patterns:

(i) Higher-deliverability wells are subject to greater flowrate reductions as a result of tubing ID reductions than low-deliverability wells because high-flow wells are typically more tubing-limited than reservoir-limited

(ii) Higher-deliverability fields are similarly subject to greater flowrate reductions from tubing ID reductions, as some, if not all, of the wells are likely tubing-limited

(iii) Low-deliverability fields, which are constrained largely by reservoir conditions, can be relatively insensitive to tubing ID reductions

How these factors could potentially affect access to the depleted reservoir storage inventory within the U.S. may be interpreted by reviewing the data obtained from the AGA report (AGA 2017)

introduced above in Section 4.2. Recall Figure 4-5, which organizes the AGA data into $Q_{avg/well}$ deliverability bins and reports occurrence of fields, wells, and working gas capacity across the U.S. by percentage. The AGA data indicate that the majority of fields and wells in the U.S. are associated with relatively low $Q_{avg/well}$, with 57% of fields containing 71% of wells associated with $Q_{avg/well} < 3$ MMSCFD. Occurrences of fields and wells also decrease rapidly with increase in $Q_{avg/well}$ so that medium- and high-deliverability fields are rare relative to the lower bins. While relatively low, the effects of liners on the low $Q_{avg/well}$ operators are fields are not necessarily zero, and some response is likely necessary to maintain their baseline field-level deliverability. An important consideration to overlay with this though is the working gas capacity associated with the range of deliverability bins shown in Figure 4-5. Working gas capacity is more evenly distributed than the number of wells and fields, so while the number of fields and operators that would be significantly affected by tubing size reductions is low relative to the general population, their contribution to the overall capacity is significant.

An attempt to illustrate these combined effects of field/well/capacity occurrence with field-level reductions for varying $Q_{avg/well}$, base casing size, and liner additions is summarized in the hybrid plot in Figure 5-22. Here, the AGA occurrence data (column data, units on left vertical axis) from Figure 4-5 are co-plotted with the deliverability modeling results (points connected with lines, units on right vertical axis) from Figure 5-21. The plot shows that the highest occurrences of fields and wells at low $Q_{avg/well}$ are also associated with the relatively low field deliverability reductions. Moving left to right, as $Q_{avg/well}$ increases, occurrence of fields and well drops sharply, working gas capacity remains about the same, and reductions in field deliverability increase to their maxima for each series at highest $Q_{avg/well}$ cases simulated for each casing size. Looking back at some of the operator concerns expressed in public literature in section 1.1, the reductions in deliverability they cited, in the range 40-60%, are consistent with the highest-flowing wells and field shown here.

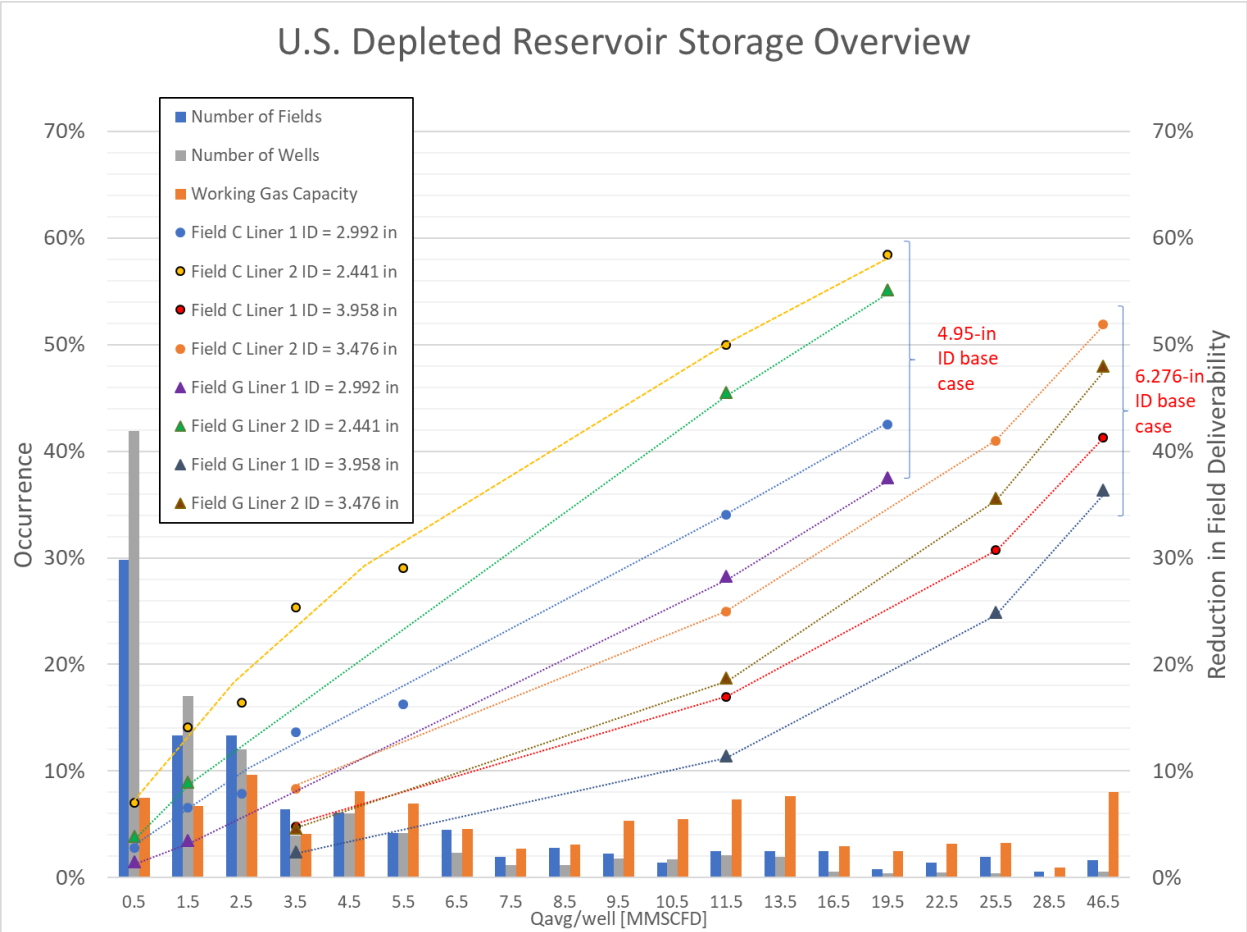

Figure 5-22. Hybrid graph showing overlay of field, well, and working gas capacity occurrence data from AGA (2017) with field-level deliverability modeling results for selected tubing size reductions.

This page left blank

6. SUMMARY

This report simulated well- and field-level reductions in deliverability from depleted reservoir underground storage as a function of tubing size reductions. The simulations were run with models developed at Sandia based on widely-accepted pipe and reservoir flow equations, verified against commercial software, and validated against field test data.

The results can be summarized as follows:

(1) Adding tubing and packer has the potential to reduce deliverability at the field- and well-level due to the addition of flow restrictions in wells, though the extent of reduction is strongly dependent on whether the current wells are reservoir-limited or tubing-limited.

   a. Tubing-limited wells will show notable reductions in flowrate with additional inner diameter restrictions.

   b. Reservoir-limited wells will show small to no reductions in flowrate with additional inner diameter restrictions.

(2) All of the simulations presented here were based on examples of hypothetical fields whose parameters were derived from a large body of averaged field data obtained from a variety of sources, both public and private. The simulations are intended to give representative results across a range of possible fields and operating conditions in the U.S. The simulations are <u>not</u> intended to be predictive for a particular field or operator.

(3) Given that the current simulations use industry-accepted modeling techniques and typical data for reservoir and well deliverability, the general behavior of actual operator systems should be analogous to what is shown here.

(4) Individual operators will have the actual well performance data and calibrated models that will best predict the response of their own fields to changes in configuration.

(5) Operator concerns noted from the public record stating that reductions in deliverability could reach 40% (Freifield, Oldenburg et al. 2016) for their current wells or even exceed 60% in some wells on the peak day (Johnson 2016) appear to be validated by the current work for the highest-deliverability wells and fields. These 40-60% reductions do not represent the majority of wells or fields in the U.S., but are possible under the right conditions for the highest-flowing wells and fields.

(6) While the effects of liners on low deliverability fields are small, they are not necessarily zero, and some response from operators may be necessary to maintain their baseline field deliverability.

(7) The modeling indicates that deeper wells experience greater reductions in deliverability than shallower wells with the introduction of liners, all other factors held equal

(8) While not explicitly modeled here, deliverability impacts of liners on directionally drilled wells could potentially be greater than shown in the current work because the length of tubing, and therefore tubing effects on deliverability, is greater for a deviated and/or horizontal well than a vertical well for a given reservoir depth.

(9) The modeling indicates that drawdowns at lower reservoir shut-in pressure (i.e. when inventory is at a relatively low level) are subject to slightly greater losses in deliverability than higher shut-in pressure (i.e. when inventory is at or near maximum capacity).

(10) This work should give Battelle/PHMSA a basis for evaluating operator concerns and identifying areas where claims are consistent, or inconsistent, with basic physics and coupled well/reservoir behavior.

7. REFERENCES

AGA (2017). "Survey of Underground Storage of Natural Gas in the United States and Canada: 2016/2017." American Gas Association. 31-Jul-2017. https://www.techstreet.com/aga/standards/aga-xu1706?product_id=2002040

API, AGA and INGAA (2016). "Underground Natural Gas Storage: Integrity & Safe Operations." American Petroleum Institute. 6-Jul. http://www.energyinfrastructure.org/energy-101/natural-gas-storage

Chaudhry, A. U. (2003). Gas Well Testing Handbook, Gulf Professional Publishing.

Crane (1982). Flow of Fluids Through Valves, Fittings, and Pipe (Technical Paper No. 410). New York, NY 10022, Crane Co.

Cullender, M. H. and R. Y. Smith (1956). "Practical Solution of Gas-Flow Equations for Wells and Pipelines with Large Temperature Gradients." Transactions of the American Institute of Mining and Metallurgical Engineers **207**.

Flanigan, O. (1995). Underground Gas Storage Facilities Design and Implementation. Houston, TX USA, Gulf Publishing Company.

Freifield, B., C. Oldenburg, P. Jordan, L. Pan, S. Perfect, J. Morris, J. White, S. Bauer, D. Blankenship, B. Roberts, G. Bromhal, D. Glosser, D. Wyatt and K. Rose (2016). "Well Integrity for Natural Gas Storage in Depleted Reservoir and Aquifers." ***SAND2016-8860R***. Sandia National Laboratories, Albuquerque, NM 1-Sep.

Frick, T. C. and W. Taylor (1962). Petroleum Production Handbook, McGraw-Hill.

Guo, B. and A. Ghalambor (2012). Natural Gas Engineering Handbook, 2nd Ed. Houston, TX, Gulf Publishing Company.

Johnson, A. (2016). "Underground Natural Gas Storage." *presented at* **2016 Government/Industry Pipeline R&D Forum**, Cleveland, OH, 16-Nov,

King, G. (2018). "PNG 301: Introduction to Petroleum and Natural Gas Engineering." John A. Dutton e-Education Institute, from https://www.e-education.psu.edu/png301/.

Menon, S. (2011). Pipeline Planning and Construction Field Manual, Elsevier.

USDOE (2016). "Ensuring Safe and Reliable Underground Natural Gas Storage, Final Report of the Interagency Task Force on Natural Gas Storage Safety." U.S. Department of Energy, Washington, DC https://www.energy.gov/downloads/report-ensuring-safe-and-reliable-underground-natural-gas-storage

USS (2014). "Oil Country Tubular Goods." ***Rev 3, 6/14***. U.S. Steel Tubular Products, Pittsburgh, PA 15219. https://info.usstubular.com/octg-catalog

This page left blank

APPENDIX A. RESERVOIR PERFORMANCE SIMULATIONS FOR FIELD C (HOCKEY STICK DISTRIBUTION)

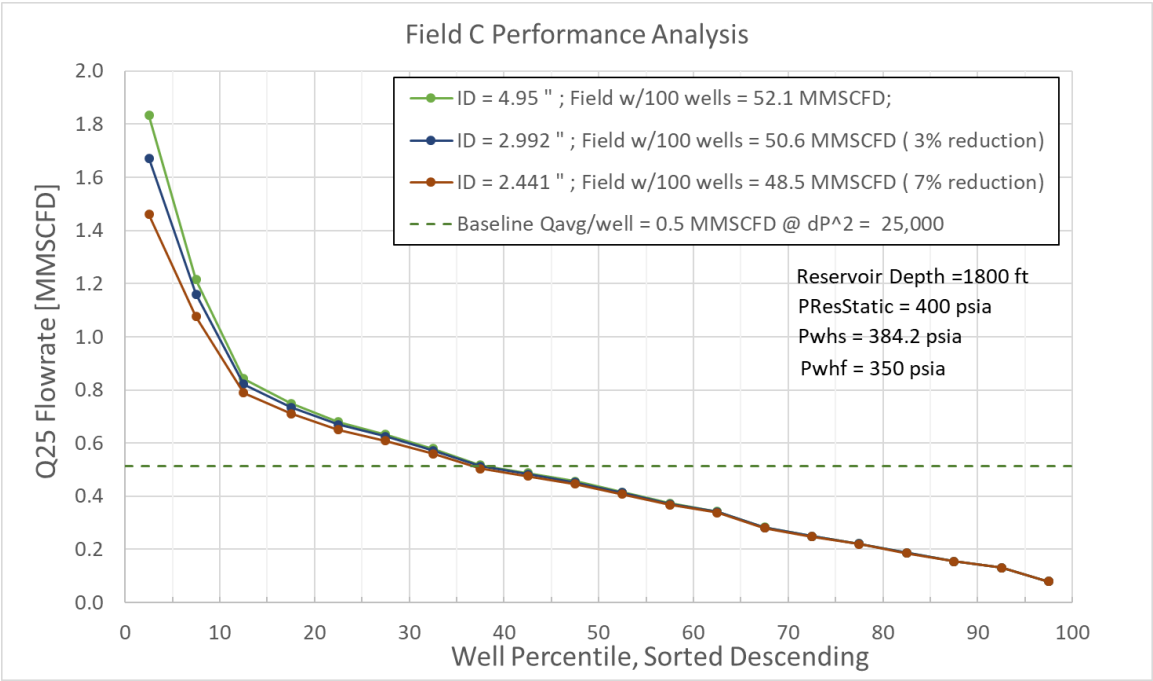

Figure A- 1. Q25 flowrates for Field C wells with baseline $Q_{avg/well}$ = 0.5 MMSCFD in 4.95" ID wells showing reductions at two liner sizes, 2.992 and 2.441"

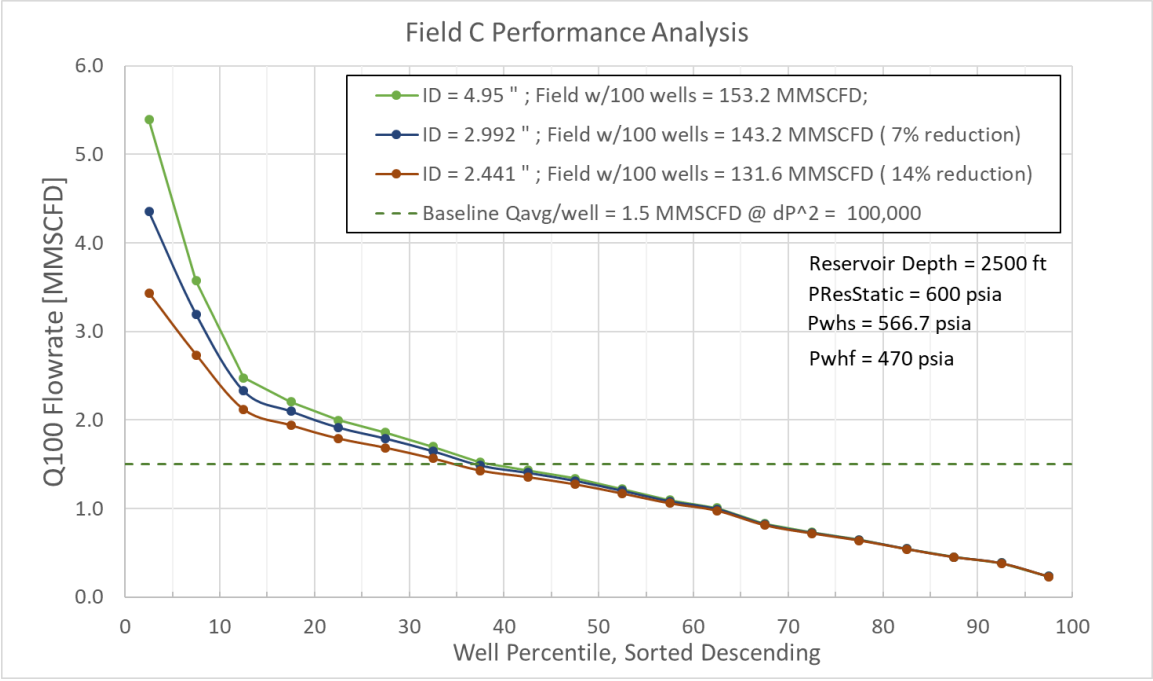

Figure A- 2. Q100 flowrates for Field C wells with baseline $Q_{avg/well}$ = 1.5 MMSCFD in 4.95" ID wells showing reductions at two liner sizes, 2.992 and 2.441"

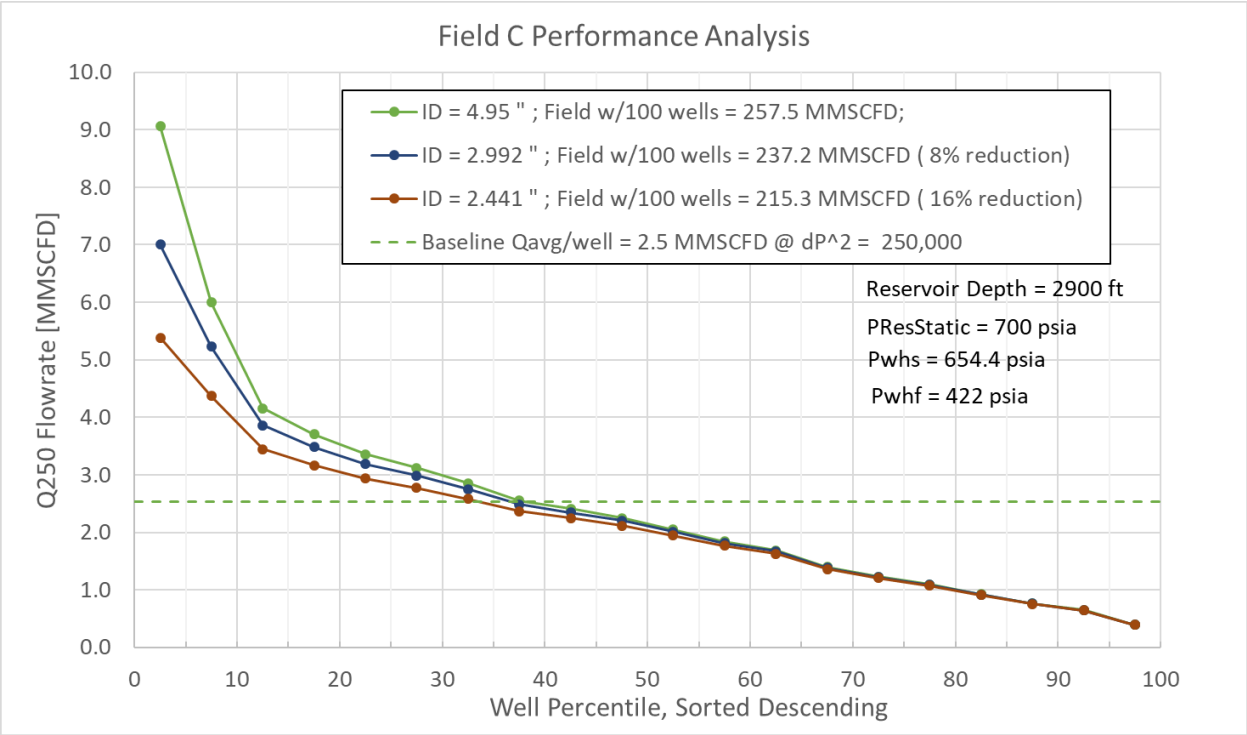

Figure A- 3. Q250 flowrates for Field C wells with baseline $Q_{avg/well}$ = 2.5 MMSCFD in 4.95" ID wells showing reductions at two liner sizes, 2.992 and 2.441"

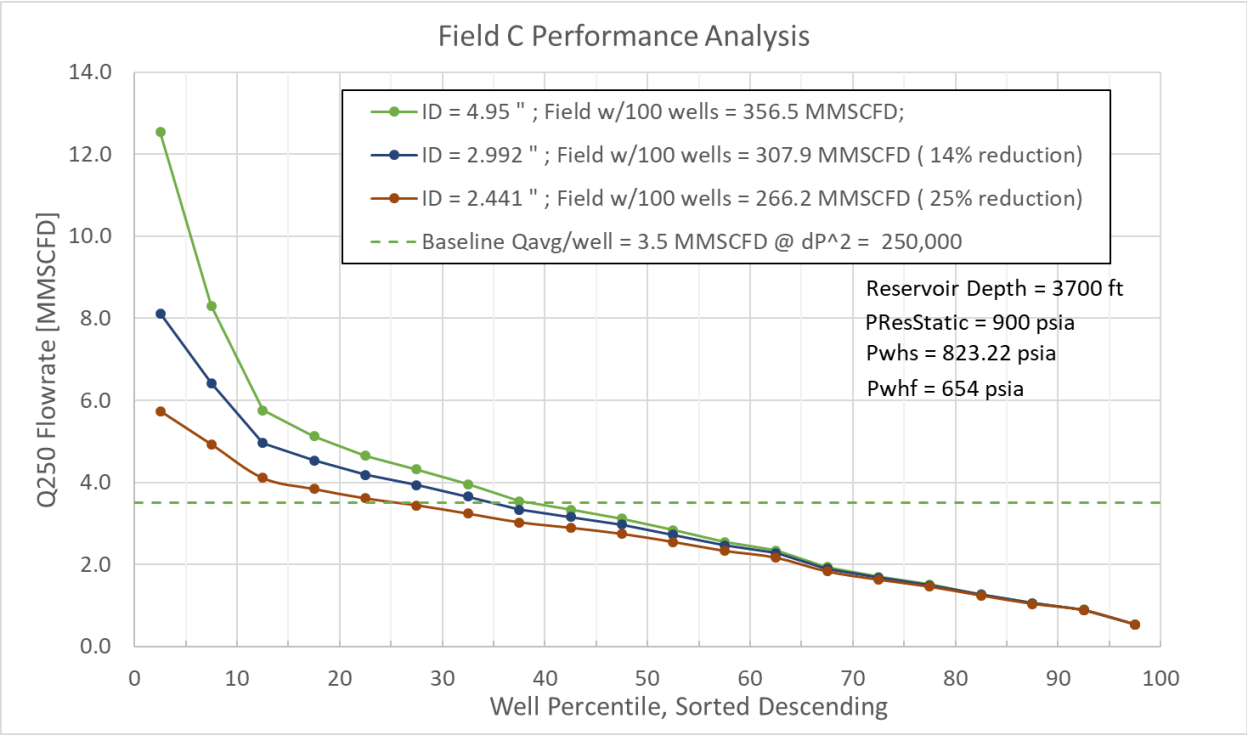

Figure A- 4. Q250 flowrates for Field C wells with baseline $Q_{avg/well}$ = 3.5 MMSCFD in 4.95" ID wells showing reductions at two liner sizes, 2.992 and 2.441"

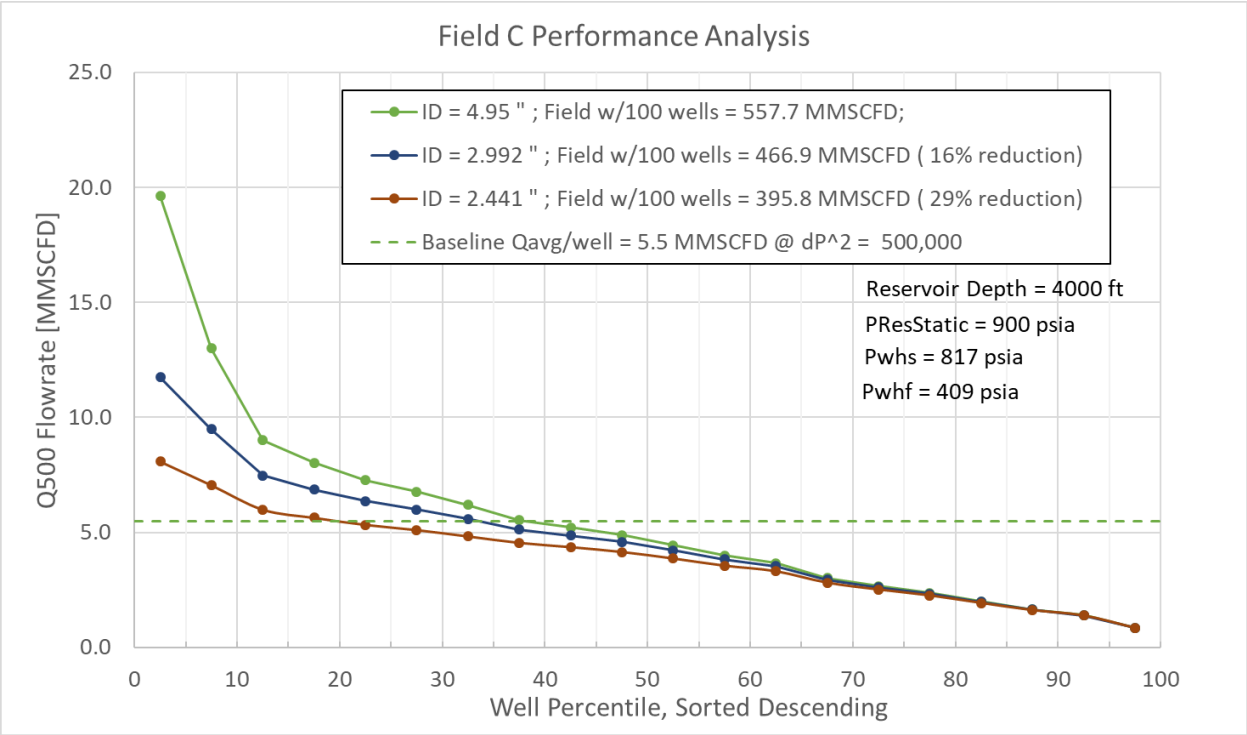

Figure A- 5. Q500 flowrates for Field C wells with baseline $Q_{avg/well}$ = 5.5 MMSCFD in 4.95" ID wells showing reductions at two liner sizes, 2.992 and 2.441".

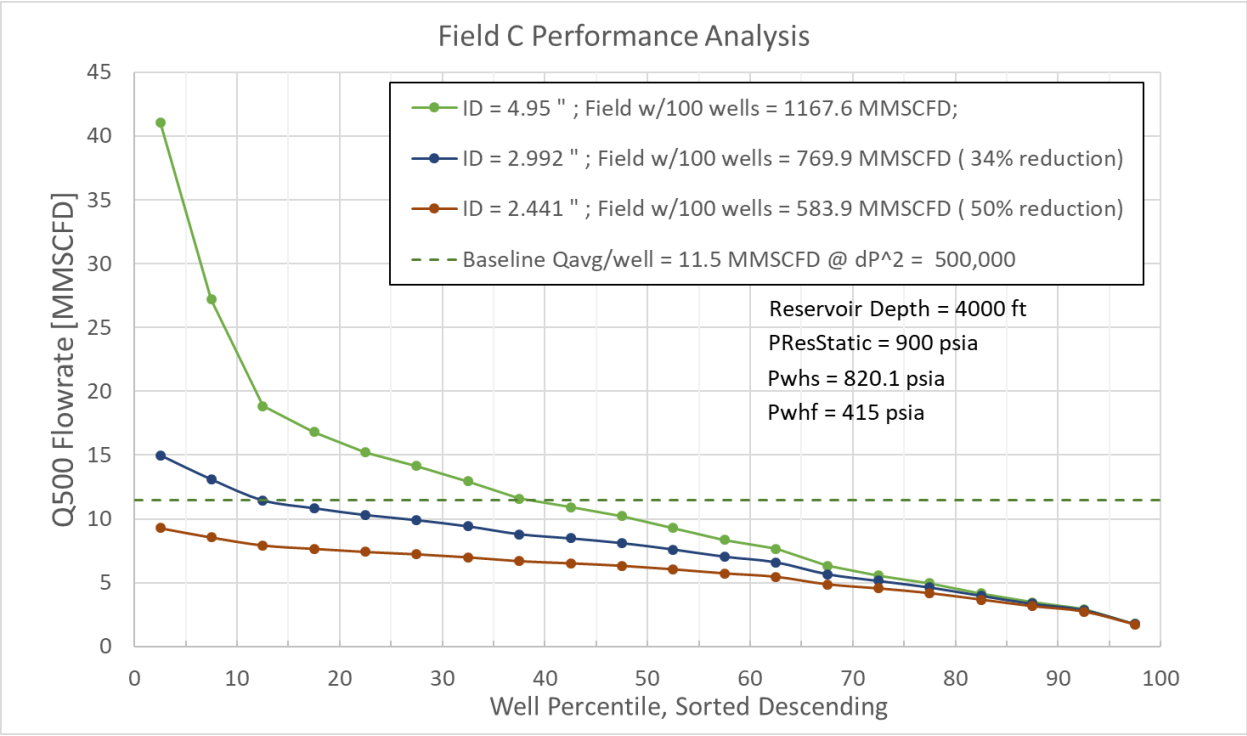

Figure A- 6. Q500 flowrates for Field C wells with baseline $Q_{avg/well}$ = 11.5 MMSCFD in 4.95" ID wells showing reductions at two liner sizes, 2.992 and 2.441".

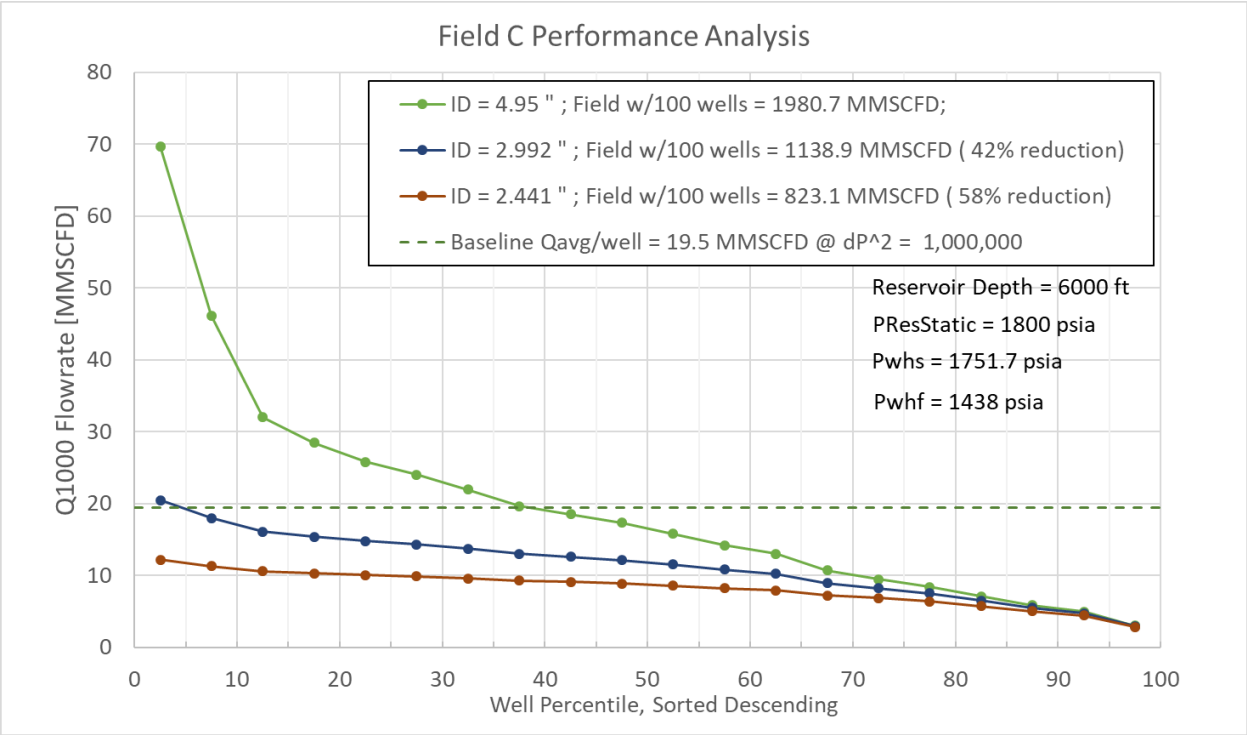

Figure A- 7. Q1,000 flowrates for Field C wells with baseline $Q_{avg/well}$ = 19.5 MMSCFD in 4.95" ID wells showing reductions at two liner sizes, 2.992 and 2.441".

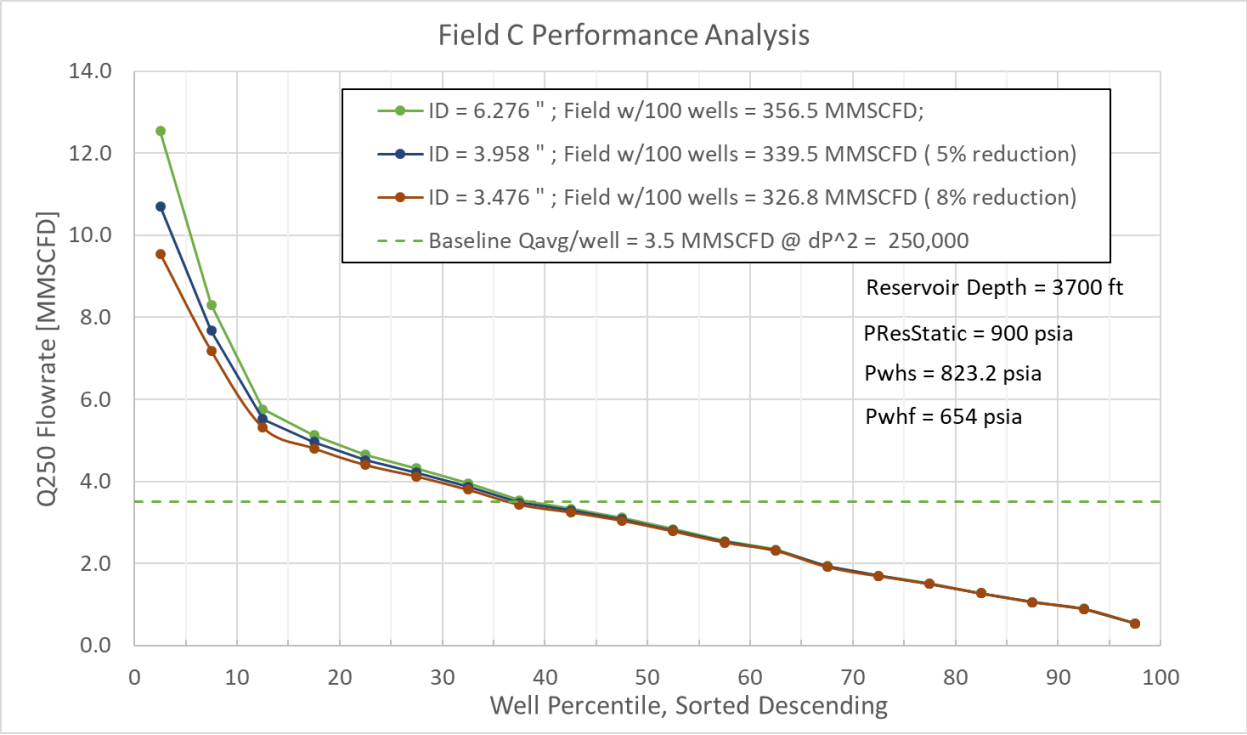

Figure A- 8. Q250 flowrates for Field C wells with baseline $Q_{avg/well}$ = 3.5 MMSCFD in 6.276" ID wells showing reductions at two liner sizes, 3.958 and 3.476".

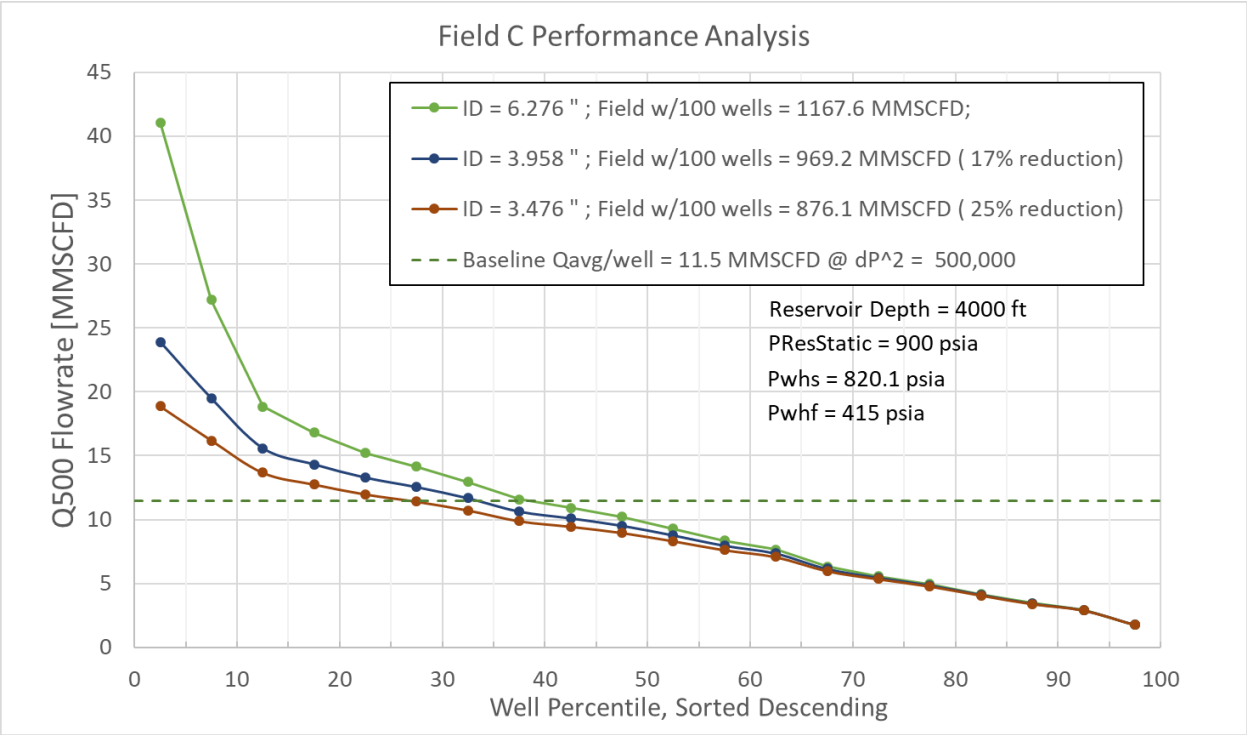

Figure A- 9. Q500 flowrates for Field C wells with baseline $Q_{avg/well}$ = 11.5 MMSCFD in 6.276" ID wells showing reductions at two liner sizes, 3.958 and 3.476".

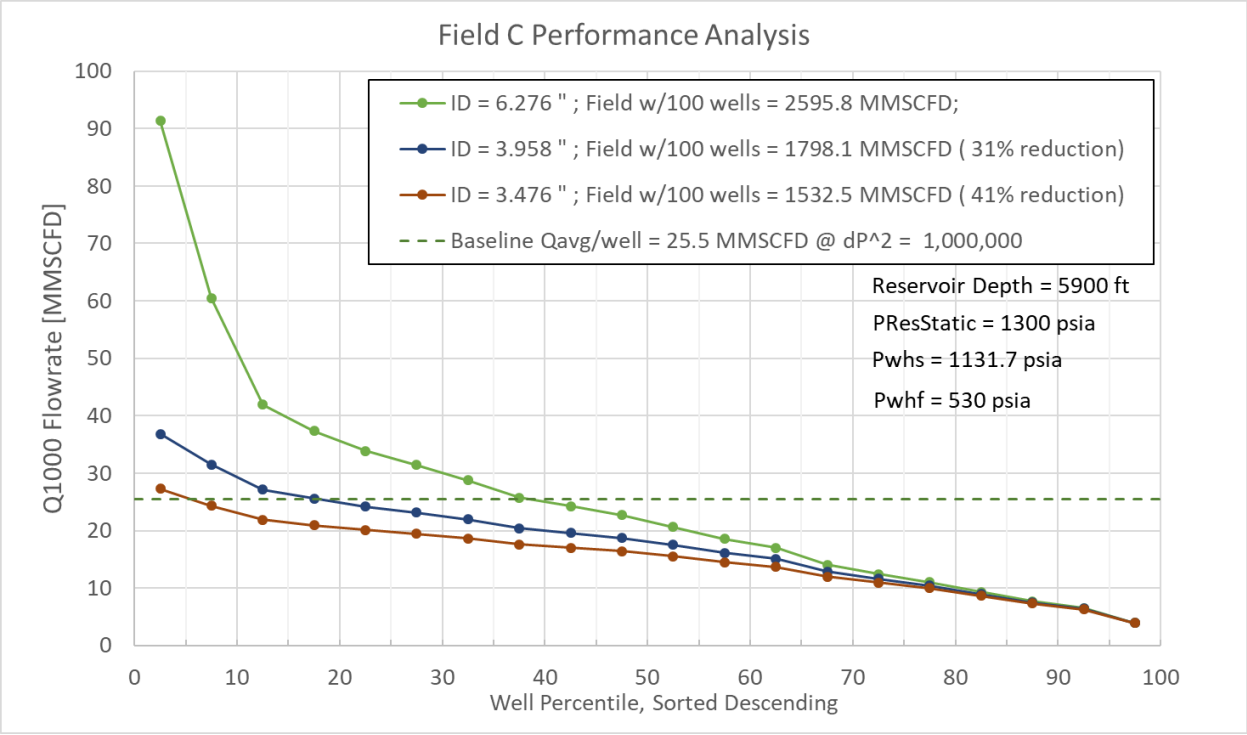

Figure A- 10. Q1,000 flowrates for Field C wells with baseline $Q_{avg/well}$ = 25.5 MMSCFD in 6.276" ID wells showing reductions at two liner sizes, 3.958 and 3.476".

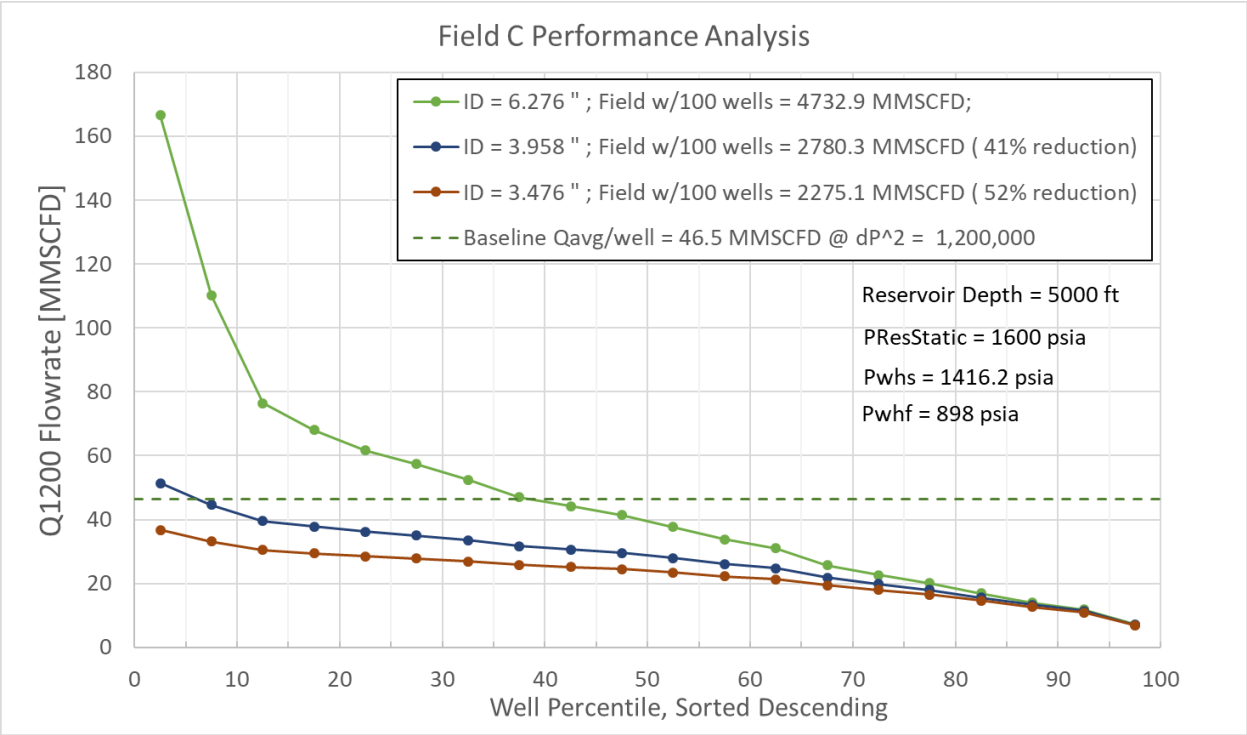

Figure A- 11. Q1,200 flowrates for Field C wells with baseline $Q_{avg/well}$ = 46.5 MMSCFD in 6.276" ID wells showing reductions at two liner sizes, 3.958 and 3.476".

Table A- 1. Results matrix for Field C showing % reductions in field deliverability for all simulated $Q_{avg/well}$ bins in 4.95" ID wells with reductions at two liner sizes, 2.992 and 2.441".

Field C Results Matrix			Base ID = 4.95 in	
Qavg/well [MMSCFD]	P_{RSI} [psia]	P_{WHS}^2-P_{WHF}^2 [psi^2]	Liner 1 ID = 2.992 in % Reduction	Liner 2 ID = 2.441 in % Reduction
0.5	400	25,000	3%	7%
1.5	600	100,000	7%	14%
2.5	700	250,000	8%	16%
3.5	900	250,000	14%	25%
5.5	900	500,000	16%	29%
11.5	900	500,000	34%	50%
19.5	1800	1,000,000	42%	58%

Table A- 2. Results matrix for Field C showing % reductions in field deliverability for all simulated $Q_{avg/well}$ bins in 6.276" ID wells with reductions at two liner sizes, 3.958 and 3.476".

Field C Results Matrix			Base ID = 6.276 in	
Qavg/well [MMSCFD]	P_{RSI} [psia]	P_{WHS}^2-P_{WHF}^2 [psi^2]	Liner 1 ID = 3.958 in % Reduction	Liner 2 ID = 3.476 in % Reduction
3.5	900	250,000	5%	8%
11.5	900	500,000	17%	25%
25.5	1300	1,000,000	31%	41%
46.5	1600	1,200,000	41%	52%

This page left blank

APPENDIX B. RESERVOIR PERFORMANCE SIMULATIONS FOR FIELD G (LINEAR DISTRBUTION)

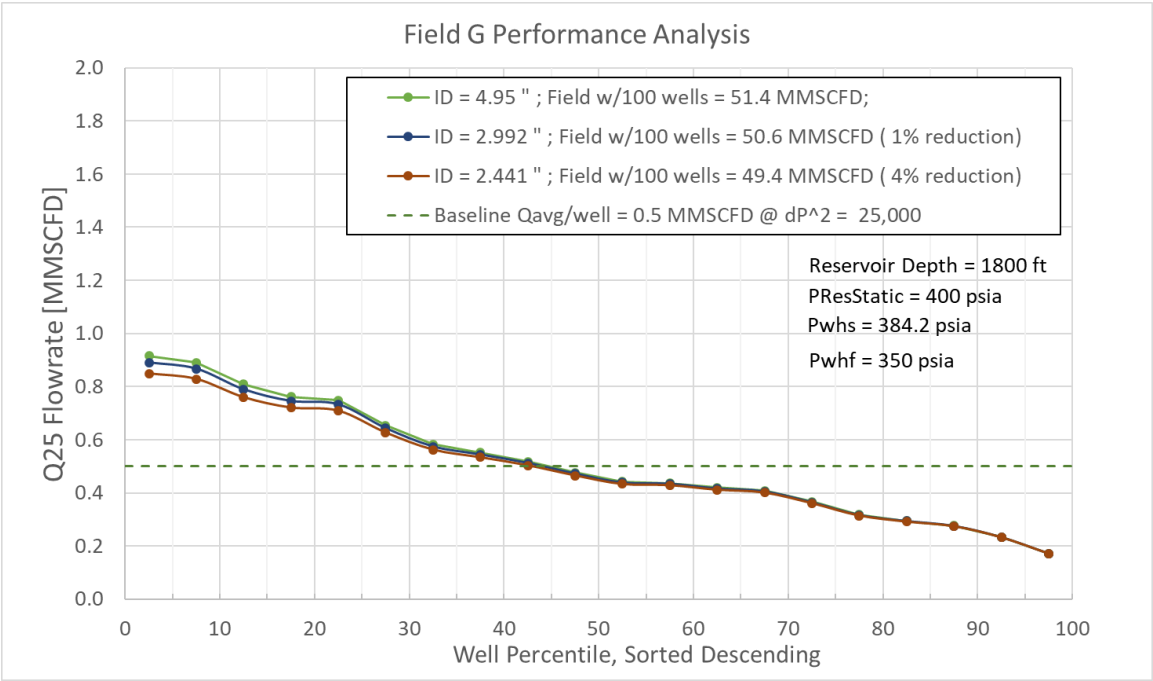

Figure B- 1. Q25 flowrates for Field G wells with baseline $Q_{avg/well}$ = 0.5 MMSCFD in 4.95" ID wells showing reductions at two liner sizes, 2.992 and 2.441".

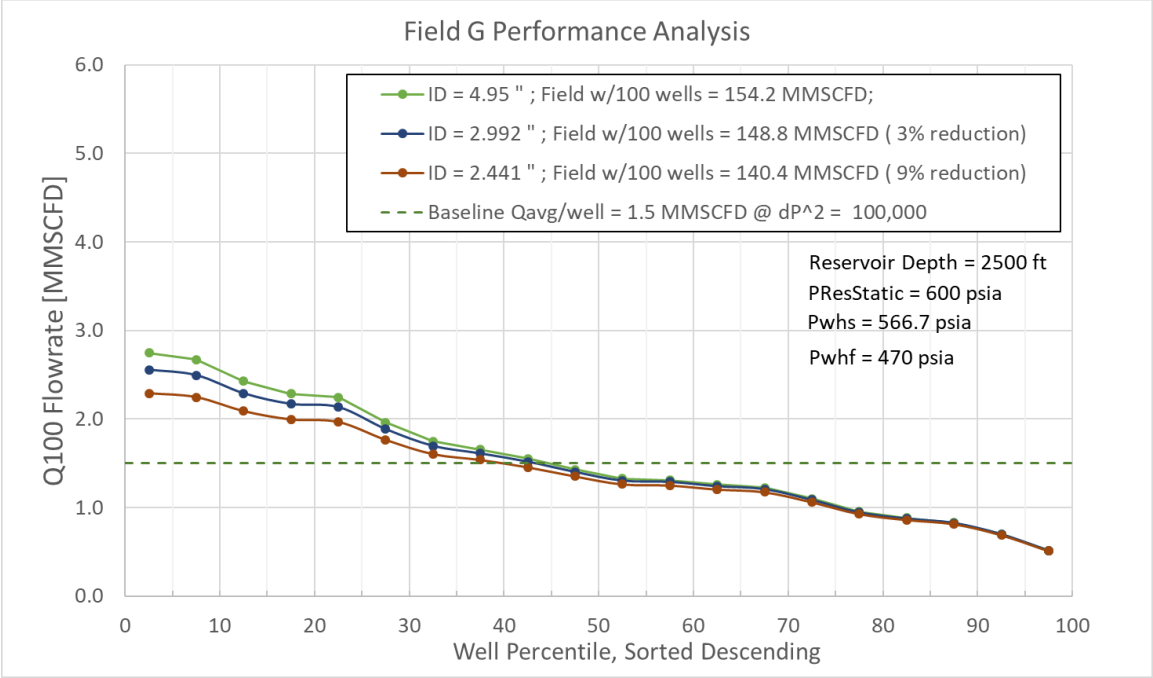

Figure B- 2. Q100 flowrates for Field G wells with baseline $Q_{avg/well}$ = 1.5 MMSCFD in 4.95" ID wells showing reductions at two liner sizes, 2.992 and 2.441".

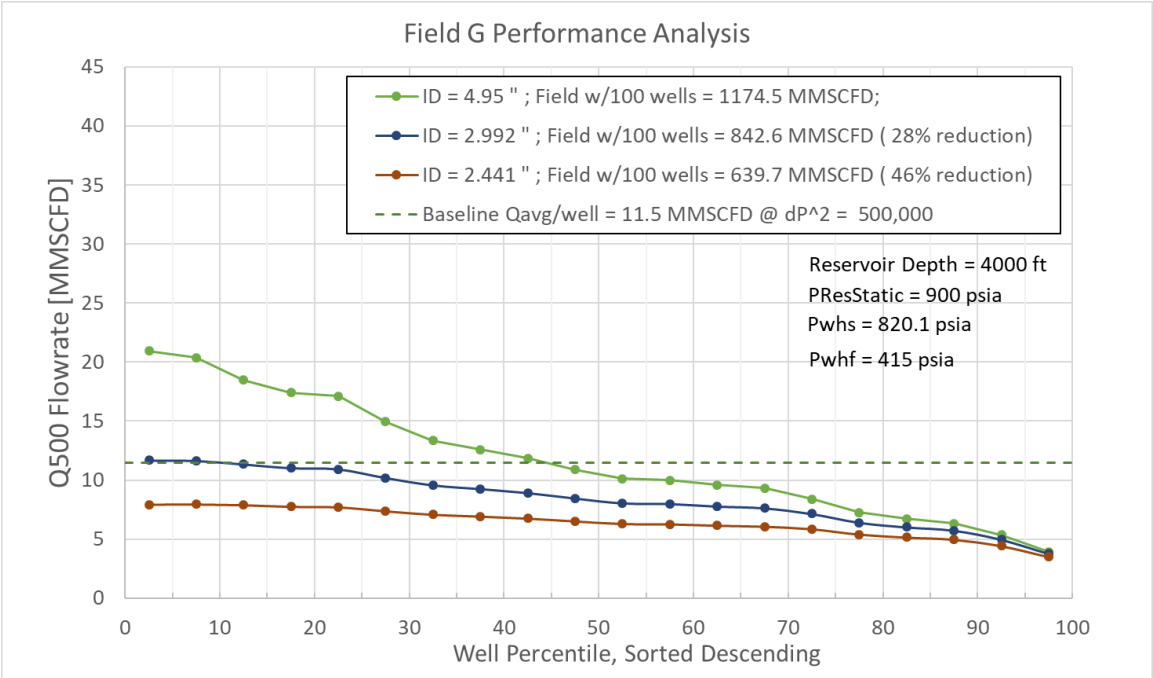

Figure B- 3. Q500 flowrates for Field G wells with baseline $Q_{avg/well}$ = 11.5 MMSCFD in 4.95" ID wells showing reductions at two liner sizes, 2.992 and 2.441".

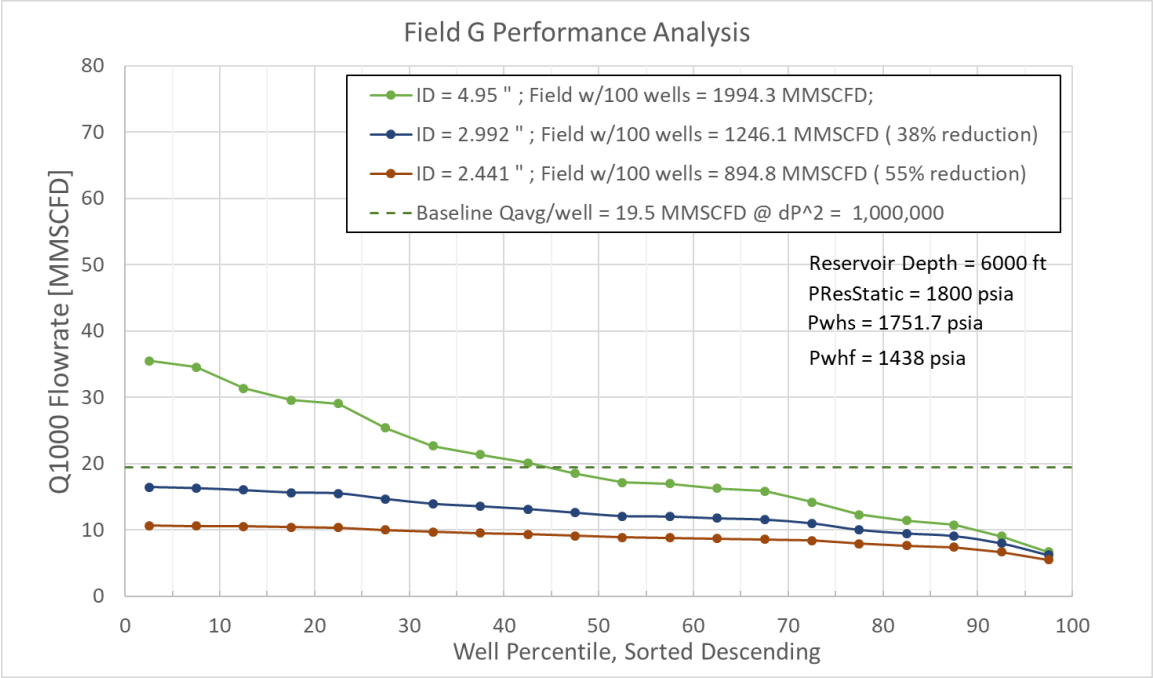

Figure B- 4. Q1000 flowrates for Field G wells with baseline $Q_{avg/well}$ = 19.5 MMSCFD in 4.95" ID wells showing reductions at two liner sizes, 2.992 and 2.441".

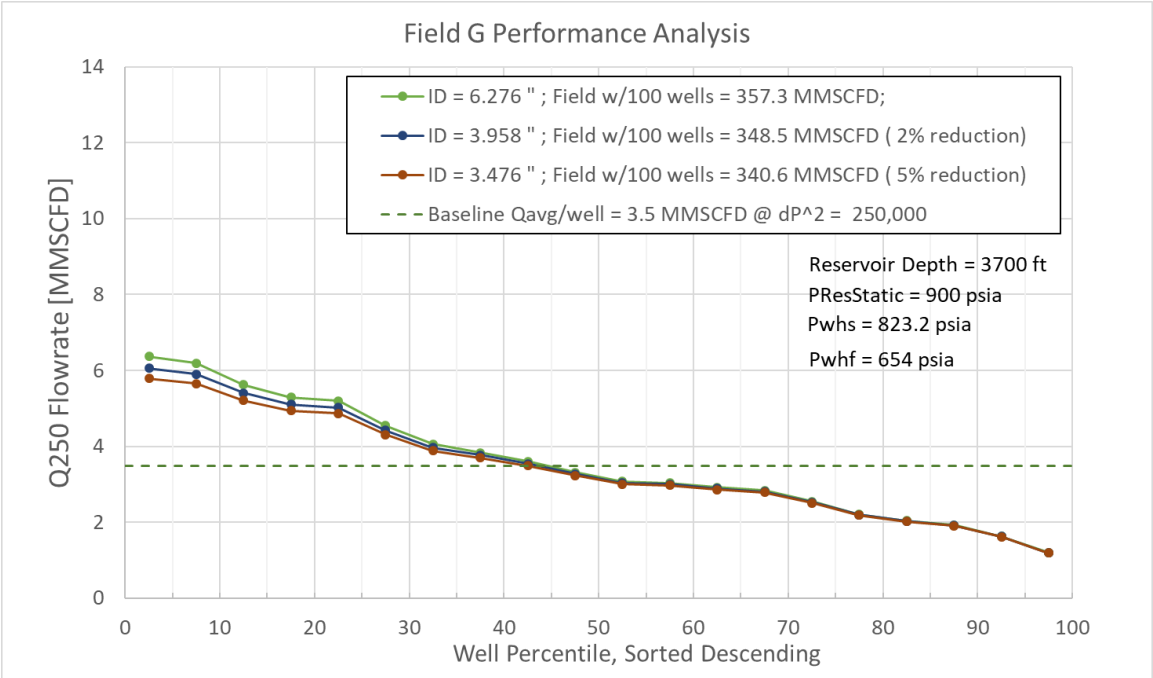

Figure B- 5. Q250 flowrates for Field G wells with baseline $Q_{avg/well}$ = 3.5 MMSCFD in 6.276" wells showing reductions at two liner sizes, 3.958 and 3.756".

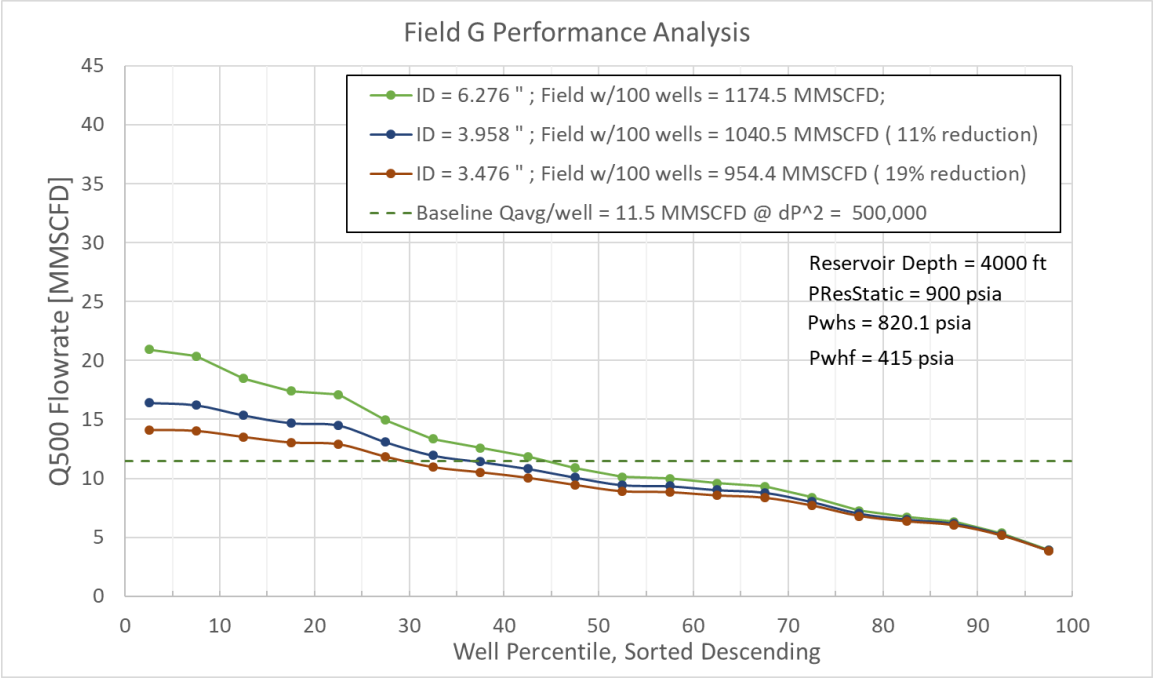

Figure B- 6. Q500 flowrates for Field G wells with baseline $Q_{avg/well}$ = 11.5 MMSCFD in 6.276" wells showing reductions at two liner sizes, 3.958 and 3.756".

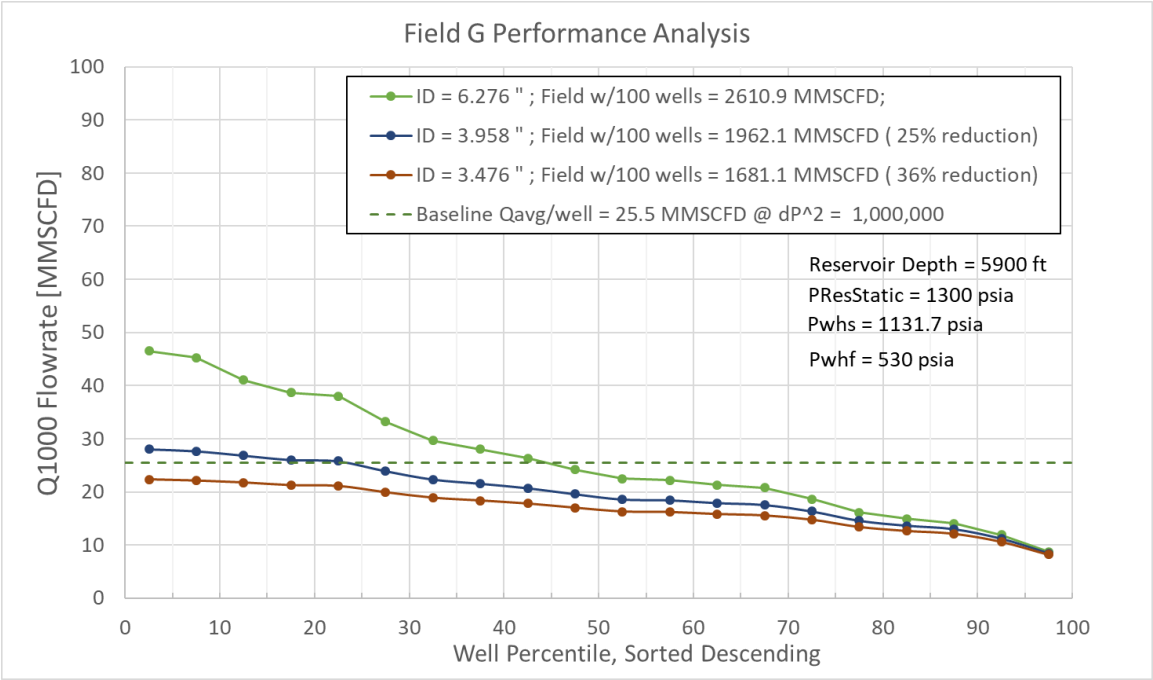

Figure B- 7. Q1,000 flowrates for Field G wells with baseline $Q_{avg/well}$ = 25.5 MMSCFD in 6.276" wells showing reductions at two liner sizes, 3.958 and 3.756".

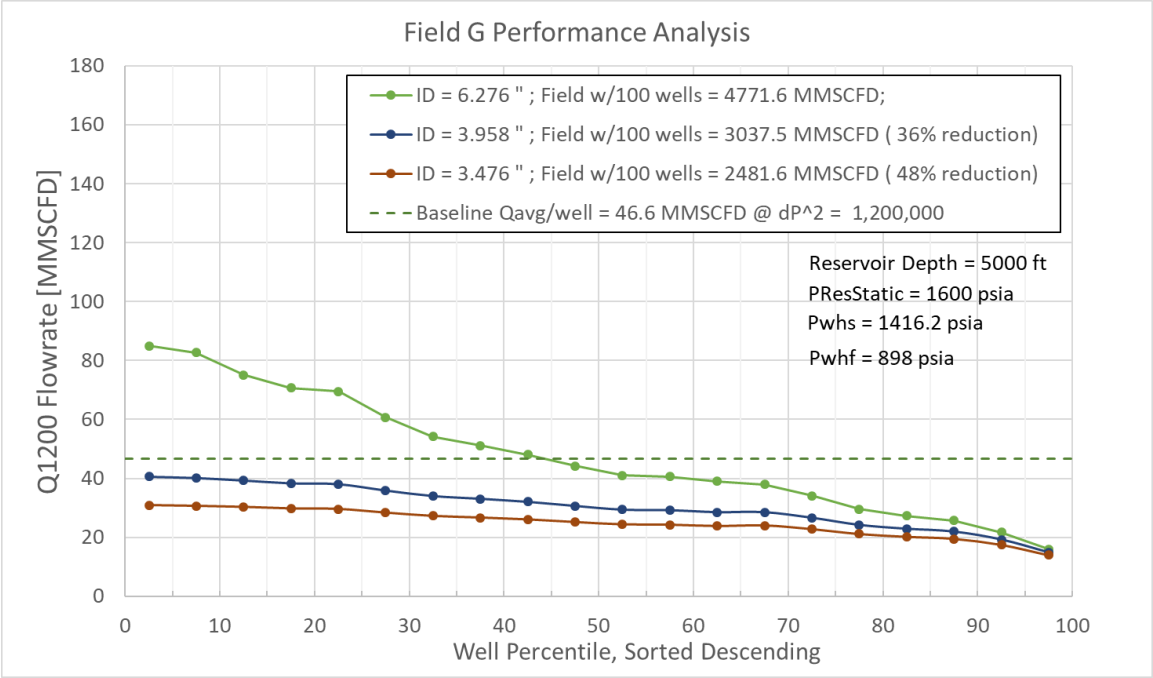

Figure B- 8. Q1,200 flowrates for Field G wells with baseline $Q_{avg/well}$ = 46.6 MMSCFD in 6.276" wells showing reductions at two liner sizes, 3.958 and 3.756".

Table B- 1. Results matrix for Field G showing % reductions in field deliverability for all simulated $Q_{avg/well}$ bins in 4.95" ID wells with reductions at two liner sizes, 2.992 and 2.441".

Field G Results Matrix			Base ID = 4.95 in	
Qavg/well [MMSCFD]	P_{RSI} [psia]	P_{WHS}^2-P_{WHF}^2 [psi^2]	Liner 1 ID = 2.992 in % Reduction	Liner 2 ID = 2.441 in % Reduction
0.5	400	25,000	1%	4%
1.5	600	100,000	3%	9%
11.5	900	500,000	28%	46%
19.5	1800	1,000,000	38%	55%

Table B- 2. Results matrix for Field G showing % reductions in field deliverability for all simulated $Q_{avg/well}$ bins in 6.276" ID wells with reductions at two liner sizes, 3.958 and 3.476".

Field G Results Matrix			Base ID = 6.276 in	
Qavg/well [MMSCFD]	P_{RSI} [psia]	P_{WHS}^2-P_{WHF}^2 [psi^2]	Liner 1 ID = 3.958 in % Reduction	Liner 2 ID = 3.476 in % Reduction
3.5	900	250,000	2%	5%
11.5	900	500,000	11%	19%
25.5	1300	1,000,000	25%	36%
46.6	1600	1,200,000	36%	48%

This page left blank

APPENDIX C. RESERVOIR PERFOMANCE SIMULATIONS SHOWING DEPTH DEPENDENCE

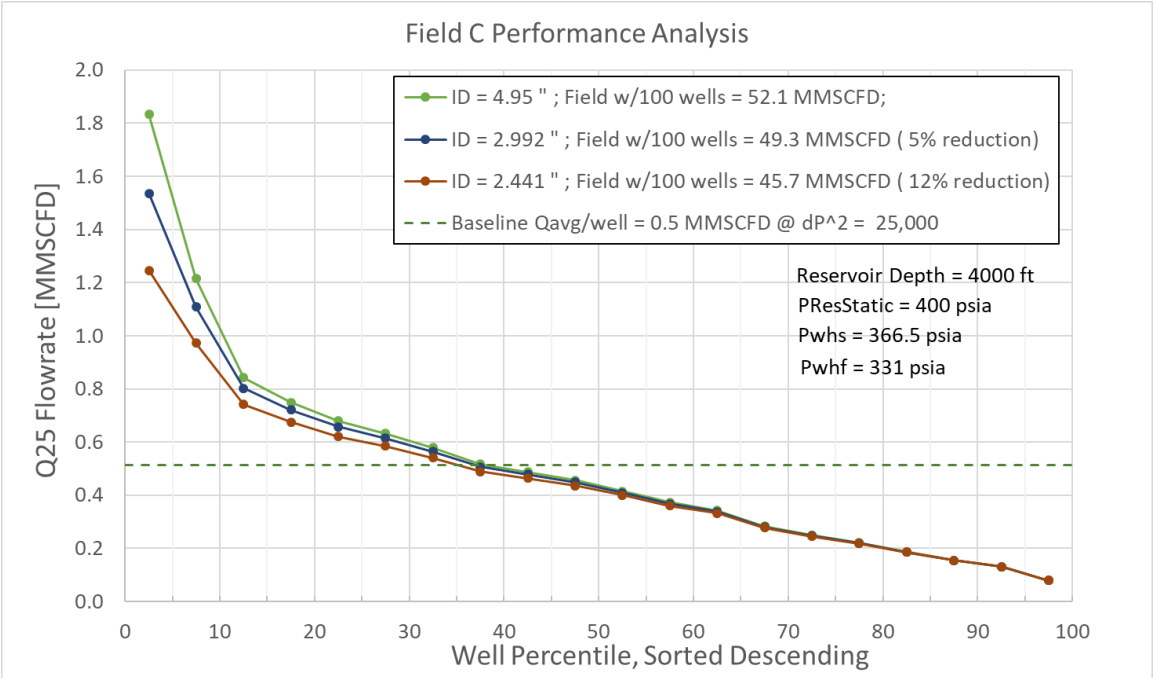

Figure C- 1. Q25 flowrates for Field C wells with baseline $Q_{avg/well}$ = 0.5 MMSCFD in 4.95" ID wells showing reductions at two liner sizes, 2.992 and 2.441" and reservoir/well depth = 4,000 ft.

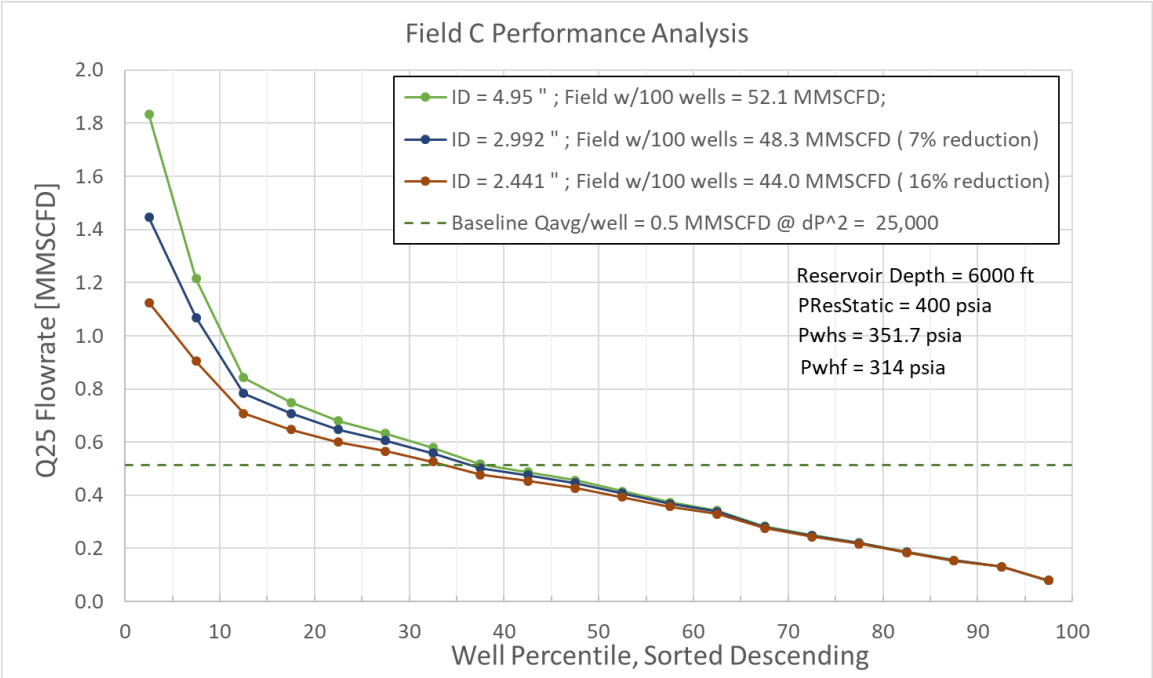

Figure C- 2. Q25 flowrates for Field C wells with baseline $Q_{avg/well}$ = 0.5 MMSCFD in 4.95" ID wells showing reductions at two liner sizes, 2.992 and 2.441" and reservoir/well depth = 6,000 ft.

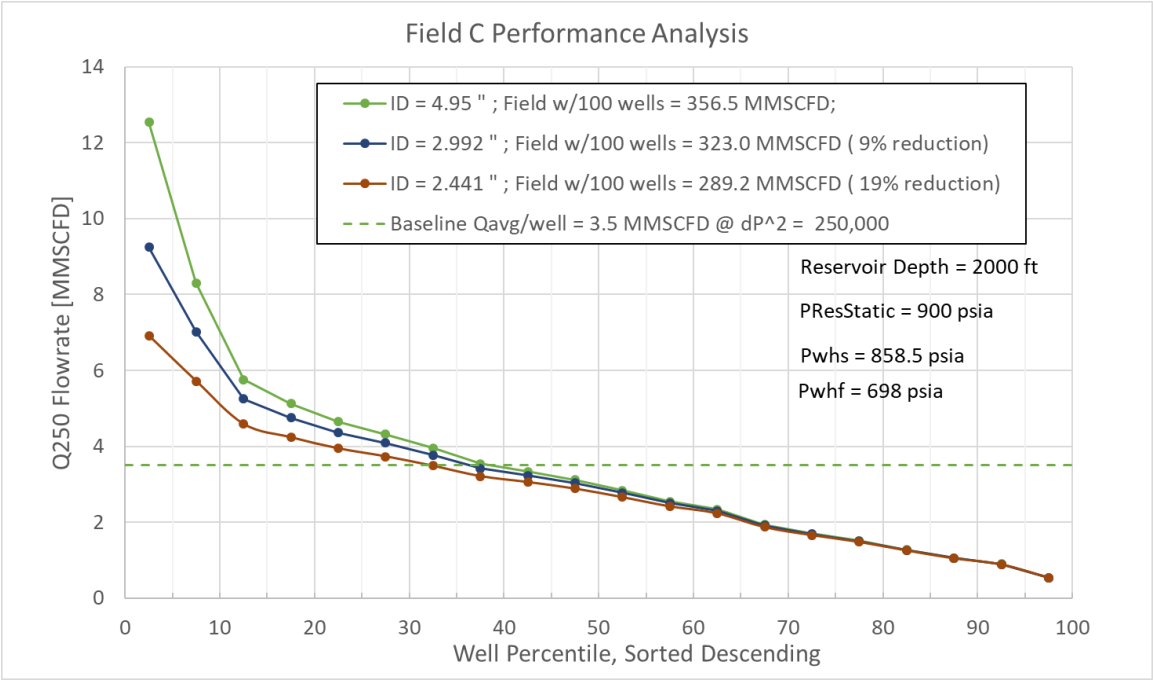

Figure C- 3. Q250 flowrates for Field C wells with baseline $Q_{avg/well}$ = 3.5 MMSCFD in 4.95" ID wells showing reductions at two liner sizes, 2.992 and 2.441" and reservoir/well depth = 2,000 ft.

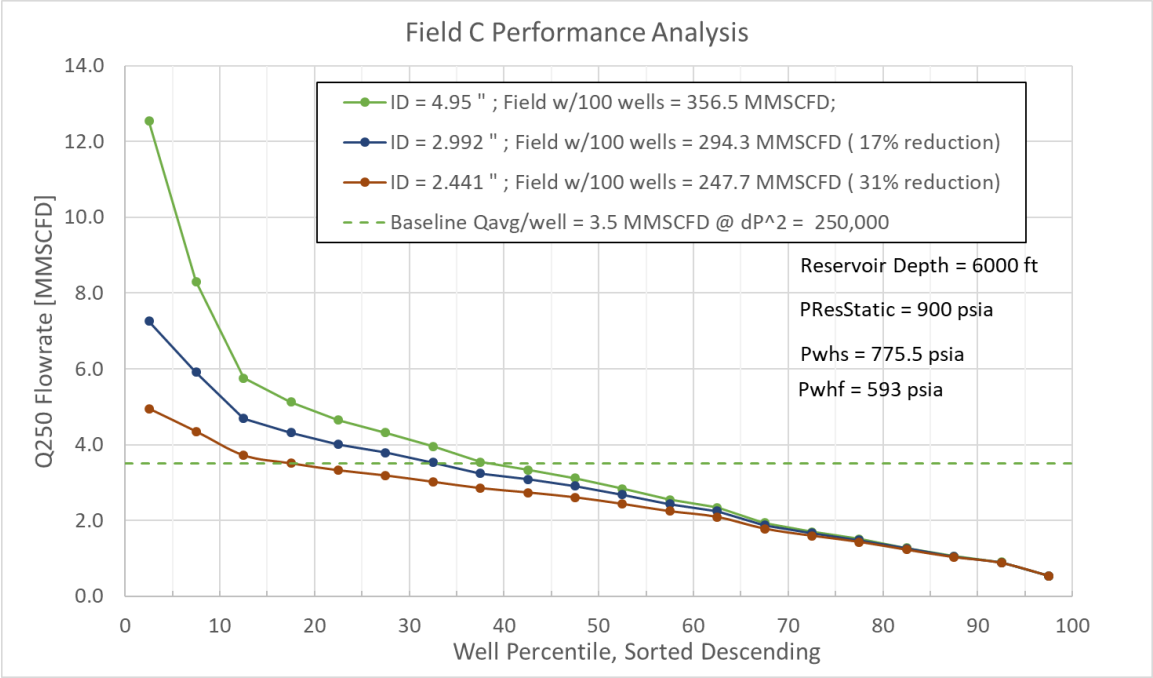

Figure C- 4. Q250 flowrates for Field C wells with baseline $Q_{avg/well}$ = 3.5 MMSCFD in 4.95" ID wells showing reductions at two liner sizes, 2.992 and 2.441" and reservoir/well depth = 6,000 ft.

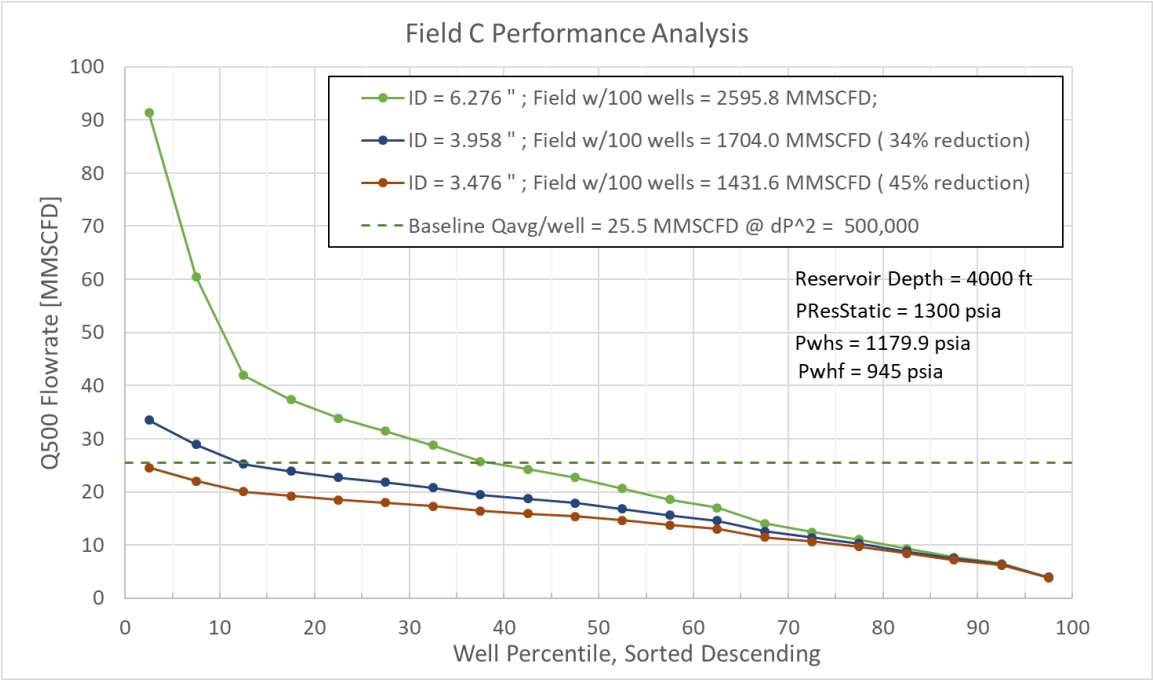

Figure C- 5. Q500 flowrates for Field C wells with baseline $Q_{avg/well}$ = 25.5 MMSCFD in 6.276" wells showing reductions at two liner sizes, 3.958 and 3.756" and reservoir depth = 4,000 ft.

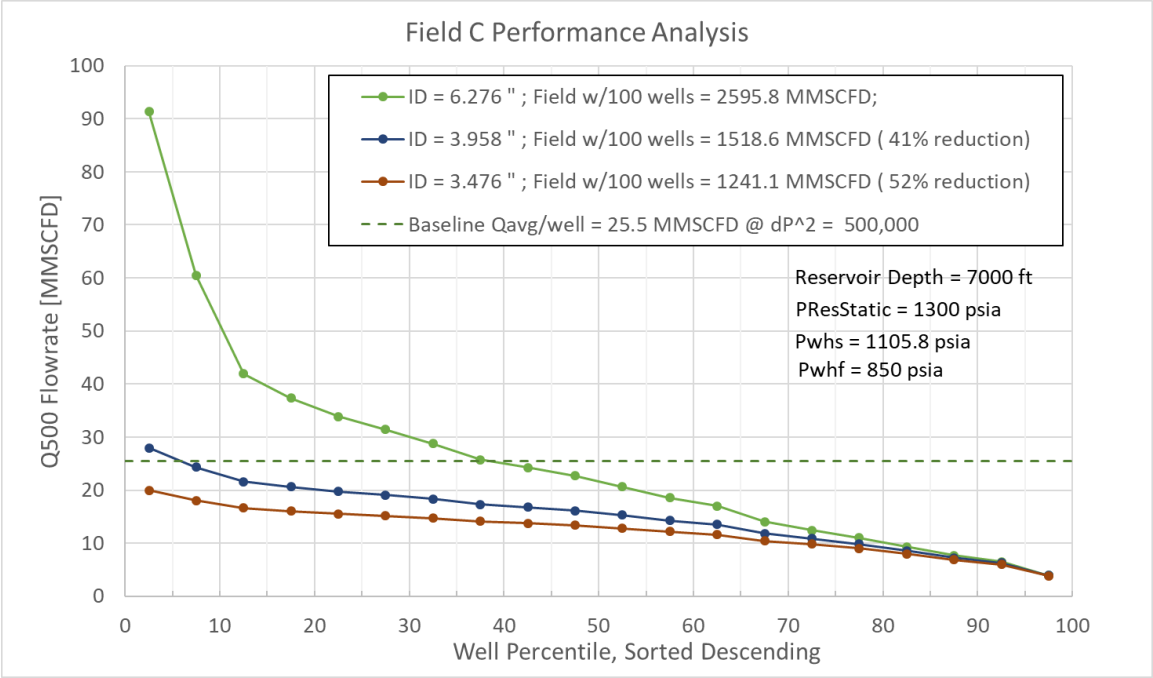

Figure C- 6. Q500 flowrates for Field C wells with baseline $Q_{avg/well}$ = 25.5 MMSCFD in 6.276" wells showing reductions at two liner sizes, 3.958 and 3.756" and reservoir depth = 7,000 ft.

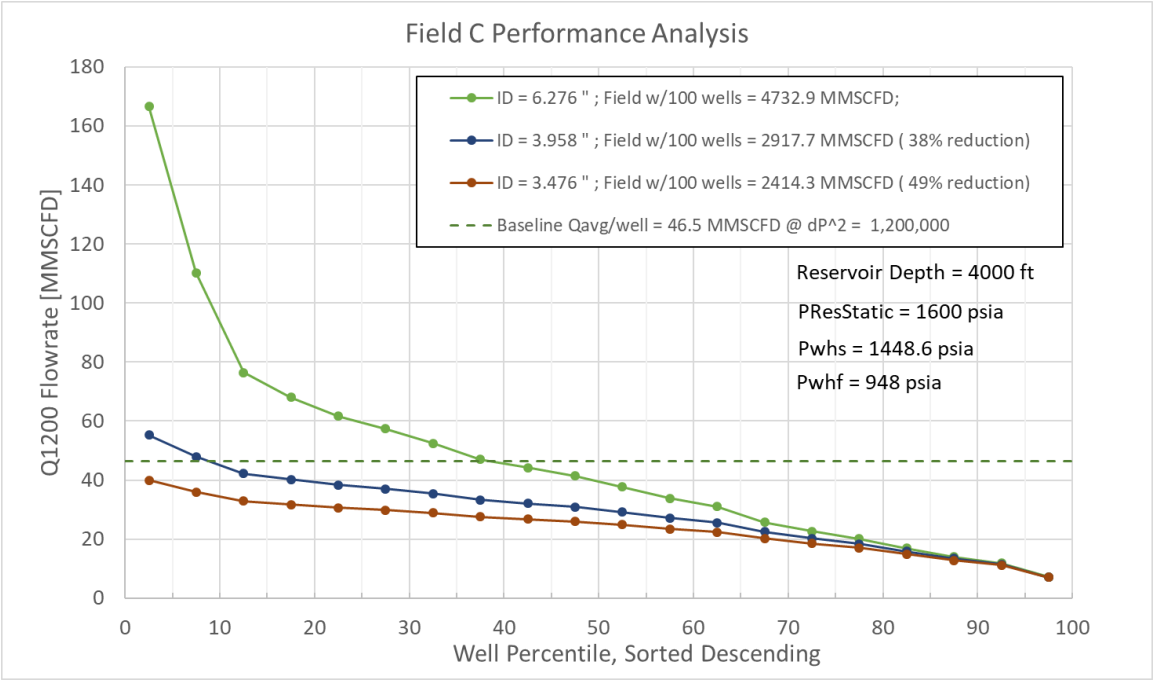

Figure C- 7. Q1,200 flowrates for Field C wells with baseline $Q_{avg/well}$ = 46.5 MMSCFD in 6.276" wells showing reductions at two liner sizes, 3.958 and 3.756" and reservoir depth = 4,000 ft.

Table C- 1. Results matrix for Field C showing % reductions in deliverability with depth for selected $Q_{avg/well}$ bins in 4.95" ID wells showing reductions at two liner sizes, 2.992 and 2.441".

Depth Series Field C				Base ID = 4.95in	
Qavg/well [MMSCFD]	Depth [ft]	P_{RSI} [psia]	P_{WHS}^2-P_{WHF}^2 [psi^2]	Liner 1 ID = 2.992 in % Reduction	Liner 2 ID = 2.441 in % Reduction
0.5	1,800	400	25,000	3%	7%
0.5	4,000	400	25,000	5%	12%
0.5	6,000	400	25,000	7%	16%
3.5	2,000	900	250,000	9%	19%
3.5	3,700	900	250,000	14%	25%
3.5	6,000	900	250,000	17%	31%

Table C- 2. Results matrix for Field C showing % reductions in deliverability with depth for selected $Q_{avg/well}$ bins in 6.276" ID wells showing reductions at two liner sizes, 3.958 and 3.476".

Depth Series Field C				Base ID = 6.276in	
Qavg/well	Depth	P_{RSI}	P_{WHS}^2-P_{WHF}^2	Liner 1 ID = 3.958 in	Liner 2 ID = 3.476 in
[MMSCFD]	[ft]	[psia]	[psi^2]	% Reduction	% Reduction
25.5	4,000	1300	500,000	34%	45%
25.5	5,900	1300	500,000	39%	50%
25.5	7,000	1300	500,000	41%	52%
46.5	4,000	1600	1,200,000	38%	49%
46.5	5,000	1600	1,200,000	41%	52%

This page left blank

APPENDIX D. RESERVOIR PERFOMANCE SIMULATIONS SHOWING RESERVOIR SHUT-IN PRESSURE DEPENDENCE

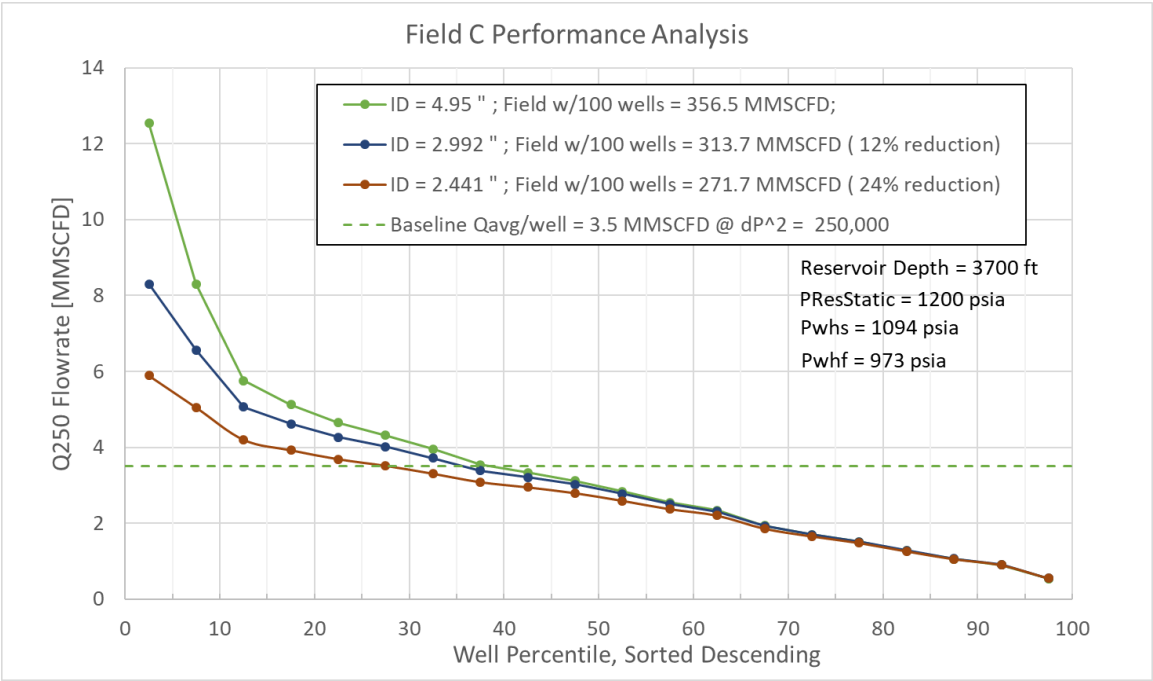

Figure D- 1. Q250 flowrates for Field C wells with baseline $Q_{avg/well}$ = 3.5 MMSCFD and P_{RSI} = 1200 psia in 4.95" ID wells showing reductions at two liner sizes, 2.992 and 2.441".

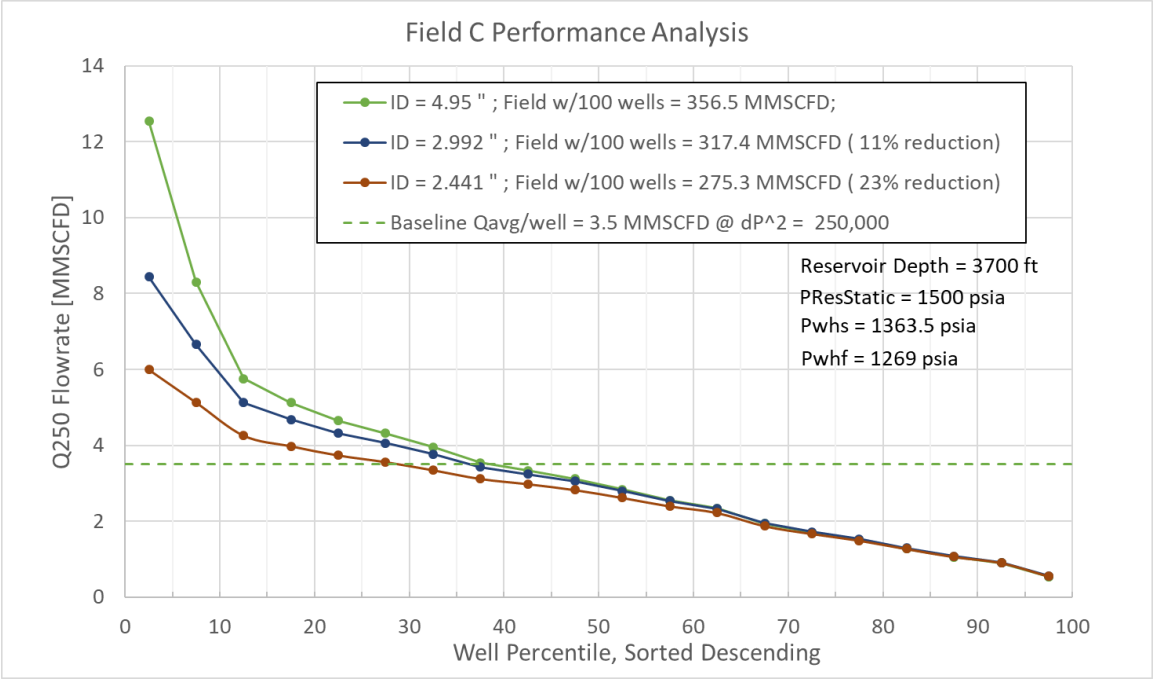

Figure D- 2. Q250 flowrates for Field C wells with baseline $Q_{avg/well}$ = 3.5 MMSCFD and P_{RSI} = 1500 psia in 4.95" ID wells showing reductions at two liner sizes, 2.992 and 2.441".

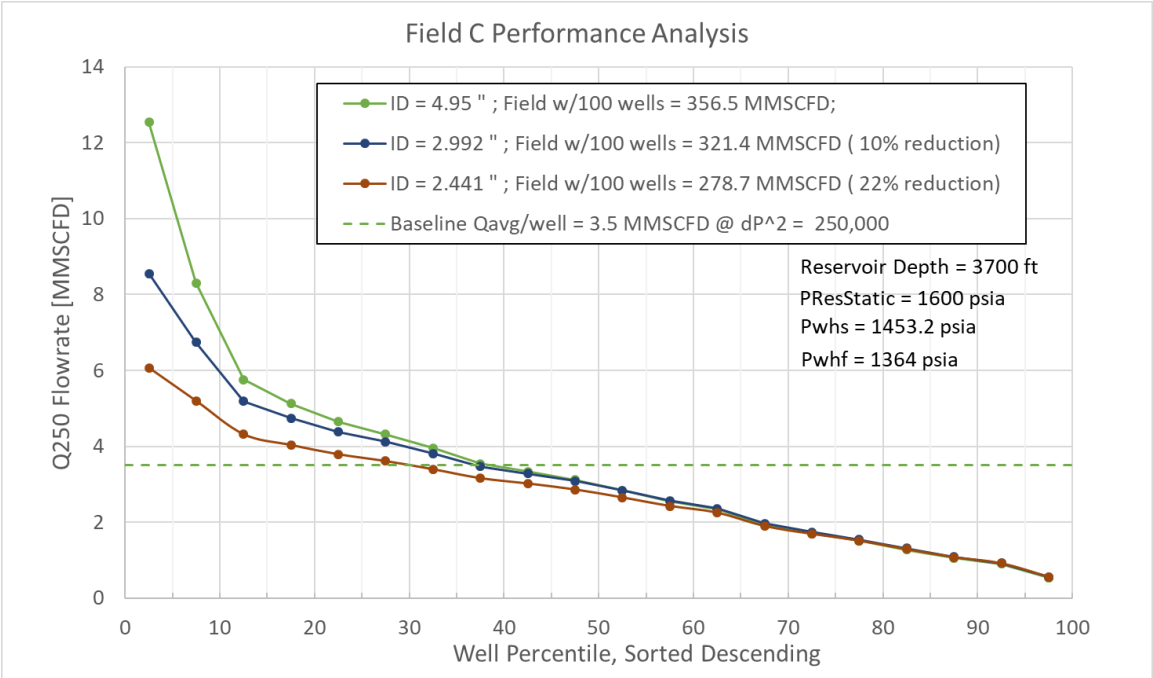

Figure D- 3. Q250 flowrates for Field C wells with baseline $Q_{avg/well}$ = 3.5 MMSCFD and P_{RSI} = 1600 (=P_{max}) psia in 4.95" ID wells showing reductions at two liner sizes, 2.992 and 2.441".

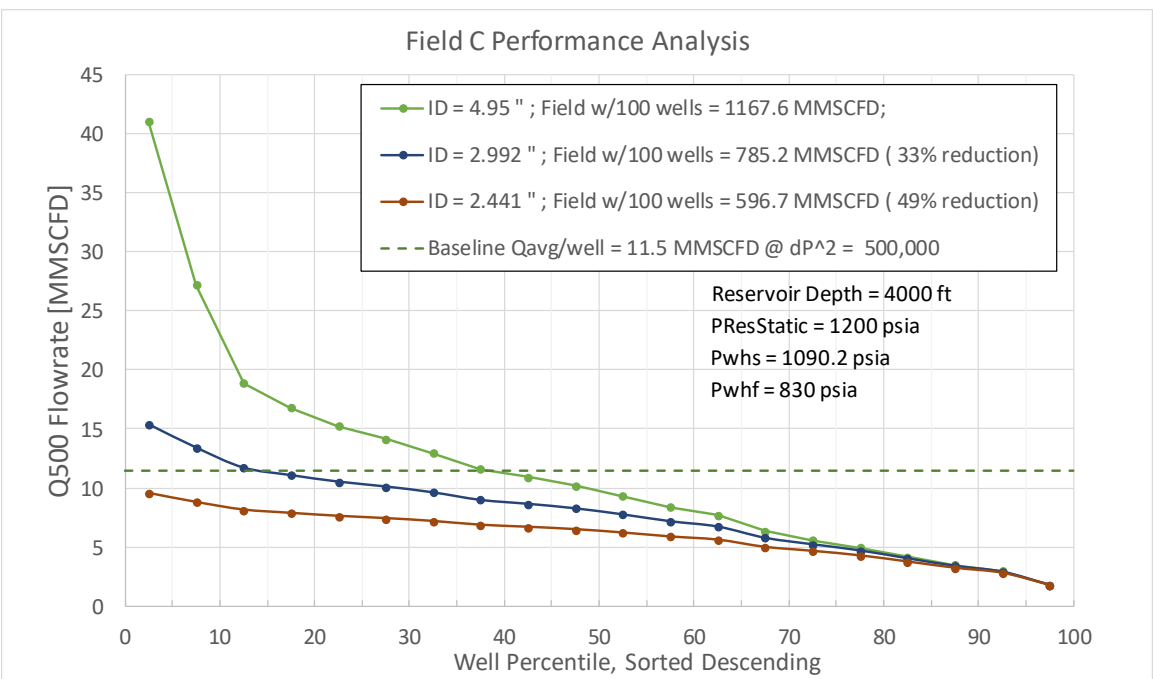

Figure D- 4. Q500 flowrates for Field C wells with baseline $Q_{avg/well}$ = 11.5 MMSCFD and P_{RSI} = 1200 psia in 4.95" ID wells showing reductions at two liner sizes, 2.992 and 2.441".

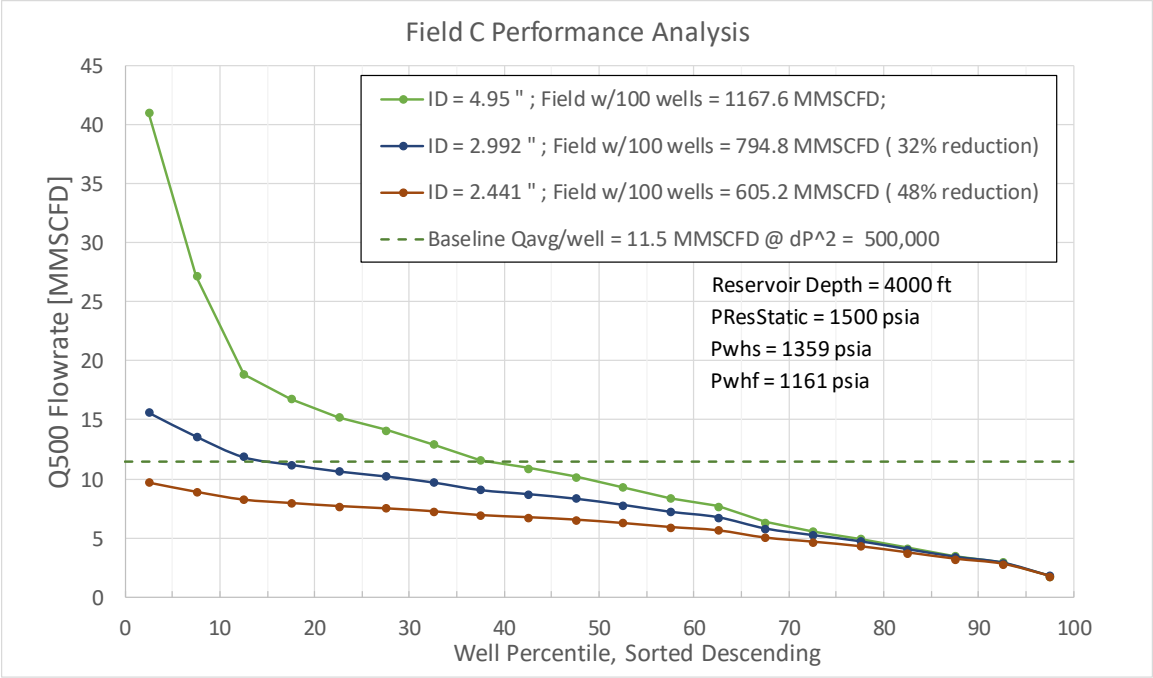

Figure D- 5. Q500 flowrates for Field C wells with baseline $Q_{avg/well}$ = 11.5 MMSCFD and P_{RSI} = 1500 psia in 4.95" ID wells showing reductions at two liner sizes, 2.992 and 2.441".

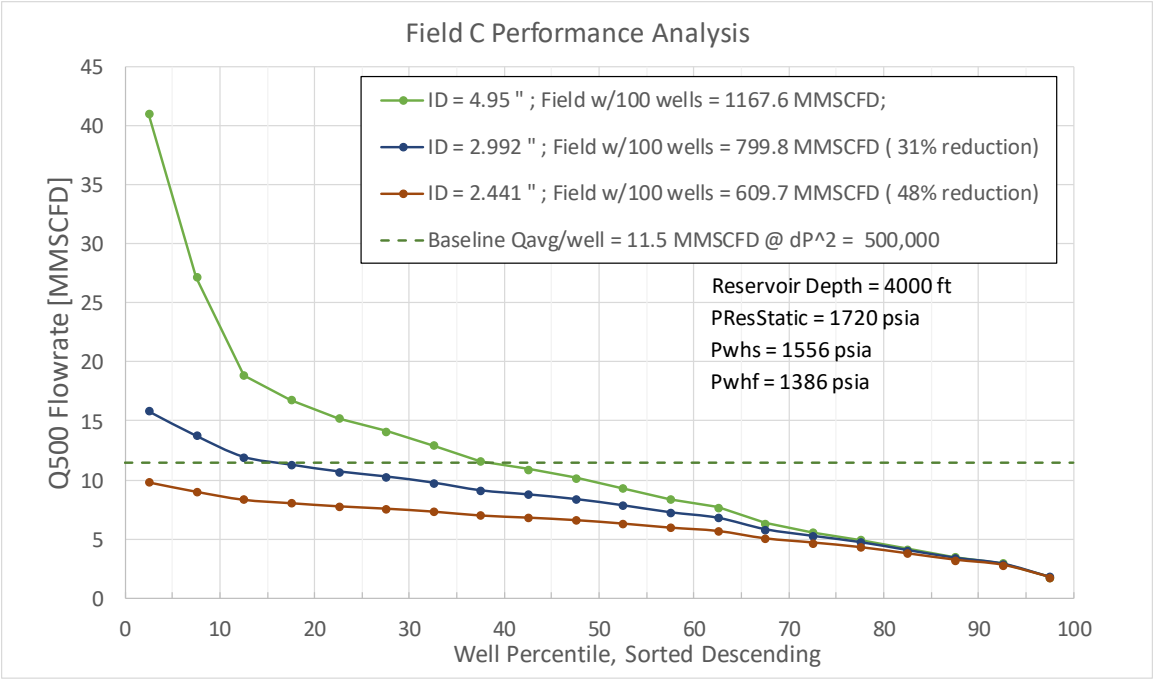

Figure D- 6. Q500 flowrates for Field C wells with baseline $Q_{avg/well}$ = 11.5 MMSCFD and P_{RSI} = 1720 (=P_{max}) psia in 4.95" ID wells showing reductions at two liner sizes, 2.992 and 2.441".

This page left blank

DISTRIBUTION

Email—External (encrypt for OUO)

Name	Company Email Address	Company Name
Kathryn Johnson	johnsonk@battelle.org	Battelle

Email—Internal

Name	Org.	Sandia Email Address
Anna Snider Lord	08862	acsnide@sandia.gov
Technical Library	01177	libref@sandia.gov

Sandia National Laboratories is a multimission laboratory managed and operated by National Technology & Engineering Solutions of Sandia LLC, a wholly owned subsidiary of Honeywell International Inc. for the U.S. Department of Energy's National Nuclear Security Administration under contract DE-NA0003525.